Experimental study of mobility control by foams : potential of a FAWAG process in pre-salt reservoir conditions

Lucas Gomes Pedroni

Université Pierre et Marie Curie

IFP Energies Nouvelles

ED 398 – Géosciences, ressources naturelles et environnement

IFPEN, Direction Géosciences

Département Fluides & Roches / Equipe Mousses pour l'EOR

Experimental study of mobility control by foams:

potential of a FAWAG process in pre-salt reservoir conditions

Par Lucas Gomes Pedroni

Thèse de doctorat de Géosciences

Dirigée par Lahcen Nabzar

Présentée et soutenue publiquement le 14 Décembre 2017

Devant un jury composé de:

Dr.William R. Rossen	Head of Petroleum Engineering Section	TU Delft	Rapporteur
Dr. Henri Bertin	Research Director	Université de Bordeaux – Trefle Lab	Rapporteur
Dr. Abdelhamid Elaissari	CNRS Research Director	Université Lyon 1, LAGEP	Rapporteur
Dr. Serge Stoll	Senior Lecturer Analytical and Biophys. Environ. Chemistry	Université de Genève	Examinateur
Dr. Amandine Cuenca	Research Scientist	Solvay Novecare EOR	Examinatrice
Dr. Pierre Levitz	Research Director	PHENIX Lab, UPMC	Président
Dr. Olga Vizika-Kavvadias	Directrice Division Geosciences	IFPEN	Invitée
Dr. Lahcen Nabzar	Ingenieur de recherche	IFPEN	Promoteur/Directeur de thèse

Dédicace

"La vie n'est pas facile pour aucun de nous. Mais quoi, il faut avoir de la persévérance, et surtout de la confiance en soi. Il faut croire que l'on est doué pour quelque chose, et que, cette chose il faut l'atteindre coûte que coûte."

Marie Curie

"The days I spent pursuing my PhD in physics were some of my darkest. It wasn't the intellectual challenges or the workload that brought me down; it was my deteriorating mental health. I felt unsupported, isolated and adrift in uncertainty. Anxiety attacks became a part of my daily life.

* * * * *

A 2015 study at the University of California Berkeley found that 47% of graduate students suffer from depression, following a previous 2005 study that showed 10% had contemplated suicide. A 2003 Australian study found that that the rate of mental illness in academic staff was three to four times higher than in the general population, according to a New Scientist article. The same article notes that the percentage of academics with mental illness in the United Kingdom has been estimated at 53%.

* * * * *

In essence, many PhD students are so accustomed to hard work and self-discipline that they beat themselves up when their efforts to manage depression fail to generate perfect results."

Jennifer Walker (Quartz, Nov 12nd 2015)

Dedicate to all those that suffer from anxiety disorder and depression. Do not give up. There is so much joy waiting for you beyond the darkness.

Acknowledgments

At last, after a long journey, this thesis is finished. This Ph.D. was certainly the most trying period of my life so far, but also the one with the richest experiences, both professionally and personally. I could not have hoped to conclude this work without the constant encouragement and support of my colleagues, friends, and family. I do not believe that words can show how grateful I am to them, but I hope to be able to express at least a glimpse of my gratitude below.

I would like to thank first and foremost my beloved *fiancée*, Angélica. Without her love, support and the joy that she brought to my life, this thesis would not be finished. She always kept pushing me forward, no matter what. You have my eternal love and gratitude, moon of my life.

I would also like to thank Jean-François Argillier and Emmanuel Manceau, not only for their support throughout this project but for offering the opportunity to develop this Ph.D. at IFPEN. They were the first to propose this collaboration and was because of their interest in this project that this dissertation is here now.

Of course, this work would not have become reality without the support of Eugenio André Campagnolo, Claudio Marcos Ziglio, Alexandre Jaime Mello Vieira, and José Roberto Fagundes Netto, from Petrobras. They not only believed in the importance of this study, they believed in my capacity to do it and defended the initial proposal inside Petrobras. My most sincere thanks to all of you for trusting me and giving me such a unique opportunity.

I would like to express my deep sense of gratitude to François Baudin, Loïc Labrousse, and Dovy Tristani from l'ED 398/UPMC, for going beyond the attributions of academic support and offering me help when I needed it the most, even if I did not know it at the time. Likewise, my special thanks go to Jean-Marc Lombard, Meriem Jehl, Louis Sylvie, Marie-Claude Lynch and Joëlle Behot, who also helped me beyond the professional boundaries of a co-working environment. Their support provided me the assistance that I needed to overcome some of my darkest hours during this Ph.D.

No amount of appreciation and thanks can be enough for all the friends and co-workers that I had the pleasure to meet during my period in France, and who helped me in and outside of the lab. A special word of appreciation goes to: the LOF team at Bordeaux, especially Emie and Amandine, who taught me so much; all the technicians and lab team from IFPEN (special thanks for letting me participate in the *Pétanque* tournament); and the other PhD students, with whom I shared friendship, experiences, mutual support, and moments of happiness and sadness (special thanks to Julia, Isabelle, Camille, Laura, Thomas, Virginie, Erica, Anouk, Richard, Vincent, and Charlotte).

I would also like to thank Dr. William R. Rossen, Dr. Henri Bertin, Dr. Abdelhamid Elaissari, Dr. Serge Stoll, Dr. Amandine Cuenca, Dr. Pierre Levitz, and Dr. Olga Vikiza-Kavvadias for serving on my dissertation committee. I feel truly honored for having you evaluating my work, and for having the opportunity to discuss it with such esteemed researchers.

This project would not have been possible without the kind words of recommendation from my professors Ana Flávia Nogueira, Marco-Aurelio de Paoli, and Luis Carlos Dias. My most sincere thanks for believing in my potential to perform such a high-level project. I would also like to thanks my advisor, Lahcen Nabzar, for the things he taught me. Special thanks to Petrobras and IFPEN for the joint funding of this project.

I could not forget to thank my family and closest friends, for their unconditional love and never-ending support. They have always stood by myself for better or for worse, and it is thanks to them that I can keep dreaming and reaching higher and higher. And last, but not least, to Arya, who gave me the final push that I needed to conclude this dissertation. I will always look after you.

Abstract

Keywords: foams, Enhanced Oil Recovery, mobility control, Brazilian pre-salt, carbonates, porous media.

The Brazilian Pre-Salt is one of the world's largest discoveries of oil in the last decade, with accumulations that could range from 115 billion barrels to over 288 billion barrels. Because of their size and the good quality of oil, these reservoirs are both a great opportunity and of strategic importance for Brazil. However, they also present some of the most technically challenging conditions for development and production. One of the main concerns is the poor sweep efficiency typically observed in carbonate reservoirs due to fractures and other large heterogeneities. Such concerned is increased by an ongoing water-alternating-gas (WAG) pilot and plans for future expansion of WAG injection, since gas-based EOR methods are subjected to sweep efficiency issues as well. To overcome these hurdles, foam flooding is being evaluated for improving sweep efficiency in these scenarios, as it holds great potential for increasing recovery in heterogeneous and complex reservoirs.

Foam flooding is one of the most promising and cost-effective methods to overcome the drawbacks associated with gas-based EOR operations. Studies have shown that surfactant stabilized foams not only reduce the mobility of the gas in the porous media but also are able to do it selectively. Hence, using foams for EOR could result in a more homogeneous advancing front especially in heterogeneous systems, thereby improving the recovery from poorly swept reservoirs.

However, foam flooding is still a developing technology. Despite the abounding works that have been dedicated to this process, and the copious attempts to describe foam rheology in porous media, major uncertainties remain, as much of the available data were obtained in different conditions. This has hindered the development of a physical model, causing current foam simulation tools to be heavily dependent on experimental results for the calibration of parameters (model tuning process). Hence, the reliability of the modeling results depends on how representative the experimental data are. Since the success of foam applications relies on

the ability to predict accurately their performance under field conditions, the lack of a physical model is one of the biggest challenges that deter the use of foams on the field.

Therefore, the present work aimed at advancing our knowledge of the physics underlying the rheological behavior of foams in porous media. For that, we performed a comprehensive systematic petrophysical study of foam flow in porous media to determine the impact of foam quality, flow rate (interstitial velocity), permeability, pressure and gas composition on foam performance. These parameters are essential for evaluating the potential of foam flooding in the scenario of interest. At the best of our knowledge, no such experimental study has been performed before using the same system and under same experimental conditions. Particularly, no similar study has evaluated so extensively the impact of pressure and gas composition on foam flow in porous media.

Our findings show that the data obtained over a range of foam qualities, interstitial velocities and permeabilities converged to a power law master curve, independently of the flow regime, once the rheological behavior of strong foam was expressed in terms of apparent viscosity as a function of shear rate. The master curve obeys a power law with a universal exponent of -2/3. We found experimental and theoretical evidence in the literature for the value of the exponent. The experimental correlation between μ^f_{app} and the determining parameters evaluated in this study might shed some light in the selection of the mathematical expressions and the value of the parameters used to represent foam flow behavior in foam models.

Regarding the impact of pressure and gas composition, our results showed that foam was less effective in reducing gas mobility as pressure increased and that at sufficiently low pressures, the gas composition has no effect on foam performance. However, as pressure increases, the gas composition becomes a determinant parameter for foam behavior, and all components must be considered. We found a master curve for foam performance when presenting the results as gas relative permeability in presence of foams as a function of gas molar density, which allows us to extrapolate foam efficiency for different compositions at different pressures.

The experimental correlations obtained by these original approaches hold immense potential to advance the physical modeling of foam flow in porous media. Therefore, both

approaches and correlations above can be used to refine foam flooding modeling, thus improving the simulation of Foam-EOR process and its reliability.

Résumé

Mots-clés: mousses, récupération assistée du pétrole, contrôle de la mobilité, pré-sel brésilien, carbonates, milieux poreux.

Le pré-sel brésilien est une des plus grandes découvertes de pétrole au monde au cours de la dernière décennie, avec des accumulations pouvant aller de 115 milliards de barils à plus de 288 milliards de barils. En raison de leur taille et de la bonne qualité du pétrole, ces réservoirs représentent une grande opportunité et sont d'une grande importance stratégique pour le Brésil. Cependant, ils présentent également certaine des conditions les plus difficiles techniquement pour son développement et sa production. Une des principales préoccupations est le faible efficacité de balayage généralement observé dans les réservoirs carbonatés en raison de fractures et d'autres grandes hétérogénéités. Cette préoccupation est renforcé par un projet pilote d'injection alternée du gaz et d'eau (WAG) et des plans d'expansion future de l'injection WAG, puisque les méthodes EOR à base de gaz sont également sujets à des problèmes d'efficacité de balayage. Pour surmonter ces obstacles, on évalue l'injection de la mousse pour améliorer l'efficacité du balayage dans ces scénarios, car elle présente un grand potentiel d'augmentation de la récupération dans les réservoirs hétérogènes et complexes.

L'injection de la mousse est un des méthodes les plus prometteurs et les plus rentables pour surmonter les inconvénients associés aux opérations d'EOR à base de gaz. Plusieurs études ont montré que les mousses stabilisées par des tensioactifs non seulement réduisent la mobilité du gaz dans les milieux poreux, mais sont également capables de le faire sélectivement. Donc, l'utilisation de mousses pour EOR pourrait entraîner un front d'avancement plus homogène, en particulier dans les systèmes hétérogènes, améliorant ainsi la récupération des réservoirs mal balayés.

Cependant, l'injection de mousse est toujours une technologie en développement. Malgré les travaux abondants qu'ont été consacrés à ce processus, et les tentatives abondantes pour décrire la rhéologie de la mousse dans les milieux poreux, des incertitudes majeures demeurent, car la plupart des données disponibles ont été obtenues dans différentes conditions. Cela a entravée le développement d'un modèle physique, ce qu'a provoqué une

forte dépendance des outils actuels de simulation de mousse sur les résultats expérimentaux pour l'étalonnage des paramètres (processus de réglage du modèle). En conséquence, la fiabilité des résultats de la modélisation dépend de la représentativité des données expérimentales. Puisque le succès des applications de mousse repose sur la capacité de prédire avec précision leurs performances dans des conditions des réservoirs, l'absence d'un modèle physique est l'un des plus grands défis qui découragent l'utilisation des mousses sur les réservoirs.

Ainsi, le présent travail vise à faire progresser notre connaissance de la physique sous-jacente au comportement rhéologique des mousses dans les milieux poreux. Pour cela, nous avons réalisé une étude pétrophysique systématique complète de l'écoulement de mousse dans des milieux poreux pour déterminer l'impact de la qualité de la mousse, du débit (vitesse interstitielle), de la perméabilité, de la pression et de la composition du gaz. Ces paramètres sont essentiels pour évaluer le potentiel d'injection des mousses dans le scénario d'intérêt. Au mieux de nos connaissances, aucun étude expérimentale n'a été réalisé avant en utilisant le même système et dans les mêmes conditions expérimentales. En particulier, aucun étude similaire n'a évalué si largement l'impact de la pression et de la composition du gaz sur l'écoulement de la mousse dans les milieux poreux.

Nos résultats montrent que les données obtenues sur une gamme de qualités de mousse, de vitesses interstitielles et de perméabilités, convergent vers une courbe maîtresse de loi de puissance, indépendamment du régime d'écoulement, une fois le comportement rhéologique de la mousse forte est exprimé comme la viscosité apparente en fonction du taux de cisaillement. La courbe maîtresse obéit à une loi de puissance avec un exposant universel de -2/3. Nous avons trouvé des preuves expérimentales et théoriques dans la littérature pour le valeur de l'exposant. La corrélation expérimentale entre μ^{f}_{app} et les paramètres déterminants évalués dans cet étude pourrait éclairer la sélection des expressions mathématiques et le valeur des paramètres utilisés pour représenter le comportement d'écoulement de la mousse dans les modèles de mousse.

Concernant l'impact de la pression et de la composition du gaz, nos résultats ont montré que la mousse était moins efficace pour réduire la mobilité des gaz lorsque la pression augmentait, et qu'à des pressions suffisamment basses, la composition du gaz n'avait aucun effet sur la performance de la mousse. Cependant, à mesure que la pression augmente, la composition du gaz devient un paramètre déterminant du comportement de la mousse, et tous

les composants doivent être pris en compte. Nous avons trouvé une courbe maîtresse pour la performance de la mousse en présentant les résultats comme perméabilité relative du gaz en présence de la mousse en fonction de la densité molaire du gaz, ce qui nous permet d'extrapoler l'efficacité de la mousse pour différentes compositions à différentes pressions.

Les corrélations expérimentales obtenues par ces approches originales présentent un immense potentiel pour faire avancer la modélisation physique de l'écoulement de la mousse dans les milieux poreux. De ce fait, les deux approches et les corrélations ci-dessus peuvent être utilisées pour affiner la modélisation d'injection des mousses, améliorant ainsi la simulation du procédé Foam-EOR et sa fiabilité.

Summary

List of figures

List of tables

CHAPTER 1.

INTRODUCTION

1.1 The Brazilian Pre-Salt

Figuring as one of the world's largest discoveries in the last decade, the Brazilian Pre-Salt consists of a cluster of accumulations that extends for 800 km in length and 200 km in width, located over 300 km from the Brazil's southeast coast, Figure 1-1 [1]. These carbonate reservoirs were formed under a rifting environment created during the separation of the continental superstructure Gondwana into the American and African continents, which allowed the formation of the microbialite rocks that constitute these reservoirs (Figure 1-2) [1]. The oil found in these reservoirs is of good quality, presenting low acidity and low sulfur content, and the volumes of the reserves are huge. Indeed, an assessment of the yet-to-find oil made by Monte Carlo simulations based on the available data suggests that total accumulations could range from 115 billion barrels to over 288 billion barrels, within probabilistic confidence levels of 95% and 5% respectively [1]. Because of their size and the good quality of oil, these reservoirs are both a great opportunity and of strategic importance for Brazil.

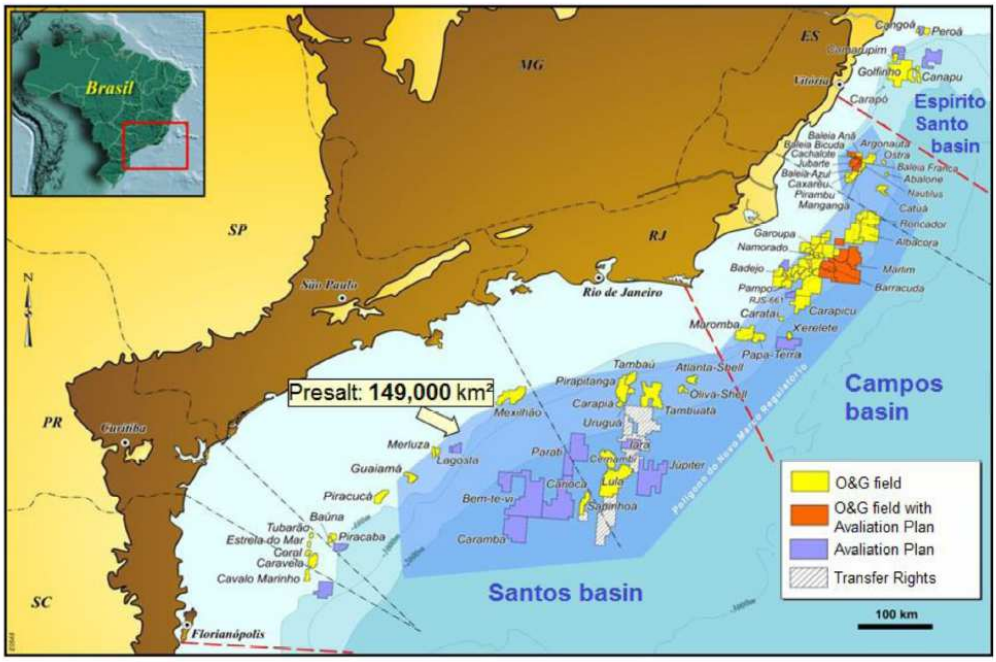

Figure 1-1: Pre-Salt province, extending throughout almost the entire southeast coast of Brazil, comprises an area of c.a. 149,000 km2 [5].

However, they also present some of the most technically challenging conditions for development and production. Found in ultra-deep water regions (1900-2400 m), these

reservoirs are hidden under layers of shifting salt that can be as thick as 2 km, at total depths of c.a. 7 km. Such depths and the high pressures associated pose serious obstacles. The extremely high salinities and hardness raise concern about scaling and the chemistry of the additives typically used in the field. Additionally, as in other carbonate reservoirs, they may be oil-wet and very heterogeneous, and present great contrasts of permeability within a short range [2]; these are characteristics that lead to low recovery factors. Furthermore, the high solution gas ratio (may be higher than 400 m^3/m^3), the presence of CO_2 in gas composition at drastic varying concentrations from field to field [3,4], and the distance from the coastline are demanding conditions regarding, e.g., the metallurgy and the managing of all the volume of gas. It would seem the challenges are as huge as the volumes in the reservoirs themselves.

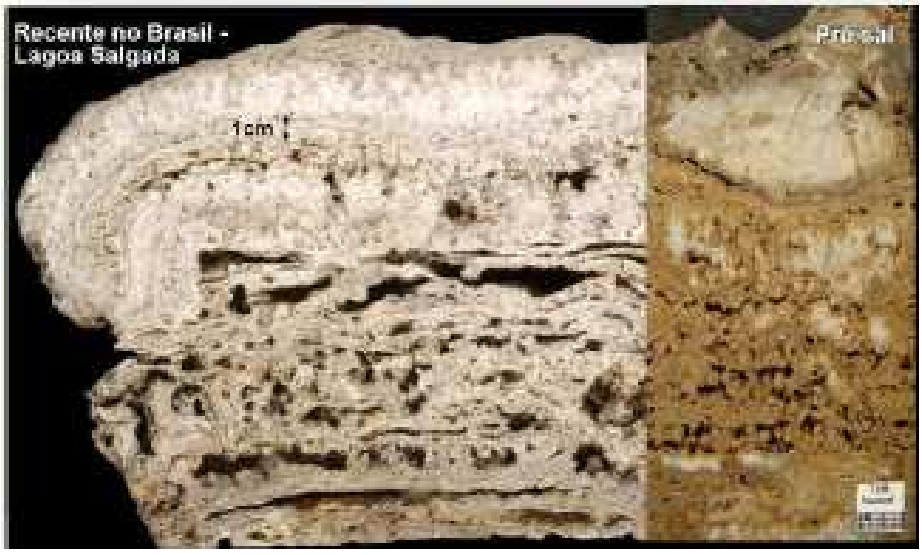

Figure 1-2: Comparison of the morphology of the stromatolites rocks that constitute the Pre-Salt with an outcrop found in Northern of Rio de Janeiro [1].

Nevertheless, Petrobras has been producing from these carbonate reservoirs recently [6]. The oil production from Pre-Salt has passed 1,000,000 bbl/d in May/2016, less than 10 years after the first oil, and less than two years after achieving the mark of 500,000 bbl/d [7]. Pre-Salt's oil production already responds for 40% of the nation's daily production, and Petrobras is responsible for 70% of this volume [7]. Figure 1-3 presents a historical of oil production in Pre-Salt fields and illustrates the fast-growing rates of production. Such impressive results were achieved thanks to an extensive and strategic planning of research to develop new technologies needed to overcome the challenges of Pre-Salt's oil production. Even more impressive, the strategy adopted allowed to achieve a production cost of 8$/barrel

currently [7]. As a part of this strategy to develop Pre-Salt fields, Petrobras is evaluating and developing technologies that may be essential to assure the future production of these fields, such as Enhanced Oil Recovery (EOR) methods [3].

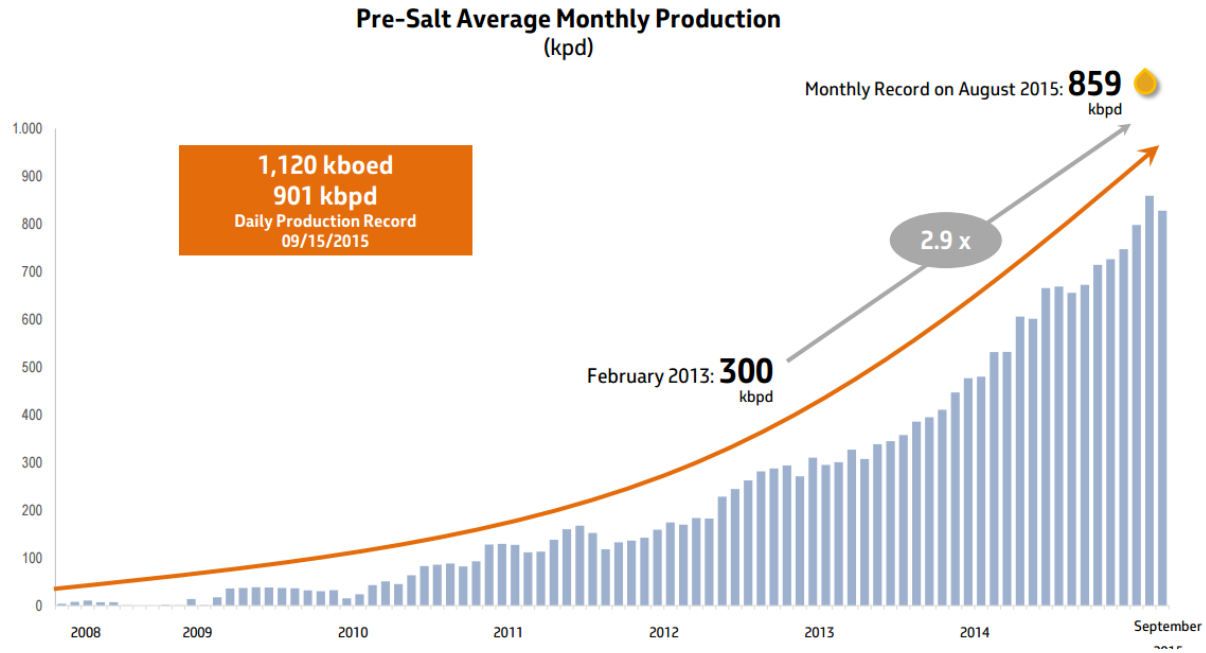

Figure 1-3: Average Pre-Salt daily production, showing the fast increasing pace of production achieved in pre-salt [8].

The application of EOR is more complex in offshore environment. Space and weight restrictions, as well as very large well spacing and less detailed information about the reservoir geology, impose constraints not present in onshore applications. Due to the lack of room in the platforms for future expansion, an EOR method in offshore scenario needs to be planned well in advance, being contemplated from as soon as the conceptual stage of the development [3,9,10]. For that reason, EOR is being studied early in the projects for Pre-Salt.

Because of the relatively high gas oil ratio (GOR) of these reservoirs and the presence of CO_2 in the gas phase, gas-based EOR methods have been considered in Pre-Salt development projects [1]. Indeed, a water-alternating-gas (WAG) pilot is already ongoing on Lula field [3], with very promising results. However, as gas based EOR are subject to poor sweep efficiency issues, and carbonate reservoirs are known for presenting fractures and layers of highly contrasting permeability, as well as other large heterogeneities (as vugs), there is a great concern regarding the sweep efficiency on the Pre-Salt. To overcome these

hurdles, foam flooding is being evaluated for improving sweep efficiency in these scenarios, since it holds great potential for increasing recovery in heterogeneous and complex reservoirs.

1.1.1 Foam Flooding

Foam flooding is one of the most promising and cost-effective methods to overcome the drawbacks associated with gas-based EOR operations [11]. Many studies have shown that surfactant stabilized foam can significantly reduce the mobility of the gas in the porous media, thereby improving the efficiency of volumetric sweep and oil recovery in both immiscible and miscible processes [12,13]. In some cases, foams have shown the ability to selectively reduce gas mobility [13,14]. Hence, using foams for EOR could result in a more homogeneous advancing front especially in heterogeneous systems, thereby improving the recovery from poorly swept reservoirs.

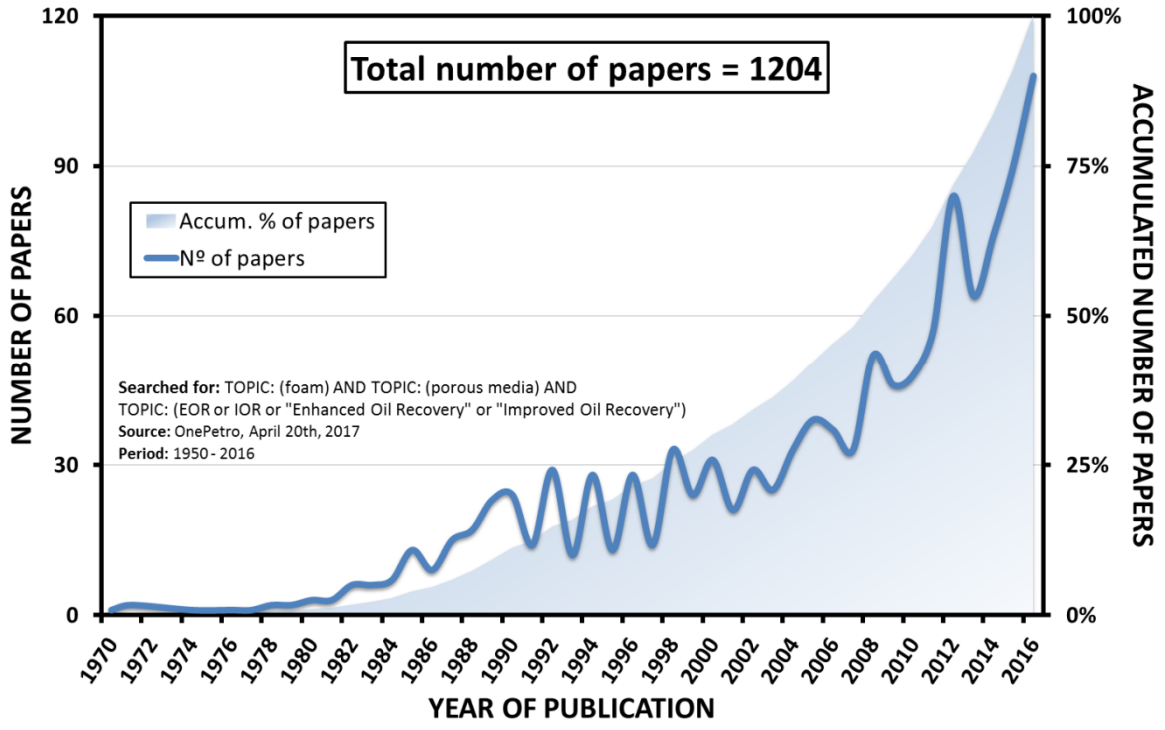

Figure 1-4: Number of publications and accumulated percentage of papers per year found by the research tool OnePetro related to Foams and EOR. The research comprises both conference and journal papers found on this platform.

Due to their large potential in boosting EOR gas flooding, foams are currently a matter of active work both at laboratory and pilot scale. An increasing interest is clearly verified in

Figure 1-4, which shows the number of publications on Foams for EOR through time. More than 50% of the papers were published since 2008, and the last year alone responds for almost 10% of the works. The potential applications of foams include in-depth mobility control, blocking agents (for thief zones and/or GOR reduction) and conformance control (fractures, large permeability contrast, and layered reservoirs) [11,14].

The flow of foam in porous media is a dynamic process that depends on the equilibrium between the creation and destruction of lamellae[15–18]. Many parameters can impact such balance, including reservoir properties (K, heterogeneity, wettability, pressure, temperature, mineralogy), reservoir fluids (nature, composition, and saturation), injection conditions, shear rate and surfactant (nature, concentration). As a result, a significant volume of theoretical, laboratory and pilot work has been dedicated to this process [11,19–21]. Nevertheless, foam flooding still is a developing technology. Major uncertainties remain regarding the rheology and transport of foam in porous media, especially in presence of oil. Consequently, current models are heavily dependent on laboratory results to calibrate their fitting parameters [22]. This dependence makes models less reliable for full-field scale predictions, especially if the results are not representative of the real conditions [21,23,24]. Since the success of foam applications relies on the ability to predict accurately their performance under field conditions, the lack of a physical model is one of the biggest challenges that deter the use of foams in the field.

With all these considerations in mind, we performed a systematic experimental study of foam rheology in porous media to gain a better understanding of the Foam-EOR process.

1.2 Motivations and Objectives

The study and evaluation of foam flooding for Pre-Salt reservoirs constitutes an innovative project in many ways. The properties of foams are influenced by a multitude of variables, and Pre-Salt has a unique set of conditions. Lula field, the target scenario of this project, for example, presents mild temperature (58°C) and light oil (28° – 30° API), but the reservoir pressure can be as high as 550 bar, about twice the highest pressure ever tested in the lab for foams [14]. Formation water salinity is c.a. 210,000 ppm and hardness is around 11,000 ppm, which represents a challenge for surfactant formulations. It has a high solution

gas ratio (200 – 300 m^3/m^3), which prompted the consideration of gas re-injection from the very beginning of the development of the field [3,10]. Moreover, the gas in solution has 8-15% of CO_2, but the facilities available for gas separation allows a stream much richer in CO_2 to be injected into the reservoir, hence injected gas composition may vary drastically during operation [4]. Furthermore, as other carbonate reservoirs, it presents several challenges mainly associated with its complex pore geometry, large-scale variation in permeability, and sometimes unfavorable wettability [2].

Such conditions are very difficult to represent in the laboratory, and sometimes even not feasible. The level of pressure comprised here typically requires tailor-made cells and setups, as commercial solutions are not usually available. Moreover, carbonate cores will dissolve during coreflood tests, due to interactions with the brine in presence of CO_2 (carbonated brine). Likewise, plugs cannot represent effectively the reservoir geology (very stratified, high contrast of permeability, presence of vugs, channels, and fractures).

As discussed in section 1.1.1, current foam simulation tools are heavily dependent on experimental results for the calibration of parameters (model tuning process), and the reliability of the modeling results depends on how representative the experimental data are [21–24]. Consequently, due to the demanding conditions of Pre-Salt reservoirs, the reliability of the predictions obtained with the current models for such complex scenario would be questionable, at least.

Additionally, important aspects for foam application that could contribute to the development of a more comprehensive understanding of foam flow behavior, as well as to improve foam modeling, have not been given enough attention. For instance, despite the considerable data and advanced studies on foams that have been published recently, correlations (either experimental or theoretical) between foam apparent viscosity and permeability are hardly ever discussed. The impact of pressure and gas composition also are poorly explored. These are aspects important for foam application in the Pre-Salt environment.

Acknowledging the intricacies above exposed, a more feasible way to evaluate the potential of foams for Pre-Salt would be developing an empirical model of the rheological behavior of foam flow in porous media, by evaluating how the most important parameters (such as foam quality, interstitial velocity, permeability, pressure, oil saturation and

composition, gas composition, among others) influence foam flow, hence allowing to predict more accurately its performance.

The main objective of this study is to gain a better understanding of foam flow behavior in porous media to verify its potential as an EOR method for improving the sweep efficiency of gas injection in Pre-Salt reservoirs. To achieve this goal, we performed a comprehensive systematic petrophysical study of foam flow in porous media. We determined the impact of the following parameters on foam performance: foam quality, interstitial velocity, permeability, pressure, and gas composition. These parameters are essential for evaluating the potential of foam flooding in the scenario of interest. At the best of our knowledge, no such experimental study has been performed before using the same system and under same experimental conditions. Particularly, no similar study has evaluated so extensively the impact of pressure and gas composition on foam flow behavior. Additionally, we performed exploratory studies on the effect of oil and heterogeneities in the foam flow. An outline of this dissertation is presented next.

1.3 Dissertation outline

This dissertation is composed of 8 chapters. Chapter 2 provides an overview of Enhanced Oil Recovery fundamentals and methods, a historical perspective and a description Foam-EOR technology. Chapter 3 is a literature review of foam flow in porous media, which covers foam generation and destruction mechanisms, flow regimes and rheology, selection and evaluation of foam formulations, as well as foam flow experiments and modeling. Chapter 4 presents the methodology and the results from the selection and evaluation process for the surfactant formulation used throughout the petrophysical characterization of foam flow. A high throughput system allied with automated image processing was used to maximize the range of conditions tested within a short time. Before starting the petrophysical studies, a high-pressure micromodel setup was used to validate the selected formulation and its foaming ability during flow in porous media. The micromodel tests and their results are discussed in Chapter 5.

Chapter 6 presents a comprehensive experimental study of the impact of foam quality, interstitial velocity, and permeability on foam apparent viscosity during flow in porous media.

We confront our results with the current understanding of foam flow, and we propose an original approach to treat coreflood data and characterize foam flow. This innovative approach allowed us to obtain a master curve for strong foam behavior over a broad range of flow conditions.

Chapter 7 explores the impact of pressure and gas composition in foam performance. Finally, Chapter 8 presents the general conclusions of the present dissertation and discusses future work initiated aiming further characterization of foam for potential application in Pre-Salt.

CHAPTER 2.

EOR: AN OVERVIEW

2.1 Introduction

Global energy demand is expected to grow by on third up to 2040 [25]. Despite the increasing share of renewable energies, hydrocarbon fuels shall remain as the major component of the energy mix. According to the World Energy Outlook 2015 from the International Energy Agency, by 2020 an additional production of 25 million b/d will be needed to equilibrate supply and consumption [26]. To secure the supply in a scenario of aging oil fields and a scarcity of new conventional oil findings, an increasing number of oil companies is trying to maximize the recovery factor (RF) of the existing reserves [27].

During an oil field's life cycle, crude oil production undergoes different processes of oil recovery. Primary recovery is the production of oil using the energy existent in the reservoir (which is found in the form of pressure, gas solution, water drive, etc.) and artificial lift devices. Typically, it can recover between 5% and 25% of the original oil in place (OOIP), depending on the reservoir and oil properties [28]. Secondary recovery consists of the injection of fluids (either water or gas) in the reservoir to either re-pressurize a depleted reservoir or to avoid depressurization. It also pushes oil toward the production wells. These methods can increase the recovery factor of a reservoir to about 40%. To further increase the RF, Enhanced Oil Recovery methods are needed. These methods act by changing the physicochemical properties of fluids and interfaces in the reservoir, thus altering the balance of forces that results in the limited recovery [29,30].

Hence, EOR can be defined as a class of methods that aim to increase the recovery factor of a reservoir beyond the levels typically achievable with primary and secondary recovery [28,29,31]. These methods can be applied at any moment of the production life of an oil field. The term has been met with much confusion and used interchangeably with Improved Oil Recovery (IOR) and tertiary recovery as well [29,30,32]. Sheng [29], Alvarado and Manrique [30], and Stosur et al [32], e.g., discuss some of the many definitions available for both terms in the literature and present their view on what should be the standard definitions. In general, the literature agrees that IOR is a broader term that encompasses just about any process (EOR included) aimed at increasing oil recovery, such as infill drilling, horizontal wells, conformance and mobility control, well stimulation, etc. [32]. However, some authors, such as Sheng [33], consider that the term should be restricted to the recovery process only, and thus practices like reservoir characterization and simulation, use of special

types of wells, infill drilling, improved reservoir management, among others, should not be included in the definition.

Regardless the definition, the potential of EOR technologies to convert huge volumes of discovered oil, which are lying in well-known locations, in reserves makes their development an area of very intense research recently [34–37]. In fact, EOR technologies are considered of strategic importance, as an increase of just 1% on the average RF would bring about 88 billion barrels of oil. Such volume is enough to replace 2.5 years of global crude oil production as it was in 2016 [36,38]. Presently, approximately only 4% of the oil production worldwide comes from EOR projects, but this share is expected to increase significantly in the near future [39,40].

Currently, the global average RF is about 35%, which means there are great opportunities for EOR. The reasons for the low RF and how EOR methods can increase the RF of a reservoir are briefly presented in the next sections.

2.2 Recovery efficiency

The recovery efficiency (E_R) of a reservoir depends on the product of the macroscopic (E_V) and microscopic (E_D) displacement efficiencies, equation 2-1. The macroscopic factor, E_V, represents the portion of the reservoir that has been contacted by a displacing fluid, like water or gas. The microscopic component, called displacement efficiency, E_D, accounts for the oil trapped by viscous and capillary forces in the zones already swept. EOR methods aim to tackle either one or both components to improve recovery factor, since E_R is a major component of the RF, as demonstrated in equation 2-2 [27].

2-1. $$E_R = E_V \times E_D$$

2-2. $$RF = E_R \times E_{con} \times E_{ec}$$

2-3. $$E_V = E_{VV} \times E_{VA}$$

E_V is by far the most impacting parameter in the E_R, and thus, the total RF of a reservoir. It is composed by the areal (E_{VA}) and vertical (E_{VV}) sweep efficiencies, equation 2-3. The main sources of poor sweep efficiency are: heterogeneities in the rock reservoir, contrast of density between displaced and displacing fluids, and contrast of viscosity between

fluids. Reservoir heterogeneities, such as zones with high contrast of permeability or fractures, allow the development of preferential paths (regions of lower resistance to flow), which eventually result in channeling of the fluids between injector and producer (Figure 2-1). In the same way, a great contrast of viscosity will conduct to a percolation-like transport, resulting in viscous fingering (Figure 2-2). Lastly, in scenarios where the vertical permeability and thickness of the reservoir are significant, gravity may act against a uniform displacement and segregate the fluids in the reservoir. This is called gravity override, in the case of a lower density fluid injection, as gas, and gravity underrunning, when the injected fluid is denser than the displaced fluids, as is generally the case for water injection. Figure 2-3 illustrates the impact of gravitational segregation in a reservoir.

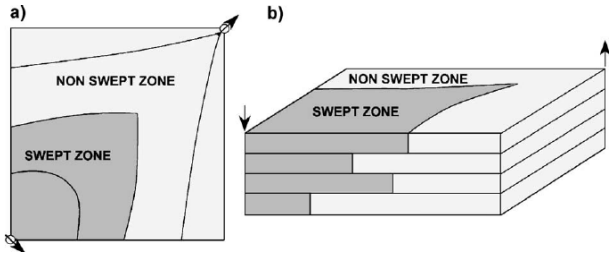

Figure 2-1: Schematic representation of a) areal and b) vertical sweep efficiency. Reproduced from [41].

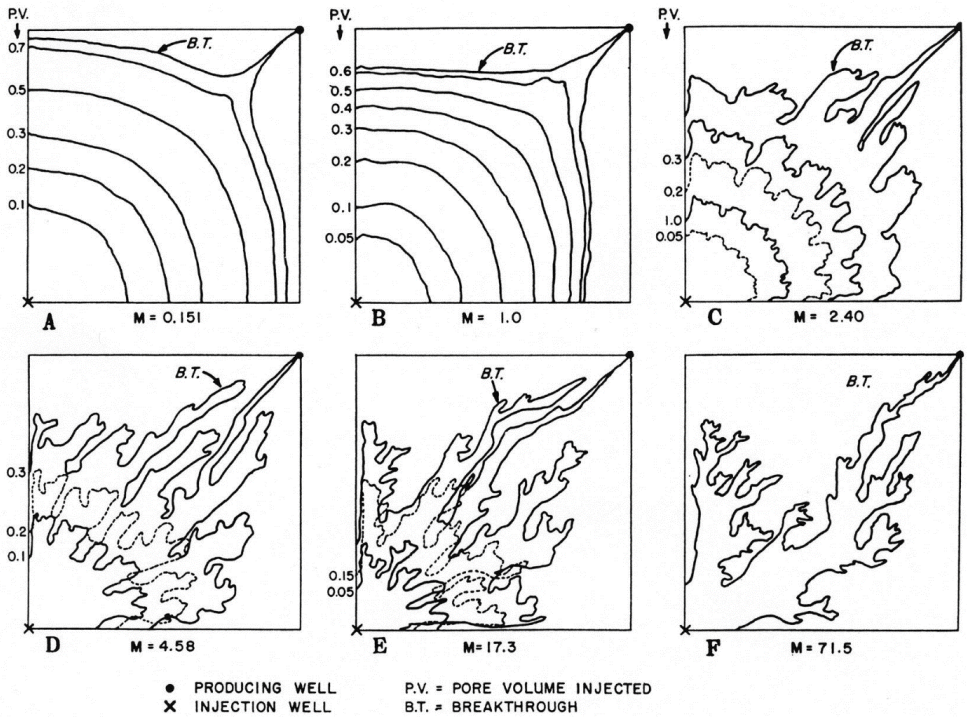

Figure 2-2: Impact of mobility ratio on the areal sweep efficiency and formation of viscous fingering [42].

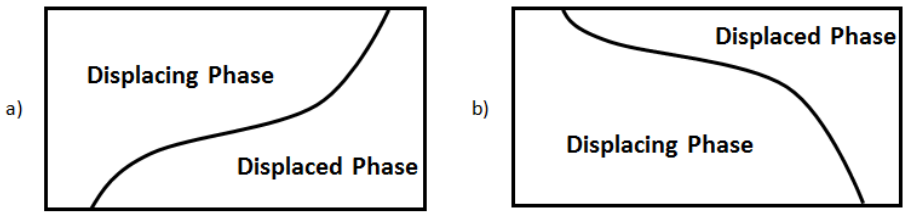

Figure 2-3: Gravitational segregation. A) Override. B) Underruning [43].

Accordingly, the sweep efficiency depends on how well the fluids move through the reservoir. Should the displacing fluid move more easily than the displaced fluid(s), than the E_V, and consequently, the RF, will suffer. The mobility of a fluid is defined as the ratio between its (relative) permeability and its viscosity. Thus, one can estimate the sweep efficiency of a reservoir determining the mobility ratio (M) of the fluids, equation 2-4 [44]. Figure 2-2 shows how the mobility ratio impacts the sweep efficiency. Therefore, E_V can be improved either by increasing the viscosity of the displacing fluid, reducing the viscosity of the displaced fluid, or altering the relative permeability of them.

2-4. $$M = k_{displacing}\mu_{displaced}/k_{displaced}\mu_{displacing}$$

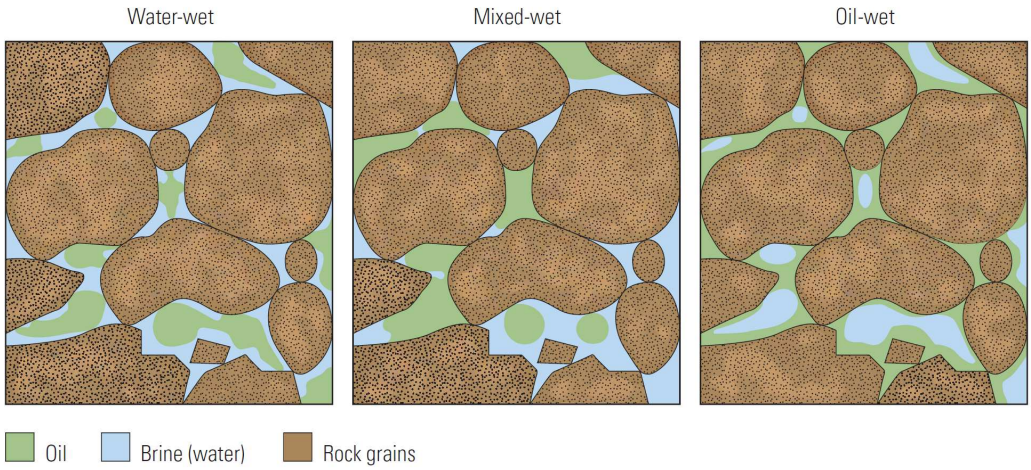

Figure 2-4: Representation of residual oil in the pore space as a function of rock wettability. For water-wet rocks (left), oil remains mainly in the center of pores, while in oil-wet conditions (right), it is the oil that covers the rock surface as a film and water remains in the center of the pore. The mixed-wet case (center) is an intermediate between both extremes, where oil can stay as droplets in the center of the pore, or contacting the rock surface [45].

Once swept, the porous medium is not completely desaturated from oil. Capillary and viscous forces trap a fraction of it, resulting in a residual oil saturation, S_{or}. The higher the S_{or}, the lower the microscopic displacement efficiency, E_D. The oil left behind in a water-wet

environment during a waterflooding exists mainly as droplets and blobs, while in oil-wet cases, it can remain as a film partially covering the surface of the porous medium, Figure 2-4.

The balance between capillary and viscous forces in the pore scale can be estimated with the microscopic capillary number, N_C, equation 2-5 [46]. As discussed by Sheng [46], N_C may assume more or less complex forms, depending on the definition. The capillary number can be used to estimate E_D, in a similar way that the mobility ratio is used to estimate Ev.

2-5. $$N_C = v\mu/\sigma \cos\theta$$

Hence, E_D is influenced by the interfacial tension of the fluids, their viscosity, and the wettability of the porous medium [44]. Wettability has a major relevance in the S_{or}. According to Muggeridge et al [27], mixed-wet and weakly water-wet reservoirs have the lowest S_{or}, followed by the oil-wet and the water-wet [27]. In practice, however, the water-wet reservoirs have higher recovery factor than the others. This happens because despite lower S_{or}, under the other wettability conditions, water breakthrough occurs earlier, and simultaneous production of oil and water produces oil more slowly, thus taking much more time and greater volumes of injected brine to achieve S_{or} than water-wet reservoirs [27]. Considering the concession periods and costs of production, mixed-wet and oil-wet reservoirs tend to be abandoned at lower RF than the water-wet ones.

As aforesaid, EOR methods try to increase the recovery factor by increasing either sweep efficiency, displacement efficiency, or both. Considering the exposed above, they can achieve that via alterations in the interfacial tensions of the fluids, their viscosities, their relative permeabilities, or the wettability of the porous medium. The following section presents some of these methods and how they are classified based on the different approaches used to increase recovery.

2.3 EOR Methods and classification:

EOR methods can be classified based on how they change the physicochemical properties of fluids and interfaces in the reservoir to increase the amount of oil that can be produced. Since several processes can be combined when operating a method, a precise

classification may be intricate sometimes [29]. Nevertheless, EOR methods may be separated in four classes according to the main agent of change of the interactions existing in the reservoir, Figure 2-5**.** The three main classes are briefly described below. More recent or immature technologies, such as Microbial EOR, low and optimized salinity injection, to mention a few, are encompassed in the category Others and will not be discussed here.

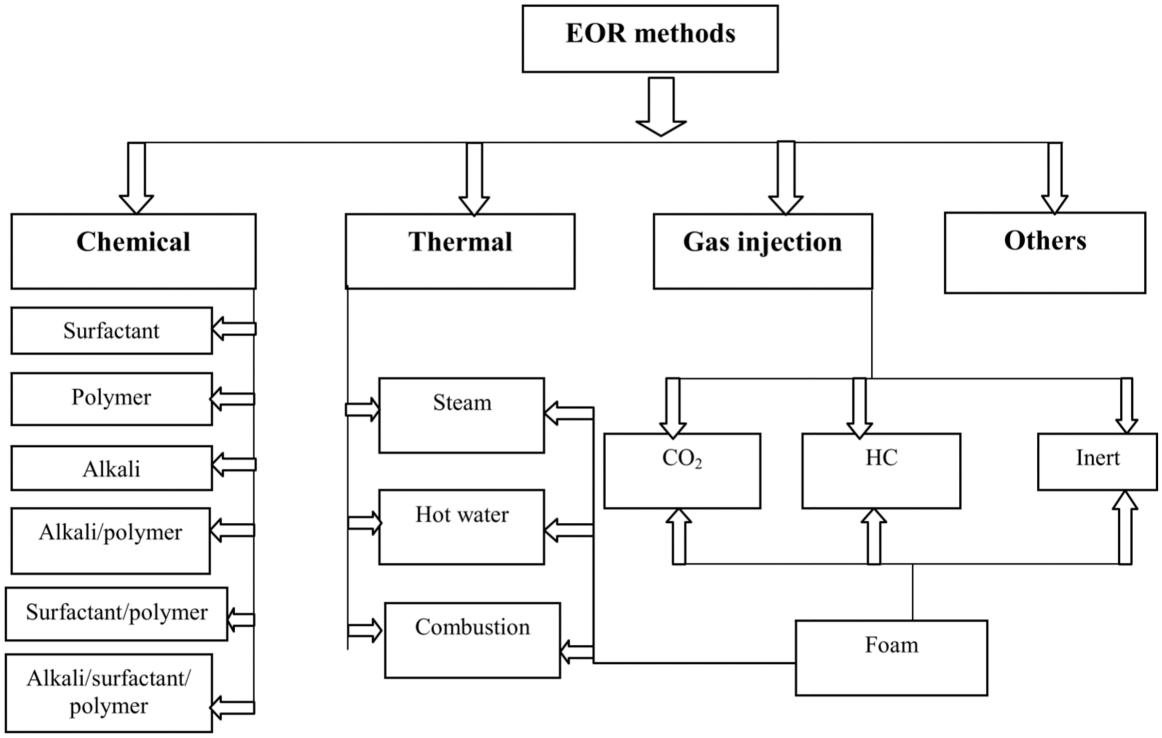

Figure 2-5: Simplified view of EOR methods [31]

2.3.1 Thermal EOR:

Methods that change the physicochemical properties inside the reservoir by supplying heat either through steam injection or in-situ combustion. They are the most used EOR methods worldwide and are responsible for a great part of the EOR's global production. Historically, they are used for heavy oils, with the main goal of reducing the viscosity of the oil. In the case of in-situ combustion, the process also seeks to improve the quality of the oil by cracking the heavier components into lighter and more valuable ones. Nevertheless, recent developments have been successful in applying these methods at light oil reservoirs [47].

Mostly, additional oil recovery comes from the increased swept area due to the reduced viscosity of the heated oil. But other mechanisms can be present as well. Lighter components can vaporize in the heated zone, condensing and mixing with the oil downstream, reducing its viscosity and improving its quality because of the incorporation of lighter components. Additionally, for in-situ combustion (ISC), the hot gases generated in the combustion zone help to displace the oil towards the producers. Nevertheless, both ISC and steam injection may present sweep efficiency issues since the gases and vapors in these processes are much more mobile than the oil.

Both steam and in-situ combustion have many variants. Here are some of them [29]:

- **Steam:** steam flooding, cyclic steam injection (huff-n-puff), steam assisted gravity drive (SAGD), expanding solvent SAGD (ES-SAGD), solvent gas vapor extraction (VAPEX), ES-VAPEX, steam and gas push (SAGP).
- **In-situ combustion:** forward dry and wet combustion, toe-to-heel air injection (THAI), THAI catalytic upgrading process in-situ (THAI-CAPRI), high-pressure air injection (HPAI).

2.3.2 Gas-based EOR:

Differently from the gas flooding used as a secondary recovery process, where the gas is injected (usually in the gas cap) with the sole purpose of pressure maintenance, gas-based EOR methods rely on mass transfer processes between the injected gas and the oil to yield additional recovery. These interactions reduce the interfacial tension (IFT) between oil and gas and the viscosity of the oil, thus improving displacement efficiency. Depending on the extension of the mass transfer processes, these methods can be either miscible or immiscible. The former is usually preferred for presenting higher potential of additional recovery and better performance on field. Although natural gas (and other gas mixtures from methane to propane), flue gas and N_2 are also used, CO_2 is by far the most used gas for enhanced recovery, since it has the advantages of being much denser and easily miscible with oils in reservoir conditions than the other options [48].

During a miscible displacement, the capillary forces vanish, as there is no longer an IFT between the gas and the oil. Additionally, the viscosity of the oil is greatly reduced

through the incorporation of the gas, which acts as a solvent. The combined mechanisms can improve the microscopic displacement efficiency up to 90% [28,49]. Depending on field conditions, such as pressure, temperature and oil composition, and the injected gas, miscibility occurs through either single (SCM) or multiple contacts (MCM) [44]. Gas composition can be adjusted to achieve miscibility more easily, e.g., through the addition of H_2S.

Immiscible gas injection also reduces the viscosity of the oil and the interfacial tension, but at much smaller scale than a miscible process. Additionally, immiscible gas can increase oil recovery through swelling the oil and vaporization of lighter components. Furthermore, relative permeability effects in tri-phasic flow also improve oil mobilization, promoting higher and accelerated recovery [50,51].

Presently, gas flooding is one of the most commonly applied and most effective EOR method worldwide [28]. Gravity stable drainage projects with RF as high as 85% have been reported [52]. Notwithstanding, the usually low density and viscosity of the displacing gas lead to gravity override and viscous fingering, while heterogeneities in the reservoir may cause channeling of the fluids. These events result in poor volumetric sweep efficiency, greatly impairing the technology's overall performance. Even though Water-Alternating-Gas (WAG) injection, which is the state of art to improve mobility control of gas flooding, is applied in almost every project, the overall recovery improvement achieved in pilots and field application is of 10-20% OOIP [49], for miscible flooding, and even lower for the immiscible ones.

Despite the drawbacks, CO_2-EOR oil production has been steadily increasing since its start in the 1970s [35,40,53]. In fact, its application is limited by the availability of affordable supplies of CO_2 rather than its performance. For that reason, this technology has been mainly restricted to the USA so far, where abundant natural sources of CO_2 are accessible [11,35,40,53]. However, the increasing worldwide concern with global warming and new politics and strategies to reduce greenhouse gas (GHG) emissions, allied with the need to prolong the lives of aging fields, has driven a number of countries to either establish or expand their CO_2-EOR projects [9,48]. Prospects look particularly favorable in Brazil, Middle East, and China, where projects are already on-going, but initiatives also exist in the North Sea [35,53,54].

2.3.3 Chemical EOR:

Methods that seek to improve either displacement, or sweep efficiency, or both, through the injection of chemical products dissolved in the injection brine [44]. These chemicals are applied as slugs, and slugs of different compositions can be combined to achieve the desired result. Mainly, the chemicals used are:

- Polymers: increase viscosity of the injected brine and hence improve sweep efficiency;
- Surfactants: used either to reduce interfacial tension between oil and brine or to alter the wettability of the rock, thus improving displacement efficiency;
- Alkalis: used to reduce IFT through reaction with acid components in the oil, but also able to change wettability and to reduce adsorption of other chemicals.

Surfactant and alkaline flooding can greatly improve displacement efficiency, as reducing IFT is the most effective and practical way of increasing the capillary number [28]. However, the reduction of IFT alters the relative permeability curves for oil and brine in a way that impairs sweep efficiency, hence these chemicals must always be used in combination with some mobility control process. Most frequently, they are associated with polymers, resulting in the following methods: alkaline-polymer (AP), surfactant-polymer (SP), and alkaline-surfactant-polymer (ASP). Nonetheless, studies have been done where gas is used either in substitution of the polymer or as an additional conformance and mobility control technique, which originate technologies such as alkali-surfactant-gas (ASG), alkali-surfactant-polymer-foam (ASPF), and low-tension gas flooding. All these processes are quite complex and reservoir specific, thus demanding extensive laboratory work to properly screen, evaluate and select formulations. Variables such as salinity, hardness, temperature, oil composition and viscosity, adsorption, need to be factored in the selection of a formulation. This constitutes a great challenge to the performance of these methods on field [44].

Chemical EOR methods have the potential to increase recovery up to 35% of OOIP and can be used in scenarios where neither thermal nor gas methods would be viable [31]. This potential makes chemical EOR a topic of intense research. Polymer flooding is the most used and successful chemical EOR method [28,31,40], despite having a lower potential of additional recovery than methods derived from surfactant and alkaline flooding. Typically,

polymer flooding additional recovery is lower than 10% of OOIP [28,44], while other methods, such as ASP, have been reported to achieve 25–30% of OOIP [28,31,55].

However, chemical EOR projects have been mostly uneconomic so far [28,56]. High total concentration of chemicals in some methods, loss of chemicals to the formation due to adsorption and trapping of microemulsions formed, and the negative impact that these methods have in the oil-water separation and water treatment processes in the topside are some of the factors that restrain economic success of these methods and, consequently, their application on field. Nevertheless, perspectives are good for the future, with the development of more efficient chemicals [28], which should allow operators to reduce chemical concentrations and adsorption, besides the experience gained from past projects.

2.4 Foam-EOR

2.4.1 Initial Considerations

Section 2.3 gave an overview of the different classes of EOR methods summarized in Figure 2-5. However, one method in Figure 2-5 is not portrayed as belonging to any single class: foams. Indeed, foam generation requires the presence of chemical additives (surfactant foamers) and, in that sense, they could be included in chemical processes. But rather than a method *per se*, Foam-EOR are hybrid processes that can be used to improve sweep efficiency of gas injection (miscible and immiscible), steam injection (and variations), and chemical methods, as already mentioned in section 2.3.3. In fact, foam is the one technology up to now capable of counteracting gravity segregation and that have the potential to deal with all the three main causes of low sweep efficiency at once.

Foams are complex fluids that consist of a gas phase dispersed in a continuous liquid* phase, which are usually stabilized by surfactants. Although sometimes it would be more scientifically accurate to say supercritical fluid emulsions, once one considers the range of temperatures and pressures of oil reservoirs, the term foam has been long used to define these systems. They can drastically reduce the gas mobility in the porous media, consequently improving volumetric sweep efficiency and oil recovery. As the reduction in mobility depends

* Although the continuous phase may also be a solid, which results in solid foams, given the systems in discussion only foams formed with a continuous liquid phase will be considered.

on multiple parameters, it can be adjusted to solve different sweep efficiency issues. Thus, foams can be used for: in-depth mobility control; near wellbore conformance control; gravity segregation channeling; and gas-oil ratio (GOR) control [11,14,57]. Additionally, multiple works have reported that foams can, under certain conditions, reduce gas mobility more strongly in high permeability zones than in the low ones [58–63]. Hence, the application of foams for EOR could promote a more homogeneous advancing front, improving recovery.

Field experience on foam injection includes both injector and producer wells, being the former kind more frequent. Foams can be injected either pre-formed, through co-injection, or alternating gas and surfactant solution (surfactant-alternating-gas, SAG). The injection mode greatly affects foam generation phenomena and, consequently, foam properties [14]. Thus, different foam injection modes are more appropriated for different issues that need to be solved. Choosing the correct injection mode for the scenario of interest is a key element for the success of a field application of foam.

Pre-formed foams present very high apparent viscosity and gas mobility reduction and are capable of completely blocking the porous medium. Hence, they are better suited to treat thief zones, like fractures and very high permeability layers, as well as gas coning [14].

Foams formed through co-injection are also capable of blocking the porous medium, though the degree of reduction of gas mobility is usually lower than pre-formed foams. They can be very effective in conformance control and gravity override. Intermittent co-injection has been particularly effective in improving sweep efficiency during steam injection, as pointed out by Turta and Singhal [14]. In-depth mobility control might be achieved on high permeability reservoirs, but co-injection is not recommended for medium to low permeability conditions due to great reductions of injectivity observed on the field. Likewise, scenarios, where injections rates need to be kept within a strict range, are not indicated for this injection mode.

For reservoirs that either have lower-than-Darcy permeability or cannot tolerate an intense loss of injectivity, SAG injection is more fitted. This mode is more indicated for in-depth mobility control but is capable of conformance control as long as both surfactant solution and gas are present in the porous medium with sufficient agitation to form foams. Differently from the previous modes, SAG cannot completely block the porous medium.

The different injection modes and the range of issues that foams can solve make this technology flexible and versatile. Likewise, the possibility to combine foam with nearly any other EOR method to improve their sweep efficiency grants foams great versatility and potential to positively impact oil recovery. Indeed, low sweep efficiency is the main reason for thermal and gas methods underperform on field. And in the case of chemical methods, polymer flooding for mobility control are the most successful projects. Thus, the potential of foams makes them a very important topic and object of intense research, as shown in Figure 1-4.

The diversity of hybrid processes resulting from such combinations ends by generating a multitude of names by which foams can be referred in the literature, which may cause some confusion. Here is a non-extensive list of names that are used: SAG, foam assisted water alternating gas (FAWAG), SWAG, low tension gas flooding (LTGF), alkali-surfactant-gas (ASG), alkali-surfactant-foam (ASF), ASP foam (ASPF), polymer enhanced foam (PEF). The use of different names for similar, if not (almost) identical processes, such as SAG and FAWAG, only causes confusion in the literature and should be avoided, as was advocated for the many terms used for EOR and IOR in the past.

Despite the many variations, fruit of being almost 60-year-old and object of intense research, foam is still an immature technology, which regained much interest in the years 2000's with the advance of CO_2 injection as an EOR technology [11]. Next is a brief history of the development of foam for EOR.

2.4.2 Historical Perspective

Foam-EOR was first proposed in 1958 by Bond and Holbrook [64], and the first field tests were done as early as 1964 in the Siggins Field [65]. However, it was not until the 1980's that foam really started to be applied on the field. Earliest foams applications were mainly designed for steam injection, which kept being the main interest up to 1990. From the 42 projects reviewed by Turta and Singhal [14], 19 were steam foam. Nevertheless, CO_2-foams were also important even in the early days of the technology, being the second most studied and applied type of foam. The first projects with CO_2 started in 1984 and lasted

through the first half of the 1990's, as indicated by the projects reviewed by Turta and Singhal [14] and Enick et al [11].

According to the works of Turta and Singhal [14] and Enick et al [11], the period of 1980's and early 1990's is marked by numerous field applications of foam. Discussions on the results of the most emblematic projects can be found in those works, as well as in the work of Lee and Kam [48]. Some of the projects that deserve emphasis are:

- Midway Sunset: one of the most successful steam foam application, design to counter an overriding problem. Injection mode was a continuous steam injection superimposed by co-injection of surfactant solution. One of the most interesting results occurred in Section 15A, where the increase of 50% in oil rate production remained for 2 years after foam injection stopped.
- EVGSAU: the most well-documented CO_2 foam pilot. Fast SAG was used in response to an early breakthrough of gas due to a thief zone. The pilot was a technical success, as foam diverted 12% of fluids injected from the thief zone to the other zones, reduced GOR in the producer well in half while doubling oil rate. Economically, however, it was only a marginal success, because of the low oil price at the time of the pilot, and because most of the surfactant was applied as a pad before SAG.
- North Ward-Estes: according to Turta and Singhal [14], it is the most successful known foam application on field. Injection mode was fast SAG with cycles of 2 days (one day for surfactant solution and one day for CO_2 injection). The GOR of producer well directly impacted for the channeling of gas was reduced 9-fold after foam injection, and oil production increased 15 times, while water cut and CO_2 requirements also decreased.
- Snorre: an offshore FAWAG project realized between 1997 and 2000. According to Enick et al [11], the most important contribution to foam-EOR was that the project demonstrated that foam can be used at full field scale to promote in-depth mobility control and produce a considerable volume of oil both successfully and profitably.

Some of the reasons for unsuccessful foam injections were: surfactant slug too small; inadequate injection mode for the issue to be solved; wrong evaluation time (pilot too short to

measure results) [11,14]. This is not surprising since much of the early knowledge of foam flow in porous media was learned by trial and error through those field operations, e.g., the way different injection modes affect foam performance. The fundamental research needed to understand foam flow behavior was still in its infancy back then. In fact, it was not until 2001, when the work of Alvarez et al [66] reproduced and extended, with consolidate rock samples, the findings of Osterloh and Jante [67], that a unified theory for steady-state foam flow in porous media was established. Both works were able to reconcile multiple contrasting results in the literature and laid the basis of the current understanding of the rheological behavior of foam flow in porous media.

The works of Alvarez et al [66] and Osterloh and Jante [67] devised a representation of coreflood results that later became known as the diagram of Osterloh & Jante. This diagram allowed Alvarez et al [66] to established some general trends about the impact of flow parameters, like gas and water flow rates, foam quality, and rock permeability, on the expected foam flow. This put these two works among the some of the most important and influential fundamental research on foam behavior in porous media.

Other prominent works on key aspects of foam-EOR were published in the period of 1980's and early 1990's. Hirasaki and Lawson [68] did one of the first works discussing the singularities of foam flow in porous media, such as the impact of texture, and how it differs from foam flow in pipes. Falls et al [69] extended the discussion and investigated the impact of pore constrictions in the flow path. Khatib et al [70] introduced the concept of limiting capillary pressure, which was later used to explain the two flow regimes defined by the diagram of Osterloh & Jante. Yaghoobi and Heller [59] observed during their experiments that sometimes foam can reduce the gas mobility more strongly in higher than in lower permeabilities, a phenomenon which they called selective mobility reduction (SMR). Ransohoff and Radke [18] identified and described the mechanisms of foam generation in porous media only in 1988.

Despite promising results in laboratory studies, the technology was impacted by a decrease of interest in the early 1990's, due to its mixed results in the field and the great success of gel technologies as conformance control, as argued by Enick et al [11]. But the interest was rekindled in the early 2000's due to a series of events, such as:

- Availability of cheap CO_2 for EOR projects in the United States stimulated these projects [53]. So much so that EOR's production from CO_2 injection surpassed that from thermal EOR projects in 2003 [40];
- Increasing concerns with greenhouse gases stimulated projects of geosequestration of man-made CO_2 coupled with EOR [48,53];
- The publication of the results of the foam injection (FAWAG) on the Snorre field [71], considered a great technical and economic success. The positive impact of these results in foam interest by the Oil & Gas industry, and consequent stimulus to its research cannot be neglected.

The regained interest shifted from mostly field-oriented projects from the previous decades to a more fundamental research, more focused on understanding the technology. Hence, a lot of works on formulation, salinity influence, foam stability, interaction with oil, surfactant adsorption, foam flow, and simulation have been performed since then. The numerous efforts in developing foam simulation are particularly noteworthy.

The ability to reliably predict foam performance on the field is a critical factor for the success of a project. Foam simulation not only allows to maximize the potential of oil recovery (via optimized foam injection strategy) but also to determine the technical and economic feasibility of the project based on the estimated additional oil production and implementation requirements. Hence, the results of foam simulation can determine whether a project is implemented or not. It is not surprising that research on foam simulation has been so prolific since 2000. This can be verified in the excellent review of Ma et al [22] on modeling techniques for foam flow. From the 41 papers reviewed to discuss the 23 models presented in their work, more than 60% were published since 2000.

Despite all these efforts, none of the models have been capable of accurately represent all different foam experiments on varying conditions so far. Hence, foam simulation remains one of the great challenges for the development of foam-EOR. A brief discussion on some of the main challenges preventing a more extensive application of foam flooding is presented next.

2.4.3 Challenges for the development of Foam-EOR

As aforementioned, despite an extensive literature and very promising results both in the lab and on the field, Foam-EOR is still a developing technology and major uncertainties remain regarding the flow and transport of foam in porous media. The main challenge to bring this promising technology to the field is to be able to probe and predict the incremental oil production to justify the associated investments and risks. To do so, an effective synergy between simulations and experimental work that allows converting laboratory data to reliable field scale predictions is needed.

There are still many unanswered questions that prevent more application and success of foam injection. Some of the challenges that need to be solved are: long distance propagation, foam stability and durability, oil impact, SMR, simulation and control. Some of the main issues are briefly discussed below. As in any other immature technology, much work is yet to be done to develop Foam-EOR. Nonetheless, the increasing number of studies and the data already obtained indicates that foams are to become a valuable tool to improve the recovery factor of old and new fields, especially in highly heterogeneous reservoirs.

2.4.3.1 Foam in-depth propagation

One of the great questions about Foam-EOR is how deep it can propagate into the reservoir. As inherently unstable systems, much has been argued whether foams may or may not promote in-depth mobility control, as it is difficult to maintain a long-term stability for foams in field applications. Among many factors, the oil itself may act as a defoamer. Hence, propagation is a complex process which involves knowledge not only of foam generation and stability, but also the impact of other factors, like oil saturation and composition, and brine composition.

Notwithstanding, the potential of mobility control foams has not been fully explored in pilot tests, especially given the immense body of promising lab-scale technical knowledge that has been reported [72]**.** Also, although there were few field tests specifically designed to assess the performance of in-depth mobility control foams**,** several other foam trials recognized that foams could be used to simultaneously improve both conformance and mobility control [11,72]**.** Additionally, new surfactants and products (as CO_2-soluble

surfactants and nanoparticles) that can enhance foams stability even in the presence of oil are being tested [11,72]. Thus, although foams propagation capacity is still uncertain, there are solid data that foams can help to sweep oil reservoirs more efficiently.

2.4.3.2 Representative lab results

The capability of lab results to represent processes that happen in the reservoir has always been an open matter of intense discussion. The scale-up of lab results is a critical step in predicting the production not only of EOR methods but even of primary and secondary recoveries. In the case of Foam-EOR, however, it is even more challenging, since foam flow through porous media is a quite complex dynamic process which involves formation, mobilization, and destruction of lamellae. How these multiple dynamic processes will take place at reservoir scales and how they will impact foam performance is still unknown [72]. Thus, how to correctly represent them in lab scale is a huge challenge.

The problem starts with defining what representative conditions for foam flow are. Foam can be affected by numerous parameters, such as: rock wettability, permeability, porosity and heterogeneity; brine salinity and composition; rock and fluid interactions; oil saturation and composition; and reservoir pressure and temperature [11,72]. Because of the number of variables that can affect foam behavior, ideally one would have to perform experiments as close as possible to the real reservoir conditions to get reliable data, which is not always possible. However, not all parameters should be significant. Certainly, some parameters have a much stronger effect than others, and hence there must be parameters that can be neglected. Thus, one way to deal with this complexity it is to do a series of consistent lab experiments to perform a sensibility analysis to identify the key parameters, as suggested by Ma et al [22].

Besides the weight of each parameter, the influence of the experimental procedure on the results of coreflood tests of foams is still unknown. There are multiple experimental protocols for these tests, and much of the data available in the literature were obtained following quite different procedures and under diverse conditions. This prevents us to determine the impact of the procedure on foam flow results simply by comparing the available similar data. To solve this issue, a systematic study comparing the different

approaches to do coreflood tests of foam flow should be performed in a well-controlled and fixed setup. However, no such study has been reported so far.

Yet, even if all the drawbacks aforementioned are taken into consideration, there is no certainty that coreflood experiments will be able to accurately reproduce the balance of the multiple dynamic processes as they will happen in the reservoir. This question can only be answered by confronting simulations results obtained from lab data with field results.

2.4.3.3 Predictive simulation

A good and sound understanding of the foam-EOR process and the actual physics underlying it is a prerequisite for predictive foam simulation. However, the rheological behavior of foam flow in porous media still lacks understanding, despite the profusion of studies available in the literature [19]. This renders the performance of foams difficult to predict and control, impairing its application on the field.

As predicting foam performance is a key factor for its success, a considerable number of models have been proposed. In the recent work of Ma et al [22], the authors presented nothing less than 23 different models for foam flow. However, none of them was capable of fitting all available data of foam flow in porous media on different conditions.

Since no physical model of foam flow in porous media is available yet, current models rely on many assumptions that are hard to verify, and need many adjusting parameters that not necessarily are independent of each other [19,22]. Hence, each group developed their models according to their own self-consisting interpretation of the physics of foam flow and their own experimental data [22]. Such approach resulted in many different mathematical formulations and made current models strongly dependent on lab results to calibrate their parameters. Consequently, simulation results for full-field scale predictions are unreliable, especially if the results are not representative of the real conditions [21,23,24]. And, as discussed in the previous sub-section, to obtain representative data is a challenge in itself.

Thus, the great challenge to achieve reliable predictive foam simulation results is to be able to justify the choice of one or another model and to understand the impact that each parameter has on foam performance on the field. For that, more knowledge of the physics behind foam flow in porous media is needed.

CHAPTER 3.

FUNDAMENTALS ON FOAMS

3.1 Basic concepts

Foams are colloidal systems where a gas is dispersed in a continuous liquid or solid phase. In this dissertation, only liquid foams are discussed. Though non-aqueous foams exist, usually liquid foams are water-based. Because of the versatility of foams, derived from the large array of possible compositions and unique rheology [73], they are found everywhere: in pharmaceuticals, cosmetics, food industry, cleaning products, fire-fighting systems, materials technology, oil and gas industry, etc. [74].

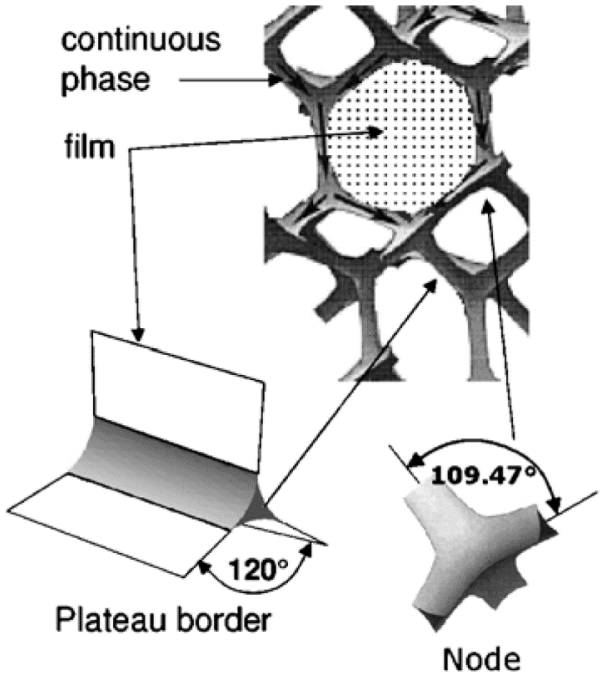

Figure 3-1: Representation of the tridimensional structure formed by the liquid phase of foams. Reproduced from [75].

In bulk foams, i.e., in foams contained in vessels or pipes with dimensions much larger than the characteristic bubble size, the continuous liquid phase forms a tridimensional structure made by lamellae, Plateau borders, and nodes, Figure 3-1. Lamella is the name of the thin liquid films remaining between the gas bubbles. Plateau borders are the edges in this 3D structure and they are created when three lamellae meet. The nodes (or vertices) are the points where four Plateau borders meet. Under equilibrium conditions, with no resulting tension, lamellae that form Plateau borders meet at 120°, which in turn meet at a 109.5° to form the nodes [73].

Depending on the ratio of liquid and gas, foams are defined as dry or wet. For bulk foams, wet foams (*kugelschaum*) present spherical bubbles separated by thick liquid films, while in dry foams (*polyederschaum*) the lamellae are thin and plane, and bubbles become polyhedra [57]. For confined foams (where the characteristic bubble size is of the same order of magnitude or bigger than the dimensions of the volume occupied by foam), such tridimensional structure may not exist, and the distinction between dry and wet foams is made differently, as discussed in subsection 3.2.4.2 below.

The ratio of liquid and gas, together with foam texture, are the main properties to characterize the rheology of foams [76,77]. Similarly, foaming efficiency of a solution is described by foam stability and foamability [74]. These properties are defined below:

- Foam quality (f_g): gas fraction, also known as foam quality, is defined as the volumetric fraction of the foam occupied by the gas phase, equation 3-1.
- Foam texture (n_f): refers to the number of lamellae per unit of volume. It is also expressed as lamellae density and bubble density and is related to bubble size.
- Foam stability: is a measure of how a desired foam property varies over time after foam generation [74]. Usually quantified by the foam half-life parameter, that measures the time for a column of foam to decrease to the half of its initial height.
- Foamability: characterizes how easily a solution can produce foam. Hence, it needs to be determined during foam formation.

3-1.
$$f_g = \frac{v_g}{v_g + v_l}$$

3.1.1 Foam stability

Foams are metastable systems (thermodynamically unstable, but kinetically stable), which means they will invariably collapse eventually. Multiple phenomena lead to the rupture of the lamellae, and hence, to foam destruction. These mechanisms are: gravity drainage, capillary suction, the influence of additional phases, gas diffusion (coarsening), and liquid evaporation and condensation [19,57]. The first mechanism is only important in bulk foams, where gravity can quickly dry out the tridimensional liquid structure, thinning and weakening

the lamellae. For confined foams, capillary forces are dominant and gravity effect can be neglected.

Capillary suction arises from a combined effect of the unbalanced intermolecular forces that originate the interfacial tension between the gas and liquid phases, and the different curvatures of such interfaces in the tridimensional structure of foams. This combined effect results in a pressure difference across these interfaces, with the higher pressure in the phase with the concave curvature. According to the Young-Laplace equation (3-2), the curvature of an interface between two phases is proportional to the pressure difference of these phases. The more curved (smaller radii) the bigger the difference. In the liquid structure of foams, the center of the lamellae has a very long radius, as they are practically flat, while near the Plateau borders and nodes, the interface is quite curved, Figure 3-2[57]. As the pressure in the gas phase inside a single bubble is the same everywhere, the liquid pressure in the Plateau borders and nodes must be smaller than in the lamellae. Hence, the pressure difference pushes the liquid from the lamellae toward the Plateau borders and the nodes, causing the thinning of the liquid films, and the consequent weakening and rupture of lamellae.

3-2. $$\Delta p = \sigma\left(\frac{1}{R_1}+\frac{1}{R_2}\right)$$

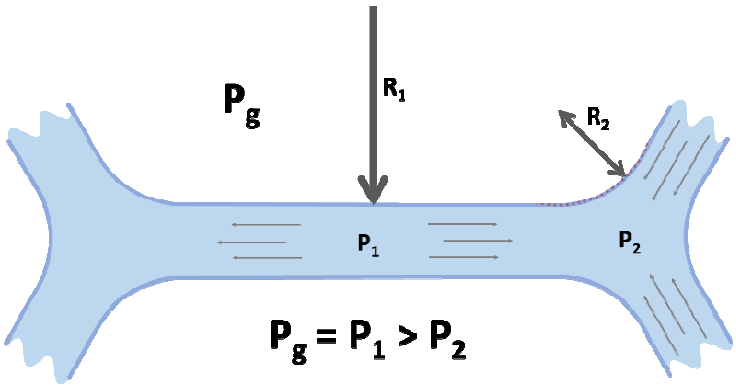

Figure 3-2: Schematic representation of the cross-section of Plateau border illustrating the capillary suction described by the Young-Laplace equation [78]

The pressure difference described by the Young-Laplace equation also explains coarsening of foams, known as Ostwald ripening. Since usually bubble size is not monodispersed, the gas pressure inside each bubble depends on its size, i.e., on its radius of curvature. Consequently, gas pressure varies from bubble to bubble, and this difference drives

gas diffusion from the smaller bubbles (higher internal pressure) to the bigger ones, causing lamella coalescence. As bubbles increase in size, lamellae become thinner and thinner, and eventually rupture.

Despite being metastable systems, the longevity of foams can be prolonged if proper stabilization is in place. Foaming and foam stability depend on the existence of foaming agents in the solution [78]. These are mainly surface active agents (surfactants), but can also be other types of compounds, such as polymers. In the presence of such compounds, mechanisms that counter film drainage either by gravity or capillary suction take place, thus making foam last longer [78]. In the case of polymers, lamellae stability is improved due to the increase of the viscosity of the liquid phase, which reduces the rate of liquid drainage. For surface active agents, besides the reduction of Ostwald ripening due to lower IFT, the stabilization mechanisms are the Gibbs-Marangoni effect and the disjoining pressure [57,78,79].

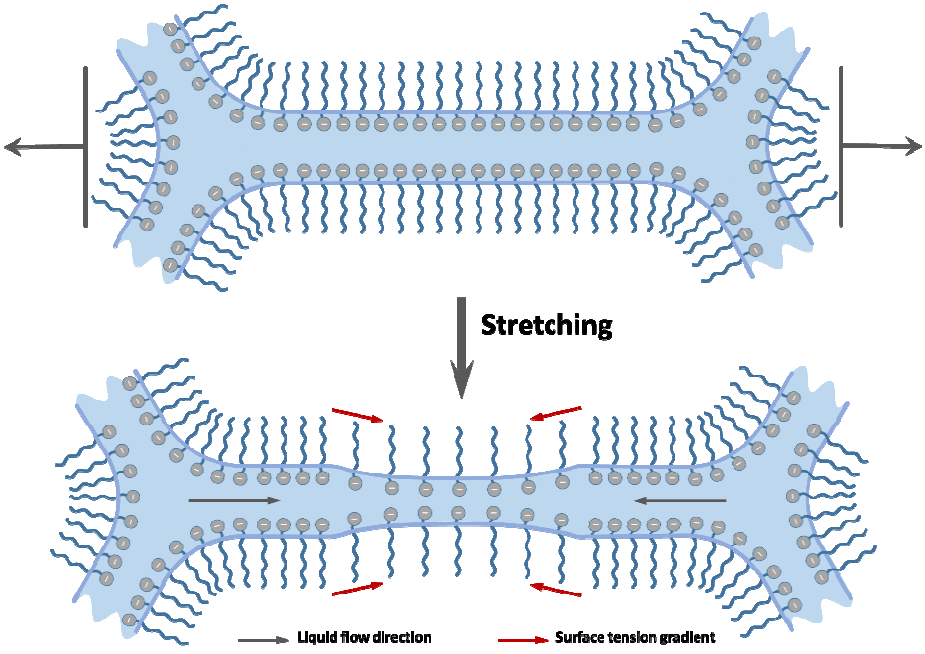

Figure 3-3: Schematic representation of the Gibbs-Marangoni effect.

Gibbs-Marangoni effect, also known as surface elasticity, occurs when a deformation of the lamella creates a thinner region and a gradient of surface concentration of surfactants. The less concentrated region (center of the lamella) develops an IFT higher than its surrounds, generating an IFT gradient that gives the lamella elasticity to resist further deformation that could cause lamella rupture. Additionally, as the higher IFT portion of the lamella contracts, it

induces liquid transport toward the thinner region, thus acting against liquid drainage and film thinning [57,78]. Figure 3-3 shows schematically the phenomena of Gibbs-Marangoni effect.

The disjoining pressure in foams is the resulting force over the two flat and parallel surfaces of a lamella originated from repulsive and attractive intermolecular forces and steric repulsion [57]. Lamellae are thin enough to allow the interaction of the molecules in the interfaces of each side. If the resulting interactions are repulsive, the parallel surfaces will repel each other, avoiding further thinning of the lamellae, and stabilization is achieved. Otherwise, i.e., given net attractive forces, film drainage would go unopposed, and foam would soon collapse [57]. This balance of forces is represented as a difference of pressures from the gas phase and the liquid phase in the lamella (equation 3-3), graphically demonstrated in Figure 3-4. Positive values mean net repulsive forces, while net attractive forces result in negative values. Disjoining pressure depends on the thickness of the lamella, ionic force of the solution (brine composition), concentration and nature of the surfactants, and temperature [57].

3-3. $$\Pi_d = P_l - P_g$$

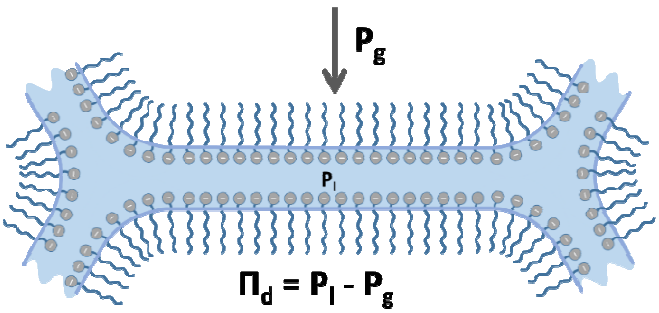

Figure 3-4: Schematic representation of the disjoining pressure.

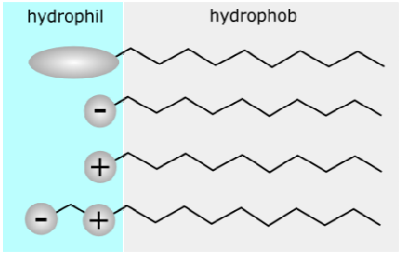

Figure 3-5: Schematic representation of small amphiphilic surfactant molecules. From top to bottom: non-ionic; anionic; cationic; zwitterionic. Source [80].

Surfactants are essential to these mechanisms due to their alignment at the interfaces and to their structures. More commonly, surfactants are small amphiphilic molecules, composed of a hydrocarbon chain as the hydrophobic part (called tail), and either an ionic, non-ionic or zwitterionic hydrophilic portion (known as head) [79], Figure 3-5. As a result, they are positioned perpendicularly to the plane of the surfaces of the lamellae, with the heads of the molecules at the surfaces opposing each other. When the heads are ionic, electrostatic repulsion of equally charged surfaces can greatly improve film stability. For non-ionic surfactants, stabilization comes from steric repulsion. However, they may present attractive intermolecular forces due to dispersion forces and van der Waals forces that reduce foam stability [57].

3.1.2 Bulk foam rheology

Thanks to their structure, foams have a unique rheology. These complex fluids behave like shear-thinning liquids when the gas fraction is low (wet or spherical foams), and as viscoelastic solids when the gas fraction is high (dry or polyhedral foams) [78]. This means that dry foams present a yield stress and behave like an elastic solid at low strain. Once the yield stress is exceeded, rearrangements in foam structure (called T1 transitions, Figure 3-6) result in plastic deformation, hence they act as a high viscosity pseudoplastic fluid [73,78]. This viscosity depends on the structure of foam, and it increases with gas content and with foam texture, i.e., the finer the texture (smaller bubble diameter), the more viscous is the foam [81]. Since most of their volume is made of gas, foams present significant compressibility as well [78]. Such diverse range of rheological behaviors allows foam to be used in several applications, as mentioned earlier. Hence, a proper understanding and control of foam rheological behavior are vital for its application. However, such knowledge is still lacking [82].

Foam rheology is usually described by yield stress pseudoplastic models, like the Herschel-Bulkley model (equation 3-4). The pure pseudoplastic model (power-law fluid, equation 3-5) can also be used if the gas fraction is low enough, since the yield stress value decreases with gas fraction, vanishing at a critical value where foam rigidity is lost, as pointed out in the review of Dollet and Raufaste [73]. However, none of these models are really

accurate in describing the rheological behavior of foams, since they do not account for the strong hysteresis observed when the direction of the shear rate is reversed [75,83].

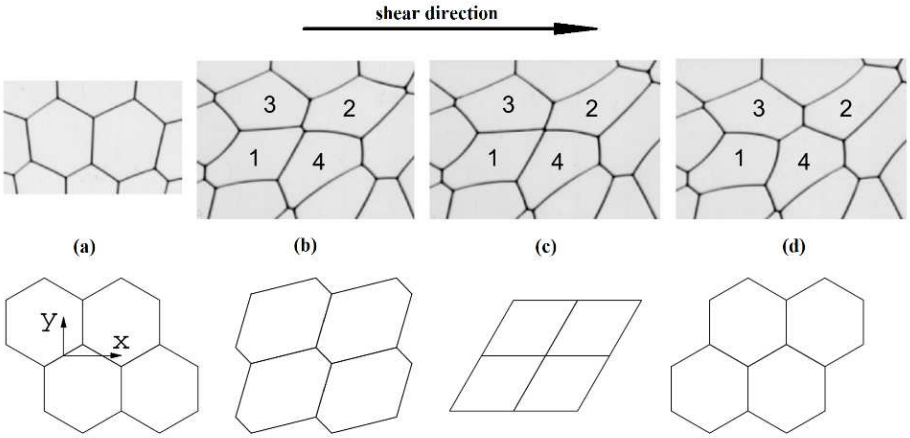

Figure 3-6: Snapshots and their corresponding schematic representation of a T1 transition occurring in a dry 2D foam. Adapted from [73].

3-4. $$\tau = \tau_y + K\dot{\gamma}^n$$

3-5. $$\tau = K\dot{\gamma}^n$$

The challenge in accurately describing, and hence, modeling the rheological behavior of (bulk) foams, comes from the difficulties in reliably measuring their parameters. Foam rheology depends on multiple parameters, such as gas fraction, bubble size and bubble size distribution (foam structure), which can change not only with time but with the magnitude of the shear forces applied [78]. Elevate shear rates can even destroy foam. To minimize these issues, highly concentrated emulsions have been used as surrogate systems to advance understanding on foam rheological behavior due to their similarities [78,84]. Furthermore, it is difficult to obtain reproducible results because of the reproducibility of the foam itself, the impact of the apparatus used (rheometer geometry), and the impact of wall slippage in the measured results [78,84]. Ergo, such complex systems demand tailor-made devices to measure foam properties in conditions as close as possible to the desired application, as stressed by Bergeron and Walstra [78]. For these reasons, the rheological behavior predicted by foam models usually differs from the empirical results.

Weaire [83] states that this lack of reproducibility and representativeness in measuring the actual rheology of foams make simulation results obtained from even the most detailed models, which consider foam structure and bubbles interactions, only semi-quantitative. He asserts that correctly describe the complexity of these systems demands a daunting number of empirical parameters, thus just fitting them to experimental data would be fruitless to further the understanding of the rheological behavior of foams.

Indeed, Weaire highlights that a great flaw in advancing our knowledge on foam rheology is the overemphasis given to fitting limited experimental data to theoretical models rather than attempting to acquire more significant and complete data sets. Thus, he advocates devoting efforts in performing more thorough and systematic experiments is needed, as such data would naturally lead to experimental and theoretical progress in characterizing foam rheology [83].

3.2 Foam in porous media

Differently from the 3D structure found in bulk foam, in porous media foam is confined in pores with a characteristic diameter smaller or of the same order of magnitude of the size of the bubbles. This causes the foam to be a train of bubbles, separated by lamellae, rather than a 3D array of liquid films, Figure 3-7. Such morphology changes its rheology and the flow of fluids in the pores. The higher entrapment of gas because of the lamellae reduces the effective permeability of the gas phase, while the additional mechanical resistance to displace the lamellae increases the apparent viscosity of fluids. These two effects result in the ability of foams to greatly reduce gas mobility.

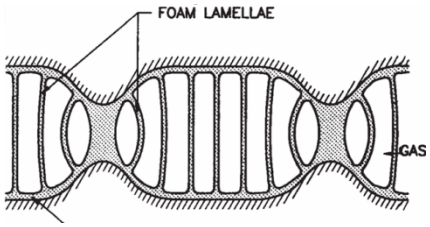

Figure 3-7: Foam morphology as bubble trains in a pore, adapted from Falls et al [69].

The flow of foam in porous media is a dynamic process that depends on the equilibrium between the creation and destruction of lamellae [15,16,18,66]. These mechanisms are presented below:

3.2.1 Foam generation

There are three main mechanisms for foam generation in porous media: snap-off, lamella division, and leave behind:

- **Snap-off:** This mechanism takes place when gas invades a pore filled with the surfactant solution, Figure 3-8a. Gas expansion creates a capillary pressure gradient between the pore and its throat (region of lower pressure), causing liquid to flow back and accumulate as a collar in the pore throat. If enough liquid is accumulated, a new lamella is formed. This kind of mechanism generates stable and so-called strong foams [85] whose bubble size is of the order of the size of the bodies of the pores. It is also important when foam flow from a region of lower permeability to a layer of higher permeability, or at the exit of the porous medium [18].
- **Lamella division:** is a process that only occurs when lamellae are already formed and can move inside the porous medium [85]. When a flowing lamella reaches a branching point and the lamella touches the wall on the junction, it can be split into two lamellae, which will then follow a different path, Figure 3-8b. Hence, this mechanism leads to increasing the number of lamellae of the foam (and thus bubbles) in the porous medium, i.e., it leads to finer foam texture. The finer foam texture increases hydrodynamic resistance in the pores by the accumulation of lamellae [86,87], and eventually, it prevents foam from entering occupied pores. First, foams spontaneously occupy the paths of less resistance (higher permeability), and then it invades other pores (of lower permeability). Such mechanism makes foam a good diversion agent. However, the lamellae accumulating in the secondary pores make it possible to deflect the lamellae towards the primary pores. Hence, intermittence between trapped and flowing foam is sometimes observed.

- **Leave-behind:** as the snap-off, this mechanism occurs when gas invades a pore filled with the surfactant solution. It takes place when two gas fronts flow through adjacent pores, leaving a liquid lens in the pore throat that connects those two flow paths, Figure 3-8c. Likewise, it happens when gas flowing from two different directions converges to the same pore, trapping liquid in a pore throat between the two fronts, thus creating a lamella. Leave-behind is associated with weak foams, as it can promote only a moderate increase in resistance to gas flow [18].

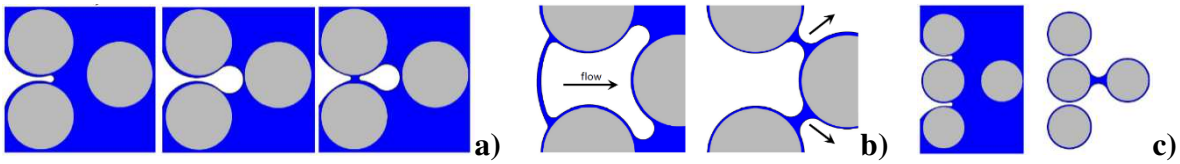

Figure 3-8: Main lamellae generation mechanisms. a) Snap-off; b) Lamella division; c) Leave-behind. Adapted from [88].

3.2.2 Foam coalescence: limiting capillary Pressure (P_c*)

Though subsection 3.1.1 discussed the main mechanisms for foam coalescence, the confinement inside a porous medium makes the capillary forces a dominant factor regarding foam coalescence and are examined in more detail here. Nevertheless, the presence of other phases (essentially, oil in the reservoir) is also crucial to foam generation, stability, and destruction [22], and will be discussed in subsection 3.4.

As previously stated, the Young-Laplace equation relates the discontinuity in pressure existing across the interface of two immiscible fluids with the curvature of the interface, thus defining a capillary pressure (P_c). In a porous medium, the capillary pressure results of the combined interfacial tensions between the phases, the interactions of these phases and the rock surface (wettability), and the pore size and geometry [89]. Consequently, P_c varies with the saturation of the fluids in the pore space, permeability, and with the natural variations from one pore to another.

According to equation 3-2, smaller pores have higher P_c than the larger ones. Hence, the capillary forces drain the wetting phase (usually water) from the larger pores to keep the smallest ones saturated and to maintain the liquid film that covers the rock surface (which is part of the connate water saturation) [11]. When foam is present in the porous medium, these capillary forces join the capillary suction intrinsic to foam structure, thus resulting in the primary mechanism for foam destruction inside porous media [90]. The disjoining pressure counters the capillary pressure destabilizing effect and, at the equilibrium, they equal each other [91].

The correlation between disjoining pressure and P_c imposes a limit to P_c regarding foam stability. If Π_d surpasses a critical value, Figure 3-9, the lamella is no longer stable and breaks. Hence, this critical Π_d establishes a limiting capillary pressure, P_c^* [70,77] [92]. Since capillary pressure is linked to the saturation of the porous medium, it also establishes a critical water saturation, S_w^*[70,77].

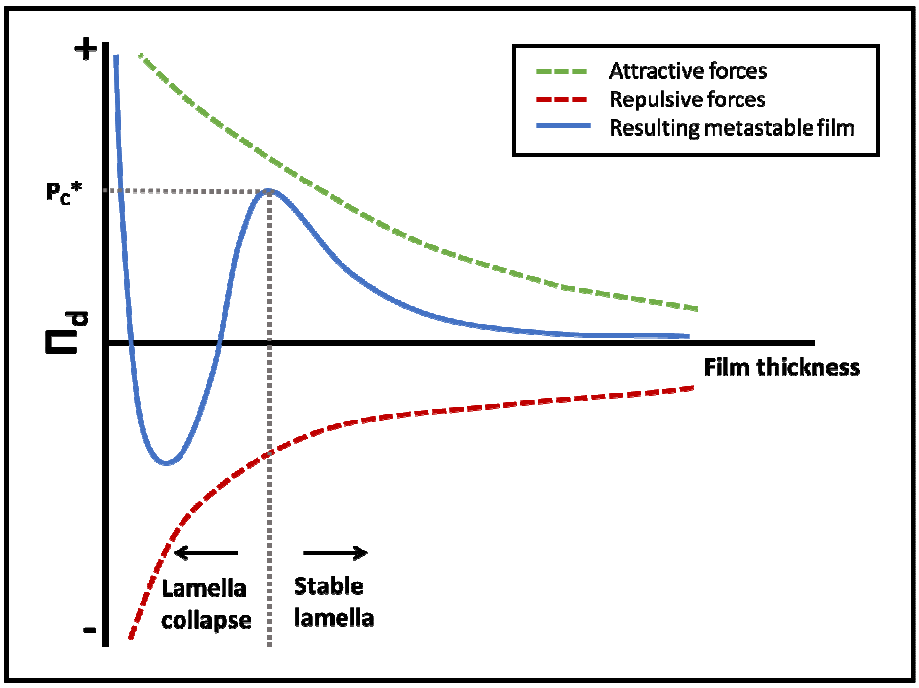

Figure 3-9: Schematic representation of the disjoining pressure curve (resultant from the attractive and repulsive forces), indicating how Πd defines a limiting capillary pressure and where is its value on the curve.

Khatib et al [70] were the first to verify the existence of a limiting capillary pressure experimentally. They investigated the impact of capillary pressure on gas mobility in presence of foams using sandpacks of different permeabilities. Their results showed that P_c^* depends

on gas velocity, permeability, surfactant type and concentration, and brine composition. However, the exact dependence yet to be determined [92].

3.2.3 Foam states

Foams are reported to exist in two distinct states in porous media, characterized by their texture or density of lamellae. Weak foams present few lamellae (coarse texture) and are not very effective in reducing the mobility of the gas phase, while strong foams have a fine texture (high density of lamellae) and can greatly reduce gas mobility, Figure 3-10. Although some transient states have been described [93], the transition between weak and strong foam (also referred as "foam generation") is yet to be clarified. There is no agreement in the literature regarding the main mechanism for foam generation, and thus, the need of either a minimum velocity or pressure gradient remains unclear [94]. Though both parameters are interrelated, supporters of snap-off as the dominant process are prone to talk in terms of minimum velocity, based on the observations of Ransohoff and Radke [18], while lamella-division defenders are more likely to discuss in terms of minimum pressure gradient to set in motion existing lamellae, as argued by Gauglitz et al [93].

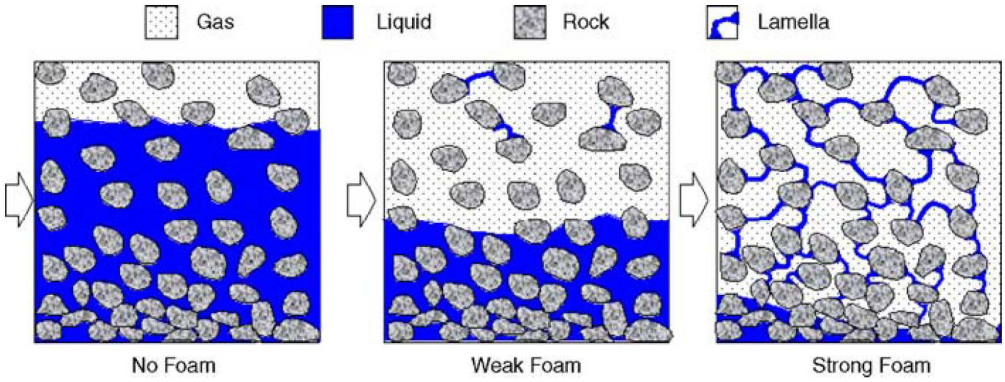

Figure 3-10: Conceptual representation of weak and strong foam in porous media compared to the two-phase flow of water and gas [95].

Once the onset of foam generation is attained, i.e., strong foam is generated inside the porous media, the rheological behavior of foam flow shows the following trends [94]:

- Firstly, foam apparent viscosity increases with increasing velocity up to a maximum;

- Then, foam apparent viscosity decreases upon further increasing the velocity beyond the maximum (shear thinning behavior);
- Finally, foam apparent viscosity shows a hysteresis effect when the velocity is decreased below the maximum of viscosity previously observed.

Figure 3-11 illustrates this rheological behavior. The shear thinning observed is advantageous to EOR application, as the viscosity near the injection well, where the foam will be formed, is smaller than further into the reservoir. This behavior results in smaller loss of injectivity and better in-depth sweep efficiency.

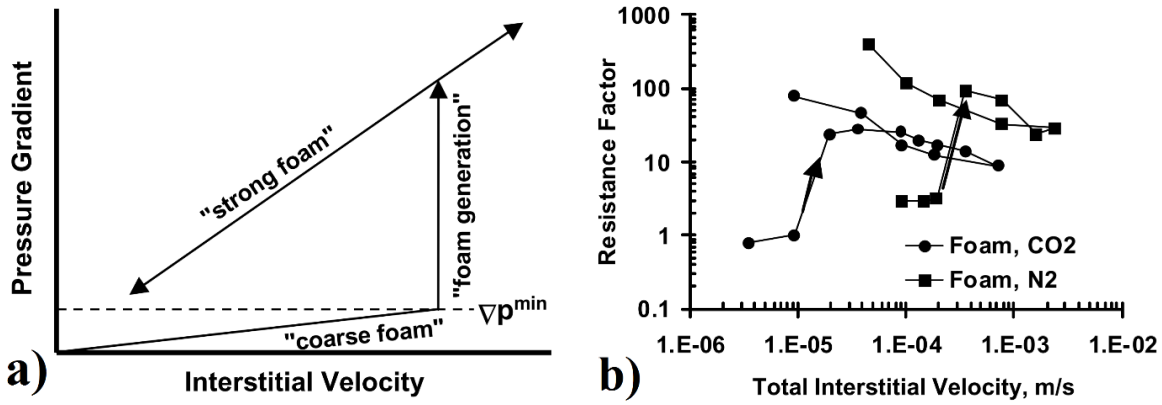

Figure 3-11: Typical foam rheological behavior. a) Schematic representation of the different states of foam and their dependence on interstitial velocity and its sequence; b) coreflood data showing the behavior represented in a) [93].

Despite the key role of foam texture on foam rheological behavior, up to date there is not enough experimental data that allow to directly relate gas mobility reduction to foam texture [19]. It has been impossible to measure in-situ foam texture so far, and off-situ measurements presented in the literature are quite debatable [21]. Though micromodels allow direct observation of not only foam texture and bubble size, but also dominating mechanisms of foam generation and coalescence, their dimensions limit the extrapolation of the results to foam flow in cores [21].

3.2.4 Foam flow in porous media

As said in section 3.2, the confined geometry imposed by a porous media affects the rheological behavior and flow of foams. These phenomena depend on the interactions

between lamellae, wetting films (liquid layer contacting the surface of pores), and solid surfaces [96]. Thus, many parameters can impact such balance, including reservoir properties (K, heterogeneity, wettability, pressure, temperature, mineralogy), reservoir fluids (nature, composition, and saturation), injection conditions, shear rate and surfactant (nature, concentration). Despite the immense volume of theoretical, laboratory and pilot work dedicated to these processes, major uncertainties remain regarding the actual physics underlying the rheological behavior and transport of foams in porous media [96].

Though the previous studies [11,12,70,94,97,98] did not allow to propose a comprehensive and satisfactory physical modeling of foam flow and propagation, they allowed to come up with a general, yet useful, phenomenological description of the rheological behavior of foams in porous media. The current knowledge on foam flow characterization and rheological behavior is discussed in the following sections.

3.2.4.1 Foam flow characterization

The rheological behavior of foam in porous media is governed by the foam texture, also called bubble density or lamellae density (n_f) [19,69,92]. Foam texture affects both the gas relative permeability and the apparent viscosity, thus being of prime importance to estimate the gas mobility reduction and foam performance. However, a direct measure of n_f is practically impossible, so n_f is usually inferred from either pressure gradient or apparent viscosity data, the latter being calculated by considering foam as a single phase and the applying Darcy's Law (equation 3-6).

3-6.
$$\mu_{app}^{f} = \frac{K\Delta P_{foam}}{v_t L}$$

Where ΔP_{foam} is the pressure drop obtained in the presence of foam, and v_t is the total superficial velocity of the combined flow. Other parameters are commonly used to experimentally measure the performance of foams in reducing gas mobility, such as foam mobility (λ_{foam}), foam relative mobility (λ^{f}_{r}), and mobility reduction factor (MRF) [11,48].

3-7.
$$\lambda_{foam} = \frac{v_t L}{\Delta P_{foam}}\ ; \quad \lambda_r^f = \frac{v_t L}{K\Delta P_{foam}} = \frac{1}{\mu_{app}^{f}}\ ;$$

3-8. $$MRF = \frac{\Delta P_{foam}}{\Delta P_{no-foam}}$$

The reference pressure drop for the MRF ($\Delta P_{no\text{-}foam}$) is obtained without surfactant at the same flow conditions that are used during foam injection.

Foam flow can also be characterized by measuring the relative permeability of gas in the presence of foam (K^f_{rg}). We can derive an expression for K^f_{rg} from the MRF. For that, we express the pressure drop in the absence and in presence of foam as follows:

3-9. $$\Delta P_{no-foam} = \frac{v_t f_g \mu_g L}{K K^0_{rg}(S^0_g)}$$

3-10. $$\Delta P_{foam} = \frac{v_t f_g \mu_g L}{K K^f_{rg}(S^f_g)}$$

Equations 3-9 and 3-10 allows rewriting MRF as:

3-11. $$MRF = \frac{K^0_{rg}(S^0_g)}{K^f_{rg}(S^f_g)}$$

MRF can also be rewritten using equations 3-6 and 3-9, resulting in equation 3-12:

3-12. $$MRF = \frac{\mu^f_{app}}{\mu_g f_g} K^0_{rg}(S^0_g)$$

By combining equations 3-11 and 3-12, we obtain an equation to determine K^f_{rg} experimentally [99,100]:

3-13. $$K^f_{rg}(S^f_g) = \frac{\mu_g f_g}{\mu^f_{app}}$$

3.2.4.2 Foam flow regimes

As discussed in section 3.2.3, there are two main states for foams to exist in porous media: weak and strong. Since only strong foams are effective in greatly reducing gas mobility (high MRF), the research and characterization of foam flow comprise only this state. Besides, the weak foam is just a transient state that exists only until the flow conditions for

the onset of foam generation are met in the porous medium, due to the hysteresis presented by foam.

Regarding the behavior of steady-state strong foams flow, the works of Osterloh and Jante [67] and Alvarez et al [66] establish two flow regimes, depending on the gas fraction (f_g): low and high quality. The transition between the two regimes occurs at a given f_g (f_g*), where maximum pressure drop is achieved. Strong foam low-quality regime exhibits shear thinning behavior, while the rheology in the high-quality regime is yet to be elucidated, with diverse behaviors reported in the literature, most probably due to the instability of foam in this regime [19].

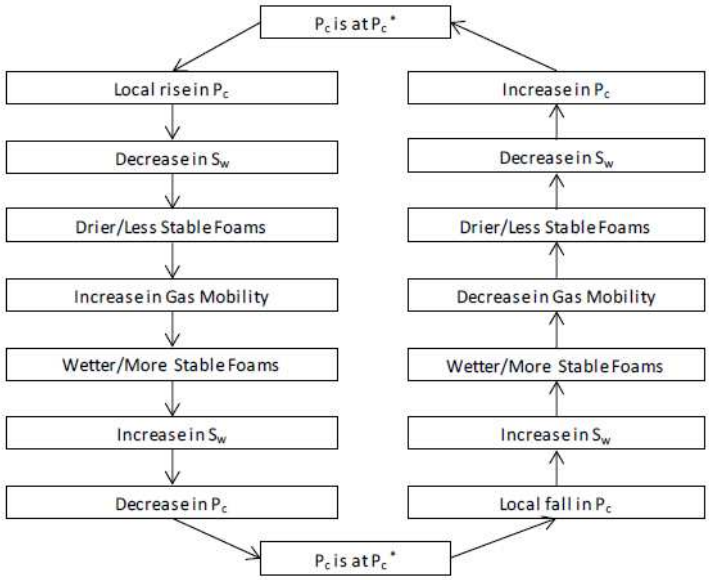

Figure 3-12: Behavior near the limiting capillary pressure, Pc*. Reproduced from [77].

The different rheology observed in each regime arises from the distinct mechanisms believed to dominate foam behavior. The high-quality regime (coalescence regime) follows the limiting capillary pressure (P_c*) model. According to this model, there exists a limiting capillary pressure P_c* (corresponding to a S_w*) over which foam becomes unstable, and coalescence takes place, causing bubble size to change to keep P_c at P_c* (S_w=S_w*) [77]. Under these conditions, pressure gradient depends only on S_w, i.e., it becomes independent of gas velocity [66,70]. This behavior near P_c* that causes coalescence and leads to a large polydispersity in bubble size is explained in Figure 3-12. In the low-quality regime, it has been assumed that bubble size is fixed and that pressure gradient depends only on bubble trapping and mobilization. As a consequence, the pressure gradient is almost independent of

water velocity and foam is shear thinning in this regime [66]. Additionally, in the low-quality regime, the lamellae are thick and bubbles are stable against coalescence.

Figure 3-13 is a schematic representation that consists of isobar contour lines representing the pressure gradient obtained in a series of coreflood tests of foam flow in porous media. These contour lines are plotted having either the velocities or flow rates of water and gas as x and y-axes, respectively. Such representation became known as the diagram of Osterloh and Jante, as they were the first to use it. However, it was not until the work of Alvarez et al [66] that the value of this type of chart was recognized and widespread in the literature. These diagrams were a fundamental tool in devising the current understanding of the rheological behavior of foam flow in porous media. They resume the characteristic behavior of foam flow in each of the two regimes (low and high quality), as well as the transition between them, represented by the two regions of the chart: one horizontal, representing the low-quality regime; and one vertical, corresponding to the high-quality regime. The two flow regimes concept with the limiting capillary pressure P_c^* is currently used in most of the foam models [92].

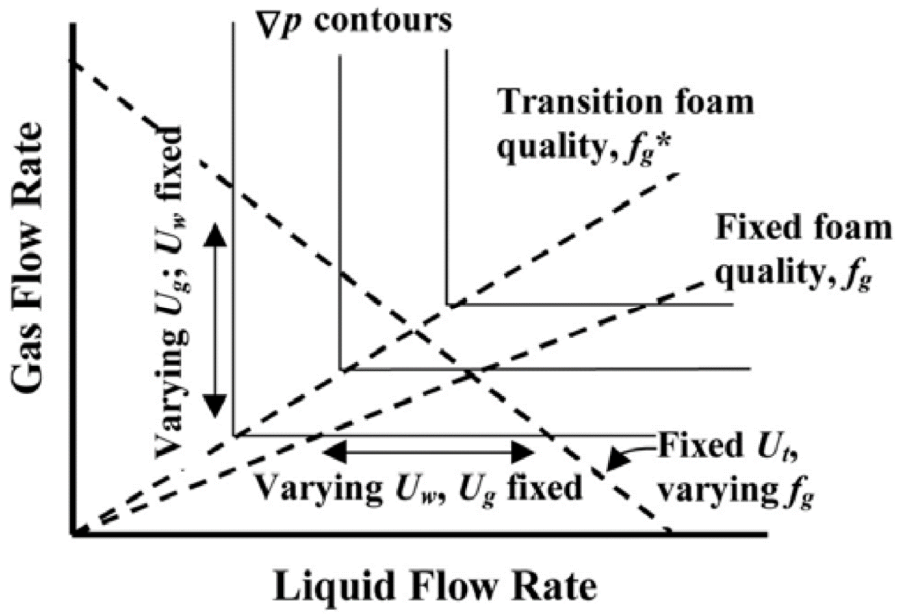

Figure 3-13: Schematic representation of an Osterloh and Jante diagram showing the two flow regimes for strong foams and identifying some important parameters [66,67].

According to the diagram of Osterloh and Jante in Figure 3-13, foam-induced pressure drops at a given total flow rate exhibit a maximum when plotted against foam quality [58,66,67,101]. This dependence of pressure drop on foam quality has been largely confirmed

experimentally [67,69]. The maximum pressure drop is reached at the optimal foam quality (f_g*), and depends on formation permeability, surfactant, and flow rate, among other parameters [67].

3.3 Foam formulations

As stated in section 3.1.1, foam cannot be sustained without a foaming agent, which almost always is a surface active agent (i.e., surfactant). Surfactants are materials that tend to adsorb at interfaces between either immiscible liquids, liquid and solid, or liquid and gas. Once at the interface, these materials alter the local balance of intermolecular forces, minimizing the total energy of the system, thus reducing the IFT. They can also modify the rheological properties of the said interface. Essentially, any compound that has these effects can be called surfactants, like proteins, particles, short polymer chains, among others. Nevertheless, the term surfactant is almost exclusively used to refer to amphiphilic molecules, where the hydrophobic tail is a hydrocarbon chain, and the hydrophilic polar head is either anionic, cationic, non-ionic, or zwitterionic, Figure 3-5.

Surfactants stabilize lamellae by reducing capillary forces (reduction of IFT), improving lamella elasticity (Gibbs-Marangoni effect), increasing disjoining pressure (electrostatic and/or steric repulsion) [74,79]. Though foam stability is essential to characterize foam performance, it does not define the performance of a formulation alone. Foamability, i.e., the easiness of formulation to produce foam, is also a key parameter to determine foaming efficiency. Here, the reduction of interfacial forces is vital for good foamability, as it allows the creation of more interface at a lower energetic cost. This means that not only less agitation is needed to generate foams, but that it is also easier to form smaller bubbles, which results in foams with a higher density of lamellae [79].

While both foam stability and foamability are needed to characterize foam performance, they belong to distinct stages of the temporal evolution of foams, and thus they concern different processes. Accordingly, the properties required for each parameter are sometimes incompatible. For instance, foam stability improves with increasing viscosity, but foamability benefits from low viscosity solutions [74]. Likewise, ultra-low IFT can greatly improve foamability but is generally considered detrimental to foam stability due to a

reduction of lamella elasticity [74]. Joseph [82], however, states that rather than the value of IFT itself, it is the rate of change of interfacial tension with surfactant concentration that determines if a surfactant is a good foaming agent (regarding both stability and foamability) or not. Regardless, this means that rarely a single compound provides both good stability and foamability. Thus, effective foaming formulations generally require the proper combination of two or more compounds to achieve the desired performance [74,82].

As colloidal systems, foam performance depends not only on its foaming agents but rather on a plethora of variables, such as: brine and gas compositions; temperature; pressure; surfactant concentration and adsorption; rock mineralogy [74,102]. Hence, properly choosing the best formulation for a given case demands a laborious screening process. Moreover, it requires performing experiments under conditions as close as possible to the aimed application. However, traditional coreflood tests are too time-consuming and expensive, so it is unrealistic to consider them to select and optimize foam formulations.

Thus, a typical screening routine involves a sequence of bottle tests of bulk foam under ambient conditions to rank formulations so only the most promising are tested in flow through porous media The usual tests are: solubility, half-life time (foam stability), adsorption, long-term stability [11]. It is important to keep in mind, however, that the differences in the physics of a bulk foam and a foam in porous media are substantial [79]. As discussed by Jones et al [102], most studies comparing foam behavior in bulk and in porous media have failed to find reliable correlations. The authors, however, did find a positive correlation between bulk foam stability and coreflood performance of foams, but only in the absence of oil. Hence, though useful, bottle tests must be regarded only as a screening tool for now [79,102].

As most of the studies have been directed to sandstones, the main surfactant is chiefly anionic, since they present lower adsorption in sandstones. Moreover, betaines are usually added to the formulations as “foam boosters” to increase foam stability in presence of oil [11,91]. Studies concerning cationic surfactants to foam-EOR are still rare, but they could be considered for reservoir carbonates [11].

Non-ionic surfactants have also been studied with promising results, but they are particularly interesting because some of these surfactants can actually be dissolved in the CO_2 phase if the injection and reservoir pressure and temperature are adequate [11,97]. Le et al

[97] argue that the possible advantages of dissolving the foaming agents in the CO_2 phase over the aqueous phase are: reducing injection costs and loss of surfactant due to adsorption and improving foam generation. Nevertheless, the research on this area is still focused on the investigation and development of surfactants molecules CO_2-soluble that also present good foamability and foam stability, so these advantages are yet to be verified by field applications.

An extensive list of the formulations that have been tested in the literature is available in Enick et al [11].

3.4 Foam and oil interactions

The presence of an additional phase is decisive to foam stability. While some compounds may improve it, others can lead to a complete collapse of foam. It all depends on the balance of forces at play (interfacial interactions, repulsive and attractive forces, capillary forces, viscous forces). So, understanding the impact of an additional phase is vital to predict and control foam performance.

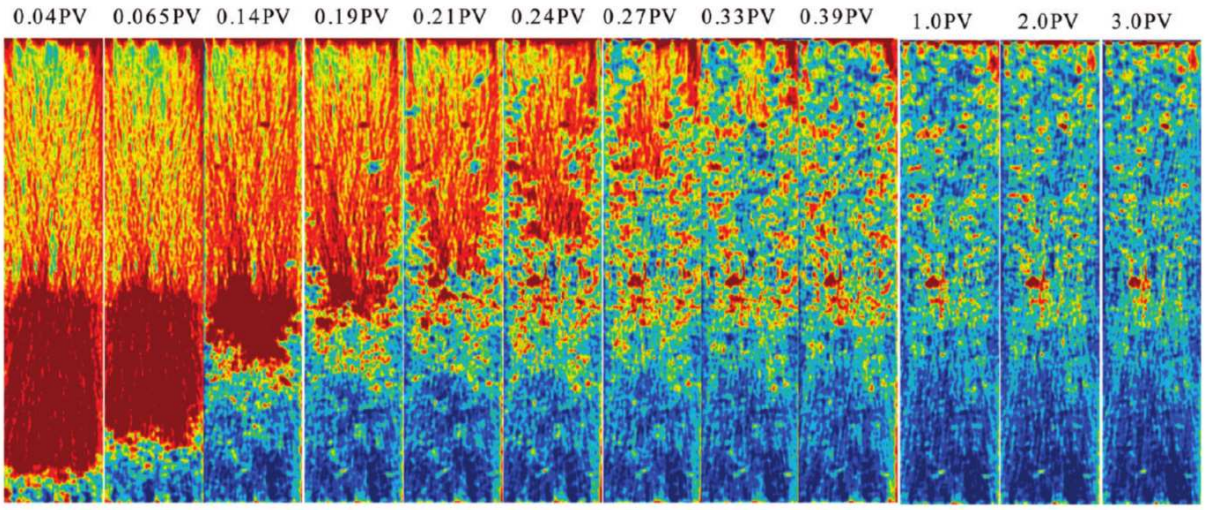

Figure 3-14: CT images obtained by Farajzadeh et al [12] showing the detrimental effect of oil on foam propagation. Blue represents foam, red is brine, and orange is remaining oil after water flooding. Oil is present only in the upper half of the core images. Foam front is stable in the lower, where oil is absent.

Regarding the use of foam injection as an enhanced oil recovery technology, live oil is the main additional phase to impact foam performance. The detrimental impact that many

types of oil have on foam stability has been observed in most of the EOR-related studies on this matter [88,91,103–109]. This negative effect depends on surfactant and oil composition, water salinity, oil saturation, etc. Among them, the impact of the oil saturation on the performance of foam-EOR is a major concern. Since oil destabilizes foam, the reduction in gas mobility in presence of oil is much lower than in its absence [91]. As oil saturation increases, foam becomes less and less effective, up to a point when oil reaches a critical saturation, and foam collapses completely [109]. Figure 3-14 exemplifies the negative effect of oil and its saturation on foam propagation in porous media. In these CT images obtained by Farajzadeh et al [12], blue represents foam, red is brine, and orange is remaining oil after water flooding. Figure 3-14 shows a stable propagation front for foam in the lower half of the image, where there is no oil. Once foam reaches the region containing oil, it propagates unevenly, as evinced by the gas fingers observed in the upper half of the core images.

Nevertheless, the available results of the influence of oil on bulk foam stability are conflicting, and there are studies that reported experiments with formulations that generate stable foam even in presence of oil [103]. Likewise, there are studies where the oil actually had a positive effect. For instance, Aveyard et al [110] reported improved foam stability by long-chain hydrocarbons, while Koczo et al [111] observed that oil can increase foam stability when a stable pseudoemulsion film is formed.

To affect foam stability oil needs first to be emulsified in droplets that can access the Plateau borders and the lamellae, so it can reach the interface gas-water. Once there, its effect depends on the balance of the physicochemical properties, especially of those at play on the interfaces [57,91,103]. The most common way to estimate the impact of oil on foam stability is by the calculating the entering (E), spreading (S), and bridging (B) coefficients (equations 3-14, 3-15, and 3-16, respectively) [57,88,102,104]:

3-14. $$E = \sigma_{sg} + \sigma_{os} - \sigma_{og}$$

3-15. $$S = \sigma_{sg} - \sigma_{os} - \sigma_{og}$$

3-16. $$B = \sigma_{sg}^2 + \sigma_{os}^2 - \sigma_{og}^2$$

When E<0, the oil droplet cannot access the gas-water interface, and the foam is stable. If E>0, then stability depends if the oil droplet will spread over the lamella (S>0), destabilizing it. When oil droplet enters both water-gas surfaces of a lamella, it originates an oil bridge, with mechanical resistance given by B. If B<0, the bridge is stable. Otherwise, it

breaks, causing lamella to collapse [102,104]. Figure 3-15 illustrates these mechanisms of oil destabilization of foam.

The stability criteria established by E, S, and B coefficients is the most used to influence of oil on foam stability, but it does not always agree with experimental results. Jones et al [102] compared the stability predicted by these coefficients with experimental results in different systems (coreflood, micromodel, and bulk/column tests) and found that it is not unusual for them to diverge. Vikingstad et al [109] found no correlation between the spreading coefficient and foam stability.

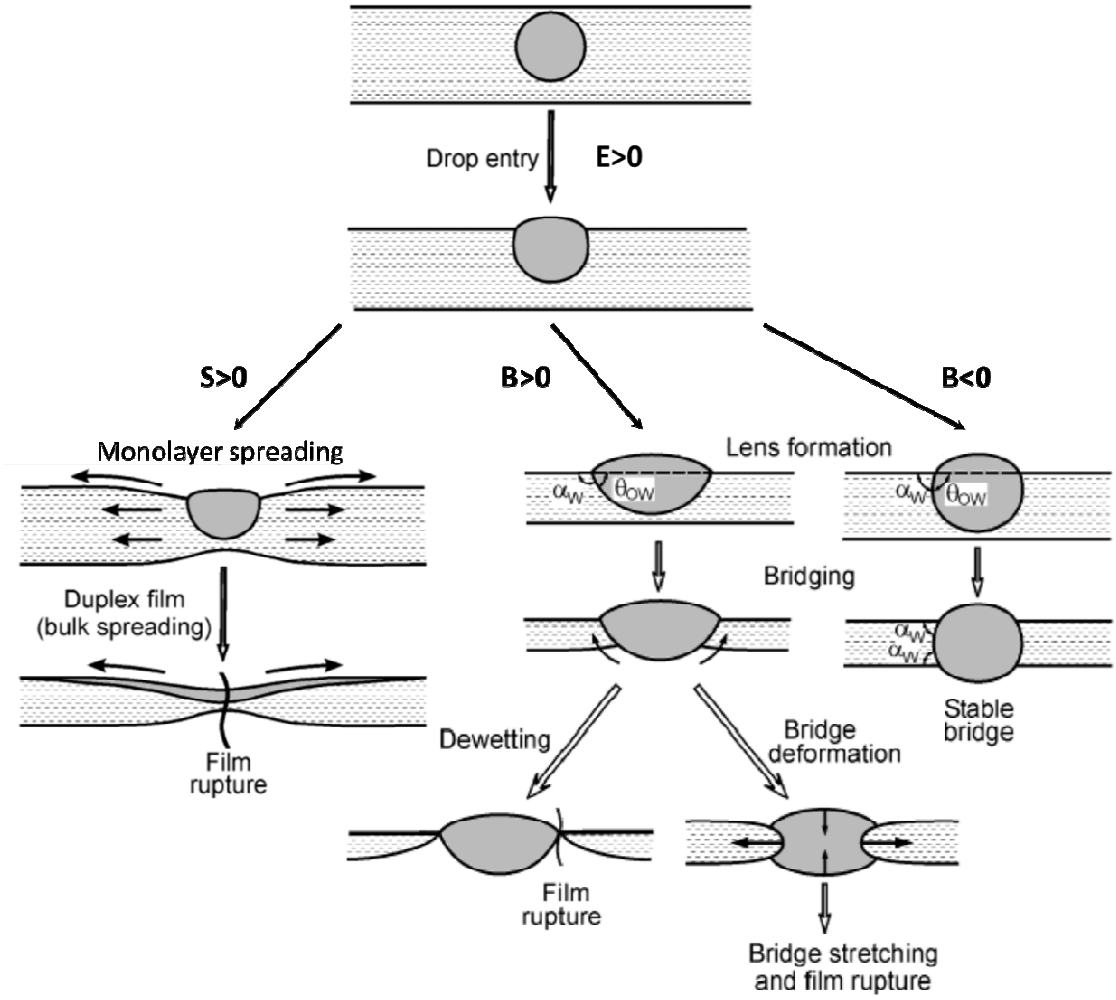

Figure 3-15: Schematic representation of the process of lamella rupture by oil according to the entry, spreading and bridging coefficients.

Other parameters have been used to estimate the impact of oil on foam stability, such as lamella number and entry barrier. Lamella number (L) was proposed by Schramm and Novosad [112] and is defined as the ratio between the capillary suction in the Plateau borders

and the pressure drop across the interface of an oil droplet and the aqueous solution, equation 3-17.

3-17. $$L = \frac{\Delta P_C}{\Delta P_R}$$

Entry barrier or the generalized entry coefficient was proposed by Bergeron et al [113] and considers both the impact of porous media and capillary forces, as the stability of pseudo-emulsion film of oil over the lamella. Jones et al [102] also presented the comparison of these parameters with experimental results; while they observed conflicting results between prediction and actual lab data for lamella number, the stability criterium defined by the entry barrier seems to be consistent with experimental results. Vikingstad et al [109] also evidenced that lamella number was not able to predict the influence of oil on foam stability. They are in agreement with the discussion in the review of Almajid et al [88], where the authors pointed out that knowing the stability of the pseudoemulsion film over the lamellae is crucial to understand lamella rupture [88].

Regardless the stability criteria used, there is some consensus on the effect of oil composition and nature on foam stability. For instance, both the works of Vikingstad et al [109] and Osei-Bonsu et al [103] showed that lower weight, shorter hydrocarbon chains are more detrimental to foam stability than longer chain hydrocarbons. Talebian et al [21] mentioned that a similar trend was observed in multiple coreflood tests with crude oils, as lighter oils had a more negative impact on foam stability. The authors questioned the validity of using dead oil instead of live oil to investigate the influence that oil will have on foam performance during an EOR operation. Since live oil is richer in lighter components, it is expected to have a more negative impact on foam stability.

Both the results of Vikingstad et al [109]and Osei-Bonsu et al [103] can also be discussed in terms of oil viscosity. The lower the viscosity of the oil, the easier it is for oil to break into droplets and emulsify, which is the first step for oil to reduce foam stability. Hence, high viscosity oil emulsifies more slowly, and are expected to impact less foam stability [21]. For the oils used in these studies, molecular weight and viscosity are proportional, thus the trend observed by both studies agrees with what is expected from the correlation between the rate of emulsification and oil viscosity.

Talebian et al [21] also remarked that experiments made with alkene solvents failed to find a correlation between hydrocarbon chain size and foam stability. This indicates that results of oil impact on foam stability obtained with pure solvents does not replicate the behavior observed for crude oil, and hence should not be regarded as adequate surrogates if the goal of the study is to reflect the influence of crude oil on foam in a reservoir [112].

Rather than the size of the hydrocarbon or the composition of oil or even its viscosity, it would be better to discuss the influence of oil on foam stability (and performance) in terms of the easiness of emulsification and the dynamic of solubilization of the oil into the surfactant micelles, as concluded by Vikingstad et al [109]. This approach would consider both the effects of oil viscosity and oil molecular density. This would also contemplate the effect of salinity and brine composition, since ionic strength plays a significant role in the interfacial forces and solubilization constants at play in these colloidal systems.

Despite the above exposed, the impact of oil remains poorly understood. No theory so far was able to contemplate all experimental observations [79]. Additionally, most of these observations were done on bulk foam at ambient conditions (bottle tests), thus not representative of conditions of interest for EOR application. It is important to remind that the physics of foam in porous media and in bulk are very different [21]. Hence, the interaction of oil with the lamellae should be different as well, since they must consider the interactions with the rock surface. The understanding of the complex interaction of oil and foam in porous media is imperative to determine their impact on foam performance and foam propagation, which are both pressing issues to advance foam-EOR technology [21].

3.5 Foam simulation

The importance of foam simulation has been presented in sections 2.4.2 and 2.4.3.3, as well as the issue that current modeling tools are not predictive due to the lack of a physical model for foam flow in porous media. In fact, Talebian et al [21] observed that commercial simulators could be improved to better represent the singular physics of foam. The authors also pointed out that these simulators depend heavily on experimental data for model tuning process, which might limit their reliability for full-field scale predictions.

Ma et al [22] also highlighted the limited predictive capability of current models. They strongly advised researchers to perform more systematic experiments to determine the sensibility of simulation results to each parameter to better describe foam behavior and improve the predictive capabilities of foam models. Likewise, Farajzadeh et al [92] stated that accurate modeling of foam rheology on field scale can only be achieved with deep knowledge of the connection between the scalable parameters of the porous medium and the fundamental properties of foam, which is still lacking. Clearly, there is still much work to be done on foam simulation.

Nevertheless, current models can satisfactorily simulate foam behavior observed in coreflood tests performed in the absence of oil. Several methods have been proposed to model foam flow in porous media. Ma et al [22] have done an excellent work on organizing and categorizing the main models in their recent review. Since foam texture dictates the rheological behavior of foam flow in porous media, the authors defined three approaches, according to how foam texture is defined:

- Dynamic texture: n_f is obtained by solving differential equations that give the rate of foam generation and of coalescence processes. Foam texture is then used to modify gas mobility through either foam apparent viscosity, or gas relative permeability (or even both). This approach can represent transient states of foam, like foam generation in the beginning of co-injection, or the modification of foam texture during FAWAG injection.
- Algebraic defined texture: in this approach, the local-equilibrium (LE) hypothesis is assumed, i.e., the processes of foam generation and lamella destruction are considered in a dynamic balance when compared to the time scale of foam transport through porous media [22]. Hence, the equations for the rates of these processes can be equated, resulting in an algebraic function for foam texture, correlated to parameters obtained through Darcy's Law and mass-conservation equations [22].
- Implicit texture: this approach also assumes the LE hypothesis, but differently from the previous approaches, it does not specify a foam texture value or expression. Instead, the effect of foam on gas mobility is modeled through a simple modification of the relative gas permeability in presence of foam by multiplying it by a factor that encompasses as many parameters as needed to

cover the impact of different variables, such as oil saturation, surfactant concentration, limiting capillary pressure, rock permeability, and injection conditions [19]. These parameters are obtained through a fitting process of experimental data, which can come from either lab experiments or field applications.

These approaches are divided into two main classes of models: local equilibrium (LE) models and population balance (PB) models. Other classes of models, such as fractional flow and percolation models, have also been reported, but these are considered to have an only qualitative purpose [21]. Figure 3-16 summarizes how foam texture approaches are associated with the main classes of foam models, according to Ma et al [22]. A complete description of these classes, as well as tables with the mathematical expressions of the main 23 foam models, are available in their review.

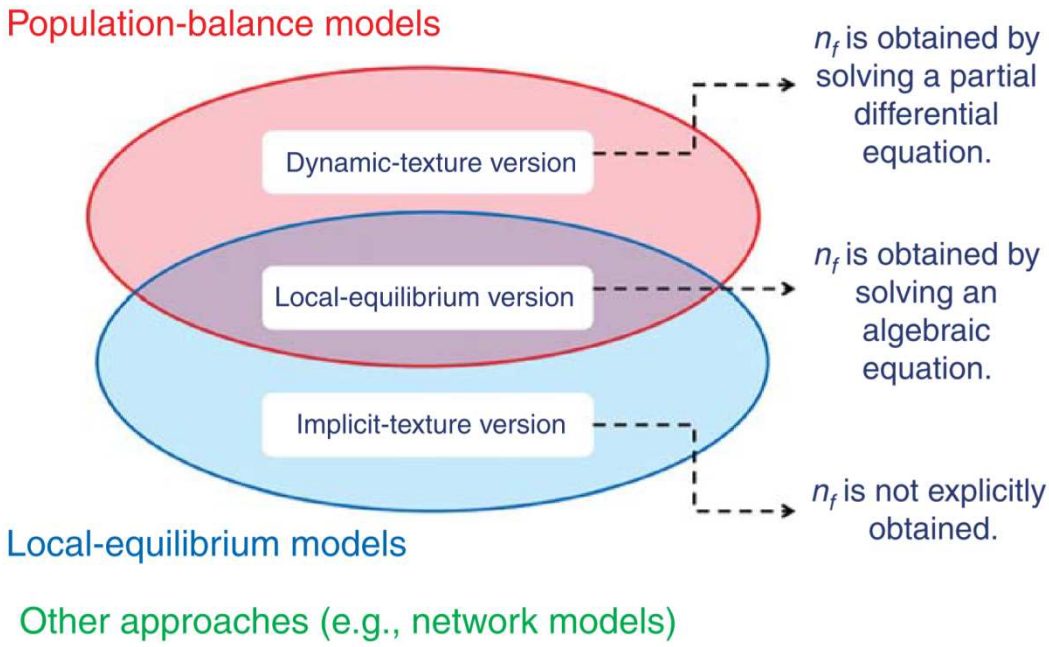

Figure 3-16: Organization of main approaches and classes of models of foam flow in porous media, according to Ma et al [22].

PB models, also called mechanistic models, are considered full-physics models, as they can track dynamically foam generation and decay (i.e., foam texture) and correlate it with gas mobility [21]. In addition, they can also account for the non-Newtonian rheology of foam as a function of bubble population [21]. The use of such comprehensive models is however limited due to the number of parameters that are difficult to obtain, measure and

scale-up to reservoir scale, and to the computational costs of solving numerically bubble population-balance equations [22]. Moreover, the mathematical expressions for the rates of foam generation and decay depend on the assumptions and hypotheses made by each group of researchers, hence differing considerably [22]. Thus, justifying the selection of one or another expression is one of the great challenges in foam modeling, as pointed out in section 2.4.3.3.

LE models, in turn, are also known as empirical or semi-empirical models, since they generally modify either gas viscosity or relative permeability according to experimental and field observations and hypotheses [19,22]. Though these models consider some of the physics of foam transport, they cannot really represent such physics since most mathematical formulations did not originate from a detailed derivation of related phenomena [22]. They can be quite complex, but mostly they are simpler, have fewer parameters, and are less demanding on computing resources than PB models. For these reasons, to date, all commercial simulators employ these models. However, the simpler approach based on experimental and field data also renders these models highly case specific, thus limiting its application and predictability [19,22].

To date, all commercial simulators (such as CMG STARS, ECLIPSE, and PumaFlow) use the LE model proposed by Martinsen and Vassenden [114]. In this model, the effect of foam on gas mobility is modeled through a simple modification (parameterization) of the relative gas permeability in presence of foam using a mobility reduction factor FM, as in equation 3-18.

3-18. $$K_{rg}^{foam}(S_g) = \mathrm{FM} \times K_{rg}^{0}(S_g)$$

Despite some differences in the name of the parameters and format of some functions that compose FM, it is basically written as follows [22]:

3-19. $$FM = \frac{1}{1+fmmob \times F_1 \times F_2 \times F_3 \cdots \times F_n}$$

Where *fmmob* is a constant that represents the maximum gas mobility reduction factor that can be obtained [22]. The functions F_i ($0 \leq F_i \leq 1$) try to capture the contributions of the main parameters impacting the gas mobility, such as surfactant concentration, water saturation, capillary number and oil saturation.

Regardless the model chose (either LE or PB models), the procedure to model foam flow in porous media involves:

- Obtaining data without foam and adjust relative permeability curves for water and gas;
- Obtaining data with foam and adjust relative permeability curve for gas;
- Obtain model parameters by fitting data in an Osterloh and Jante diagram, for example;

It is important to notice that the values of model parameters depend on the method of fitting, and the initial values used during the fitting process. Ma et al [22] remarked that the fitting methods are rarely presented in detail, and conclude that the approaches used to fit parameters to experimental data need further development, as this is also a major challenge to foam simulation.

CHAPTER 4.

SELECTING A FOAMING FORMULATION

4.1 Introduction

Selecting and optimizing a chemical formulation for EOR process (especially the ones that employ surfactants) is a rather complex and time-consuming task due to the great number of variables that need to be considered, as the interactions between the chemicals to be injected and the injection fluids (water and/or gas), the reservoir fluids (formation water, oil and gas), and the reservoir rock itself [115,116]. All this complexity usually makes the selected formulation reservoir-specific, and the entire process needs to be repeated if the technology is to be applied to another target (either field, reservoir, zone, or even well) [10,116]. The costs associated with extensive lab tests and the timeframe of evaluation of formulations can be a critical issue in the beginning of an EOR project [117], possibly affecting the decision making process. Particularly, if the proposed method is a new one (either generally or company-specific), this time-consuming phase could lead to the early elimination of the method under consideration.

In the case of SP/ASP flooding, companies are able to considerably hasten this first step due to the overwhelming amount of experimental studies, pilots and field applications, which has built a consistent database that provides some solid guidelines not only on how to pre-select chemicals based on target conditions, but also on what lab tests are essential to effectively evaluate and optimize a formulation [115,116]. However, that is not the case for foams. There is no comparable body of work neither on how to select a foaming agent, nor understanding on how the formulations affect the performance of foam-EOR [57]. Additionally, even though some studies were performed comparing different formulations, most of the experimental work realized so far, either at laboratory or pilot/field scale, has used a rather small diversity of formulations [11,13,58,118–120,120]. Consequently, fast screening techniques may play an important role in advancing foam technology for EOR [117,121–123].

To address this challenge, a collaboration was established with Solvay (the Laboratory of the Future – LOF) to obtain a chemical formulation that could be effective under the desired conditions that were considered in this thesis. The LOF, a joint team between CNRS, Solvay, and University of Bordeaux, is specialized in developing new methods based on high-throughput screening (HTS) tools combined with advanced data treatment specifically dedicated to research in chemistry. The methodologies created at LOF allow to considerably

speed up the evaluation of complex physical-chemical systems, reducing the timeframe of tests from weeks to hours in some cases. These methodologies are being applied to the development of products for a variety of applications, including chemical EOR [66,124,125].

Based on the traditional tests reported in the literature, the LOF´s EOR team proposed a workflow for the evaluation and selection of foaming agents. The proposed methodology was applied on two pre-selected surfactant formulations (one especially conceived for dense CO_2 applications, and one best suited for non-dense scenarios), since the chemical optimization is not one of the goals of this Ph.D. Nevertheless, this knowledge is essential for the development of the project.

4.2 Methodology:

All formulations were prepared on a Genesis Tecan robotic platform (a fully automated robot for liquid handling tasks) using stock solutions of the salts and pre-selected surfactants. This platform supports a gamma of different racks for both stock solutions and formulation vials, giving it the flexibility to perform all the steps of a formulation screening (Figure 4-1).

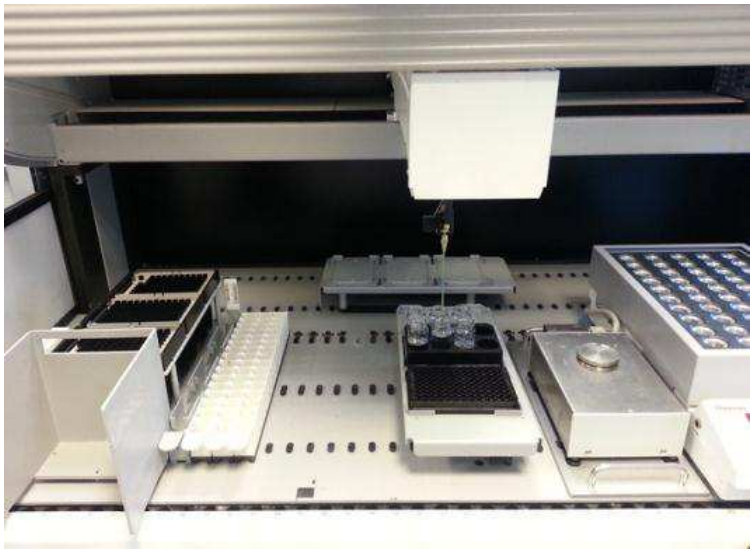

Figure 4-1: Genesis Tecan robotic platform with the different racks used during formulation screening.

The pre-selected surfactants proposed by Solvay were the following:

- SurfEOR dC-40R, a proprietary formulation specially developed by Solvay for high-density CO2 foam, available as a 40% active matter solution;
- Rhodacal A246L, an alpha olefin sulfonate with an average 14-16 carbon chain length, also available as a 40% active matter solution;
- Mackam CB 35, a betaine with an average 12 carbon chain length, available as a 35% active matter solution.

The active content of foaming agent in all formulations and water compositions tested throughout the selecting process was kept at 5000 mg/L.

The range of salinity and hardness were chosen based on the most relevant water compositions of the Pre-Salt oil field that serves as the ultimate target of this project. Due to the rock-fluid interactions between the carbonate reservoir rock and the CO_2 present in the injected gas, these water compositions included not only the injection and formation brines, but also the water composition achieved once the reactions between the injected fluids and the rock had reached chemical equilibrium. Based on the scenarios that were being considered for gas injection at the beginning of this thesis (section 7.2.1), three equilibrated water compositions were provided by Petrobras. Their salinities and hardnesses are presented in Table 4-1. The stock solutions of salts employed throughout the experiments at LOF are shown in Table 4-2. As a standard procedure to avoid contamination by microorganisms and degradation of products, new batches of stock solutions were prepared fortnightly.

Table 4-1: Salinity and hardness of the most relevant water compositions for the scenario under consideration.

Water Composition	**Salinity** (mg/kg_w)	**Hardness** (mg/kg_w)	**Hardness Solvay** (a.u.)
Injection Water	28112	134	0,0121
EW-P-d	28112	596	0,0518
EW-I-d	28112	941	0,0794
EW-P-dc	28112	958	0,0807
EW-R-d	28112	1079	0,0900
EW-I-dc	28112	1554	0,1247
EW-R-dc	28112	1795	0,1413
Formation Water	206160	11027	0,1329

Where:
EW: Equilibrated Water;
P, I, R: Poor, Intermediate, and Rich gas compositions, respectively;
d: equilibrated with dolomite;
dc: equilibrated with dolomite and calcite;

Table 4-2: Concentration of stock solutions employed in the experiments developed at LOF.

Substance	Concentration
NaCl	300 g/L of Na^+
(Concentrated) $CaCl_2.2H_2O + MgCl_2.6H_2O$	50 g/L (48,642 g of Ca^{2+} and 1,358 g of Mg^{2+})
(Diluted) $CaCl_2.2H_2O + MgCl_2.6H_2O$	5 g/L (10x dilution of the above solution)
SurfEOR dC-40R	50.000 ppm (5%) of active content
Rhodacal A246L (AOS)	50.000 ppm (5%) of active content
Mackam CB 35 (Betaine)	50.000 ppm (5%) of active content

Hardness Solvay, also called R-factor, is defined as the ratio between the total concentration of divalent cations and the total concentration of cations in solution, quite similar to the ionic force definition. This parameter has shown better correlation to the results obtained in previous experiments at LOF, facilitating the determination of tendencies and the understanding of the behavior of the complex colloidal systems investigated in this facility.

4.2.1 Solubility tests:

The solutions of the surfactant formulations at different salinities and hardnesses were prepared in plastic microboards containing 96 wells (8x12) of 300 µL each. Based on the water compositions supplied, 6 salinities and 8 hardnesses were chosen for these tests, therefore allowing the evaluation of 2 formulations per run. The formulation indicated for dense gas injection was the dC-40R, a proprietary formulation still under development. For the non-dense scenario, the proposed formulation was a mixture 1:1 of Rhocadal A246L and Mackam CB 35.

Once formulated, the microboard is transferred to a home-made device called Turbiscan. As the name suggests, this equipment evaluates the solubility in each well by a turbidity-like measurement. The samples are placed on a metallic frame connected to a thermostatic bath and covered with a sheet of glass, so to avoid evaporation during the analysis. A backlight (LED plate) is placed over the glass, while a digital camera is located under the microboard. The controller software then starts a ramp of temperature from 5ºC to 90ºC over 2 hours, taking pictures at intervals of 2 minutes. The software then compares the image of each well with a picture of an empty microboard (taken at the beginning of the analysis), attributing a greyscale value for each well as a function of time, which is registered on a worksheet. These files were then processed in a Matlab software to plot a map of

greyscale value as a function of hardness and salinity at fixed temperatures, Figure 4-4. The darker the region of the map, the less soluble the formulation is under those conditions.

Table 4-3: Salinity, total dissolved solids (TDS), and hardness of the chosen water compositions guides for the solubility tests

Water Composition	**Salinity** (mg/kg$_w$)	**TDS** (mg/kg$_w$)	**Hardness** (mg/kg$_w$)	**Hardness Solvay** (a.u.)
IW	28112	28150	134	0,012
EW-Pd	28112	28613	596	0,052
92,5%IW+7,5%FW	41466	41646	951	0,058
EW-Pdc	28112	28974	958	0,081
EW-Idc	28112	29571	1554	0,125
85%IW+15%FW	54820	55141	1768	0,0810
EW-Rdc	28112	29812	1795	0,141
60%IW+40%FW	99331	100126	4491	0,113
35%IW+65%FW	143843	145111	7214	0,125
FW	206160	208089	11027	0,1329

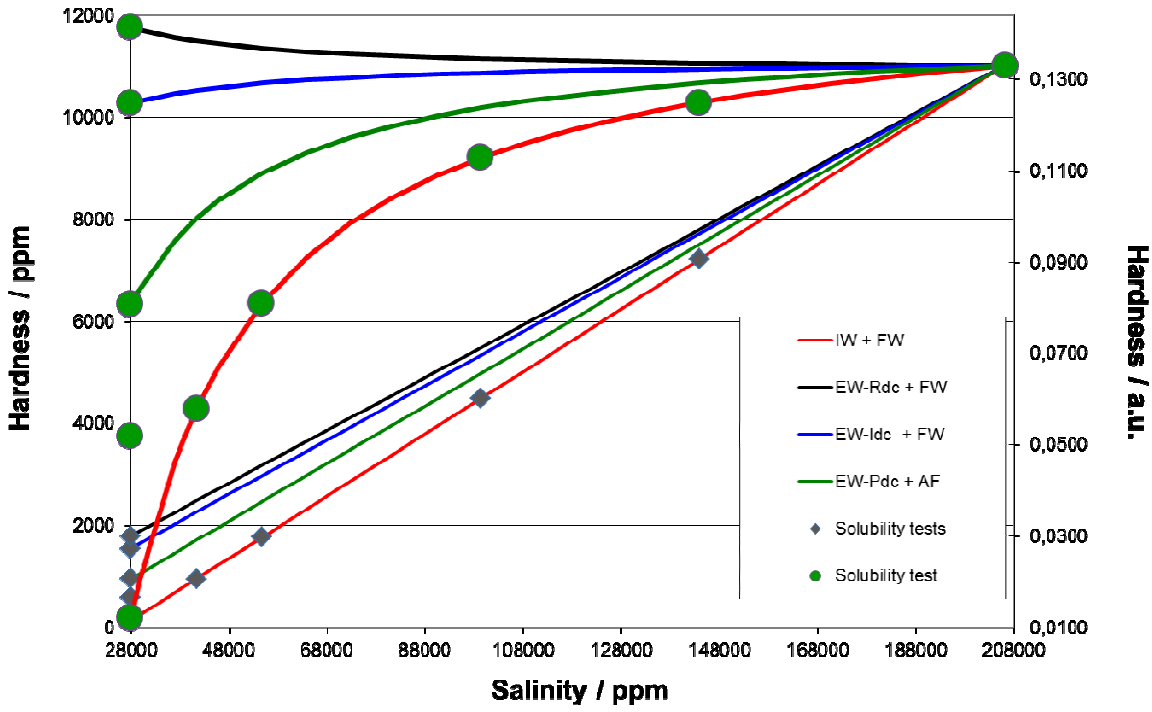

Figure 4-2: Mixtures of either injection brine or equilibrated water compositions with the formation water as water injection proceeds. The highlighted points represent the water compositions in Table 4-3.

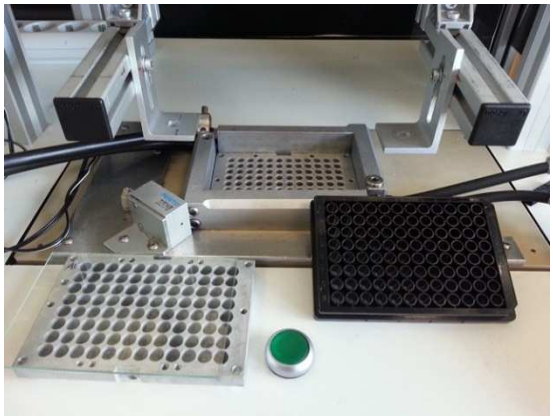

Figure 4-3: Turbiscan setup with blank microboard.

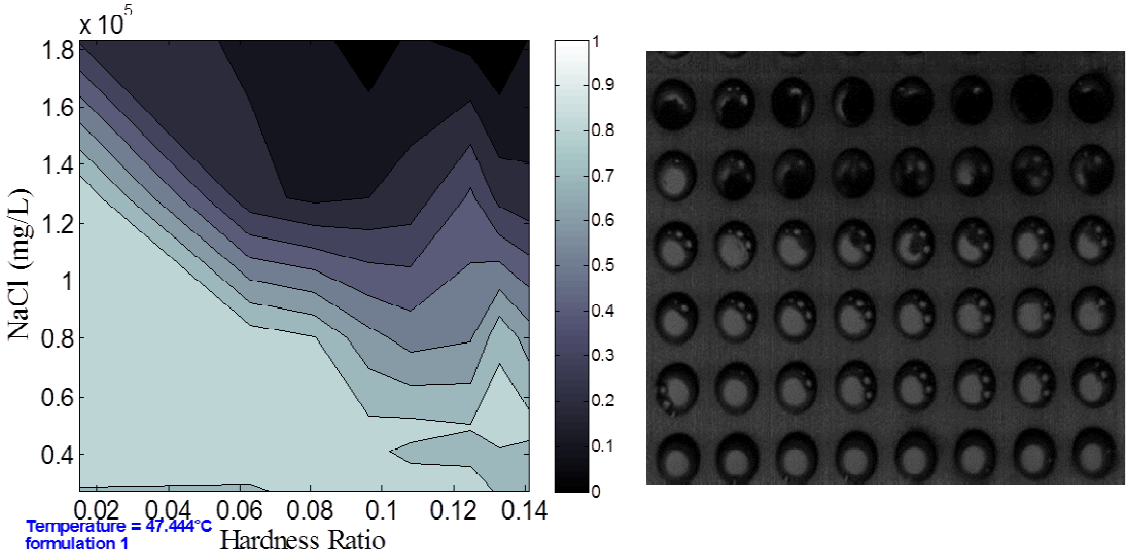

Figure 4-4: Example of picture and corresponding greyscale map obtained from the solubility tests.

4.2.2 Stability tests:

The foam stability of the selected formulations was evaluated by measuring the decay of a foam column with time. The time at which a foam column has decayed to half of its initial height is called the half-life of the foam, and it is widely used as the main parameter to select a foaming agent [11,124,125]. The effect of salinity, hardness, formulation, and temperature was evaluated. A few tests regarding foam resistance to model oil and foaming ability in presence of crude oil were realized as well.

For the half-life tests, the solutions of foaming agents were prepared in 8 mL glass vials with the aid of the Tecan platform. A volume of 2 mL of solution was placed in each vial. Ten water compositions were used in these tests, Table 4-4. After formulation, the foam was formed by two techniques, depending on the temperature at which the stability would be evaluated. For ambient temperature tests, the solutions were foamed by injecting 8 mL of air at a flow rate of 50 mL/min using a syringe pump and then positioned in front of a digital camera that was inside a dark chamber.

Table 4-4: Salinity and hardness of the chosen water compositions for the foam stability tests

Water Composition	**Salinity** (mg/kg_w)	**Hardness** (mg/kg_w)	**Hardness Solvay** (a.u.)
IW	28112	134	0,012
EW-Pdc	28112	958	0,081
EW-Idc	28112	1554	0,125
EW-Rdc	28112	1795	0,141
60%IW sal. + Pdc hardness	99331	3101	0,081
60%IW sal. + Idc hardness	99331	5031	0,125
60%IW sal. + Rdc hardness	99331	5812	0,141
35%IW sal. + Pdc hardness	143843	4440	0,081
35%IW+65%FW	143843	7214	0,125
35%IW sal. + Rdc hardness	143843	8322	0,141

For reservoir temperature (60ºC) tests, a small curved metal bar was placed inside each vial. The vials were positioned in an oven and allowed to equilibrate at the desired temperature for at least 1 hour. Then, they were individually agitated with the aid of a vortex mixer for 10-15 seconds and repositioned inside the oven on a metallic support backlit by LED plates. The digital camera and black chamber were then positioned in front of the glass door of the oven.

Two different kinds of foam-oil interactions were assessed. The first was the foam resistance to oil, which judges the ability of the foam to resist to the contact of oil. The second was the foaming ability in presence of oil. For the first kind, the tests were realized at ambient temperature by dripping 200 µL of dodecane over a formed foam. The second was tested at reservoir temperature by adding 200 µL of crude oil to the vials previously to their heating.

In all cases, the vials were observed for a period of up to 6 hours. A digital camera controlled by a computer acquired images of the vials at intervals of 2-3 minutes. A maximum of 10 vials could be used per run. The image sequences were analyzed in ImageJ, a public

domain, Java-based image processing program. Figure 4-5 shows an example of the different steps of the image processing.

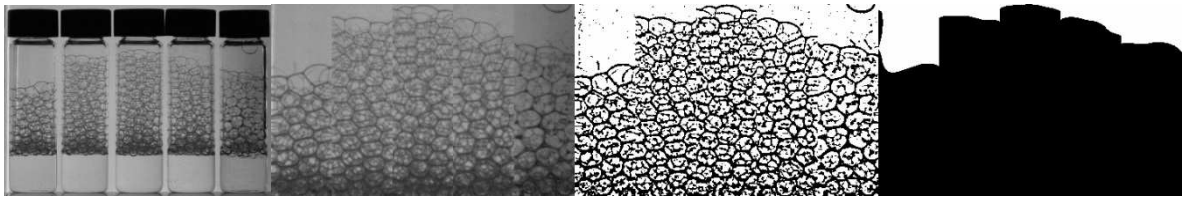

Figure 4-5: Automated image processing for foam stability tests. From left to right: original photography; selection of areas of interest and conversion to 8-bit greyscale; filtering to highlight lamellas and conversion to a binary image; filling all spaces enclosed by lamellas and calculating the percentage of the area of interest is dark.

4.2.3 Adsorption tests:

The adsorption tests were performed by mixing 4 g of crushed rock samples with 10 mL of solutions of the selected non-dense formulation at different salinities and hardness. The solutions were allowed to contact the rock samples for 24h at 40ºC before being separated by centrifugation. The concentrations of the foaming agents were measured by HPLC before and after contacting the rock samples, and adsorption was determined by the difference in active content. Samples of Indiana Limestone, Clashach sandstone, and Silurian Dolomite were tested.

4.2.4 High-pressure stability tests:

The influence of pressure and, consequently, of gas density, were evaluated by half-life stability tests performed in a high-pressure visualization cell with sapphire windows. The cell consists basically of a cylindrical chamber of approximately 10 mL surrounded by a heating system, and three visualization windows: one at the top of the chamber, one in the bottom, and the last one positioned perpendicularly halfway between the top and bottom (Figure 4-6).

Tests were realized with pure CO_2. Previously to gas injection, the system is heated to the desired temperature and rinsed three times with the formulation´s solution to be tested.

When the system was completed saturate with the solution of interest and no air bubbles were left, the chamber pressure was adjusted using a backpressure valve. Once temperature was stable, gas was injected at 0.8 mL/min at the base of the chamber so to form foam. The gas injection was stopped before the limit between foam and liquid phase were no longer visible in the halfway window. As in the ambient pressure tests, a digital camera was used to acquire images at fixed time intervals. Experiments were done in triplicates, and the total observation time was 3 hours per run. Half-life times were determined manually by observing the images taken.

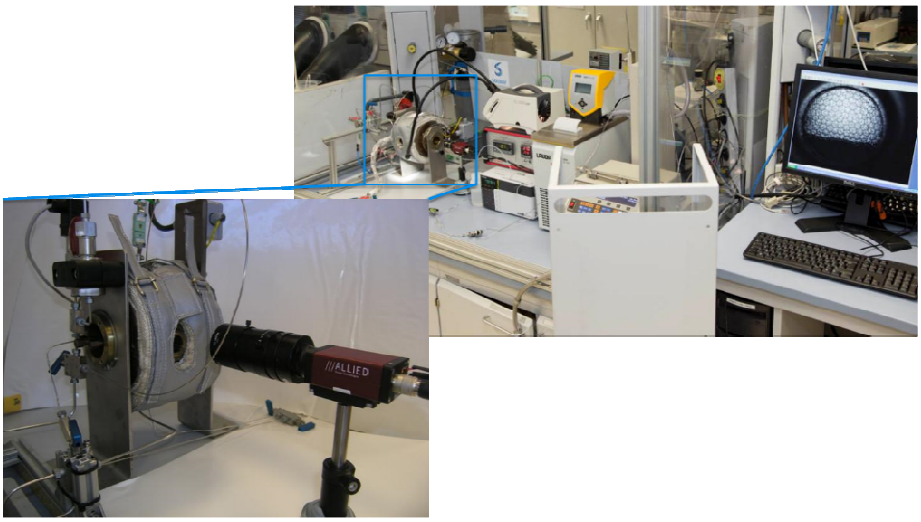

Figure 4-6: High-pressure visualization cell used for evaluating half-life of selected foaming agent formulations.

4.3 Results and Discussion:

4.3.1 Non-dense formulation

The initially suggested formulation consisted of a 1:1 mixture of AOS and betaine products (Rhodacal A246L and Mackam CB 35, respectively) since it has shown superior performance in past experiments performed at LOF. However, as the hardnesses considered for the desired field are very elevated, an adjustment of the ratio between AOS/Betaine could be necessary. Therefore, three ratios of AOS/Betaine (3:1, 1:1, and 1:3) were tested. Table 4-5 shows the concentrations of divalent cations needed to obtain the 8 hardness x 6 salinities matrix for the solubility studies. Figure 4-7 shows the solubility maps obtained for such compositions, as well as for the pure surfactants, at various temperatures.

Table 4-5: Matrix of Salinity and hardness used for the solubility tests, with the calculated concentration of divalent cations (in mg/L) to achieve the desired R factor, given the salinity of the solution. The highlighted cells (in blue) represent the water compositions in Table 4-3.

		Calculated Hardness ($[Ca^{2+}]+[Mg^{2+}]$) in mg/L					
R factor / a.u.	**0.012**	134	190	246	433	620	882
	0.052	596	847	1097	1931	2765	3933
	0.058	670	951	1232	2168	3105	4416
	0.081	958	1360	1768	3101	4440	6315
	0.113	1387	1969	2551	4491	6431	9147
	0.125	1554	2206	2858	5031	7214	10247
	0.133	1673	2374	3076	5414	7753	11027
	0.141	1795	2548	3301	5812	8322	11836
		28112	**41466**	**54820**	**99331**	**143843**	**206160**
		Salinity (mg/L)					

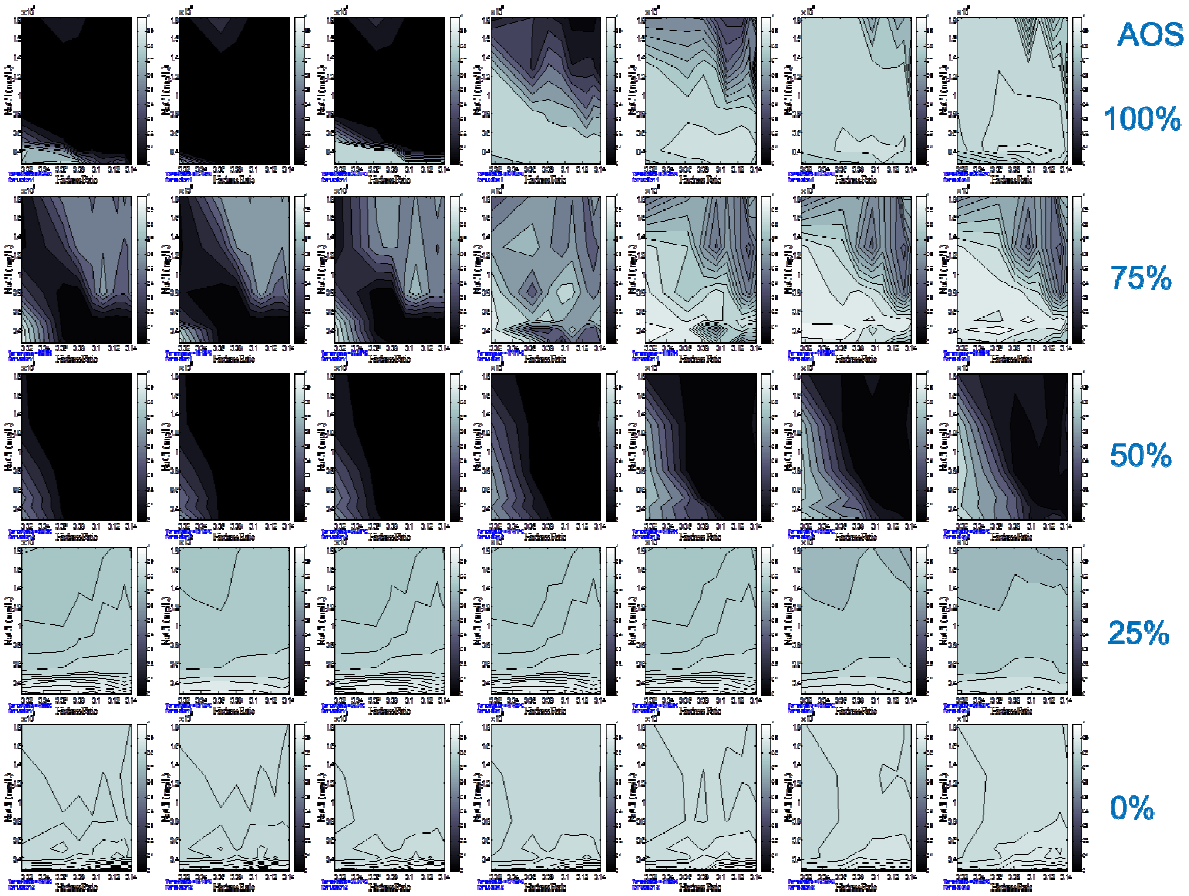

Figure 4-7: Effect of AOS/Betaine ratio on the solubility of the foaming agent formulation at various temperatures (from left to right: 5ºC, 20ºC, 33ºC, 48ºC, 62ºC, 76ºC, and 90ºC).

As the maps show (Figure 4-7), initially, the mixture of the betaine to the AOS solution decreases the solubility of the system. But at some point, after the betaine turns into the major component, the system becomes completely soluble in all salinities and hardnesses.

Regarding the temperature effect, the general trend is to increase the solubility as the temperature rises. Additionally, the results evinced that the originally proposed formulation has very limited solubility within the range of salinity and hardness analyzed, even at higher temperatures.

Given that the 1:1 ratio was the initially chosen due to its superior performance, additional ratios where tested in order to determine which is the highest AOS content that still presented good solubility. Solubility maps were obtained for formulations with 30%, 35%, 37.5%, and 40% content of AOS, and are presented in Figure 4-8.

According to these maps, the solubility of the 40% AOS formulation has considerably improved in comparison to the 50% AOS formulation; nevertheless, it still presented limited solubility at higher hardnesses. All other formulations seemed completely soluble in all water compositions tested.

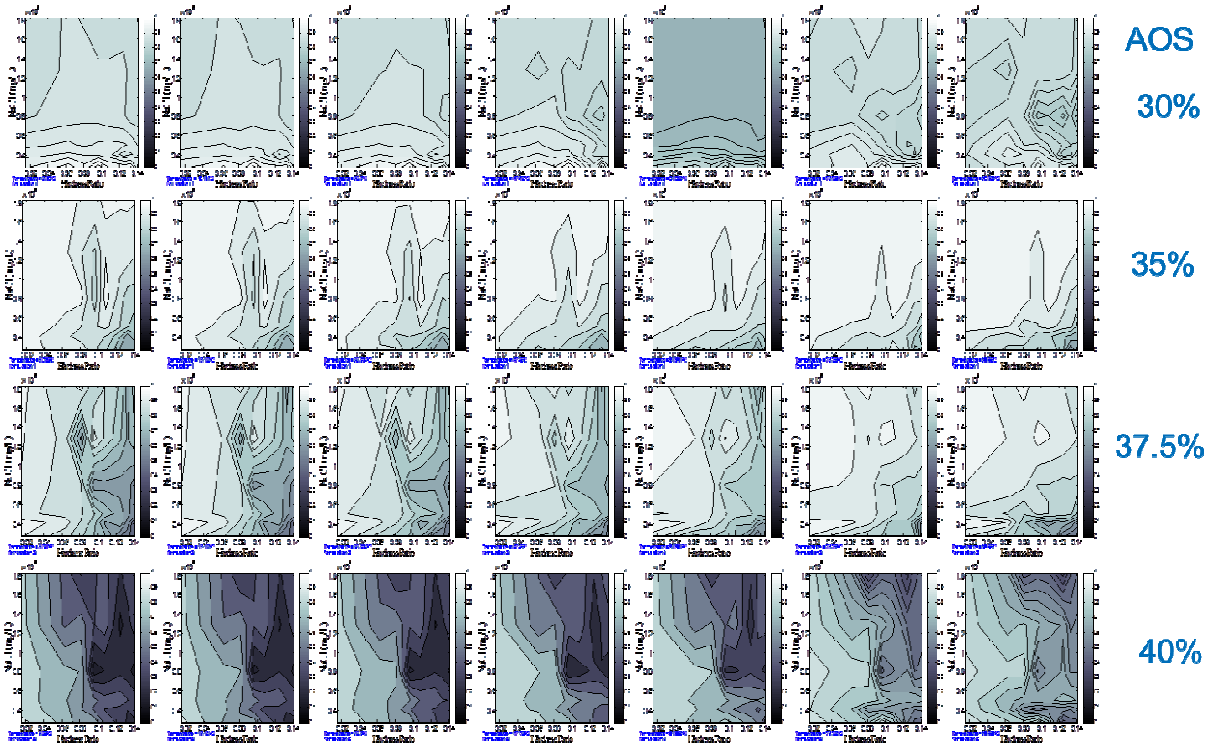

Figure 4-8: Solubility maps for formulations AOS/Betaine containing 30%, 35%, 37.5%, and 40% of AOS. (from left to right: 5ºC, 20ºC, 33ºC, 48ºC, 62ºC, 76ºC, and 90ºC).

Notwithstanding, when larger volumes of these formulations were prepared (in 8 mL vials, for example), phase separation was observed when the AOS content was over 30%, Figure 4-9. Since the separate phase does not alter significantly the greyscale value of the well

in the images taken (as shown in the upper right wells), the Turbiscan gave a false positive. However, upon agitation (lower right), the solution becomes much more cloudy, reducing the probability of a false positive. The presence of artifacts as this is not unknown in image analysis, and though it evinces some limitations in the technique, it does not undermine the methodology. In fact, it just stresses the importance of comparing the maps with the actual photos to check the accuracy of the results. Therefore, the input of the analyst is crucial to ensure the effectiveness of the automated analysis.

Figure 4-9: Limitations of the adopted methodology for solubility evaluation. The image on the left shows a 35% AOS formulation where a hazy phase is visible; hence, the solubility of the formulation is not adequate at this salinity and hardness. The images on the right evince that agitation improves the ability to detect this kind of situations.

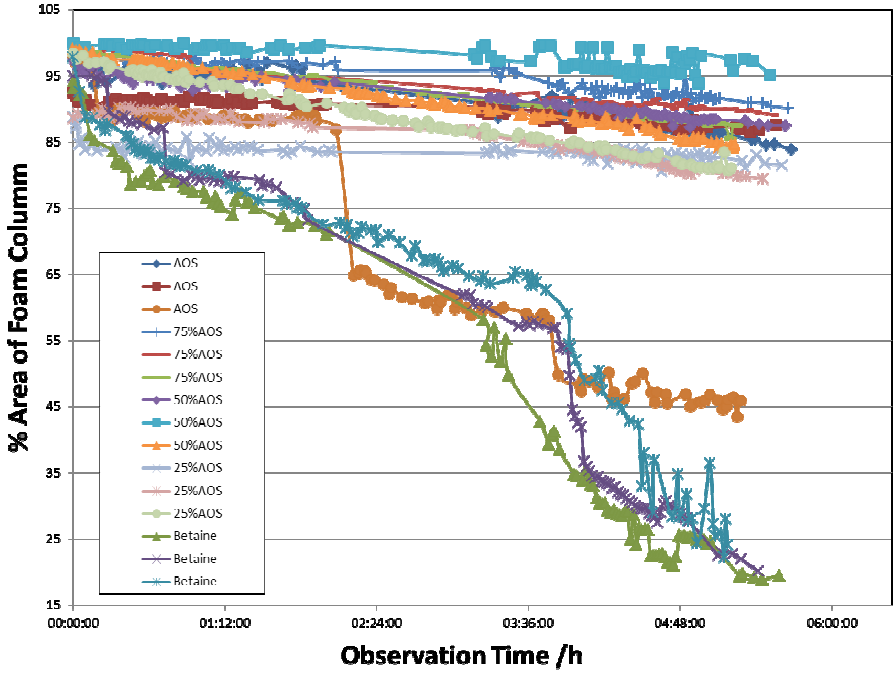

Figure 4-10: Foam stability at ambient conditions for different ratios of AOS/Betaine.

Once the effect of AOS/Betaine ratio in the solubility was determined, the next step was to verify its influence on the stability of the foam. For this test, the injection water

composition was used, since it was the only one in which all ratios were soluble at ambient conditions. Figure 4-10 shows the curves of the area of foam column with time. The tests were realized in triplicate. No significant difference was observed between all formulations with some content of AOS, which were very stable. Only the foams formed with pure betaine decayed beyond the 50% level within the 6 hour period of observation.

The following test (Figure 4-11) sought to evaluate the effect of AOS/Betaine ratio on the foam resistance. The foams made of pure surfactants (no mixture) showed no resistance to oil, breaking almost completely within minutes after the oil contact, while the 3 mixtures tested showed some resistance. However, the results varied widely for each composition, presenting curves that showed both very good resistance and rather unstable foams (Figure 4-11). Thus, no clear trend was found.

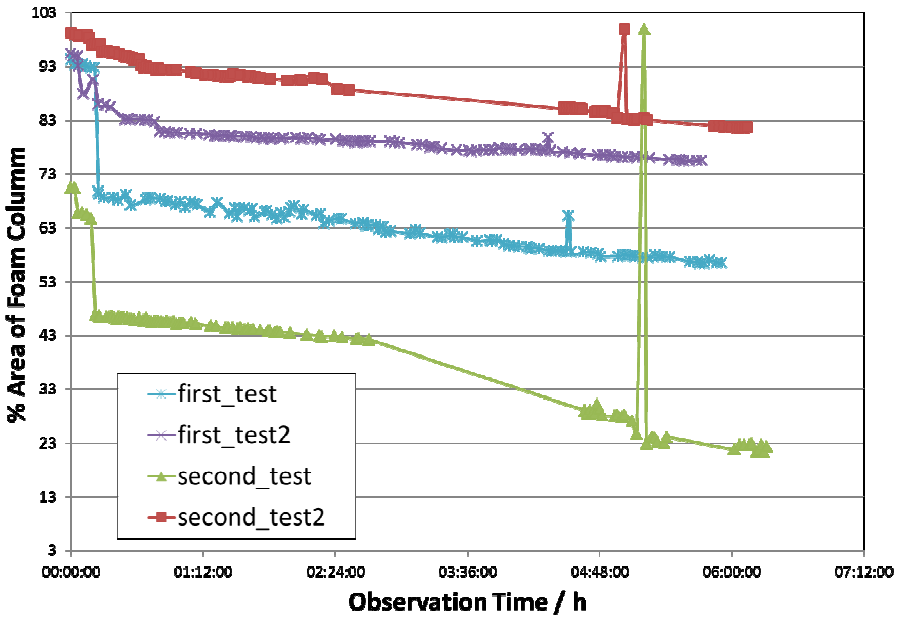

Figure 4-11: High variability of foam resistance to oil contact for 1AOS:3Betaine formulation.

These results indicate no major loss of performance should occur from changing the initially chosen formulation (1:1 AOS/Betaine) to one with a ratio of 1:3 AOS/Betaine, which has a better solubility, to perform the petrophysical studies. Therefore, the experiments henceforth used this formulation.

Next, the influence of hardness and salinity on foam stability was investigated (Figure 4-12 and Figure 4-13, respectively). In both cases, the stability of foams initially increased

with higher hardnesses and salinities, reaching a maximum from where no further changes were observed. This can be attributed to an increase in the viscosity of the solutions, which could be verified qualitatively during the experiments. A higher viscosity reduces the gravity drainage, retarding the collapse of foams.

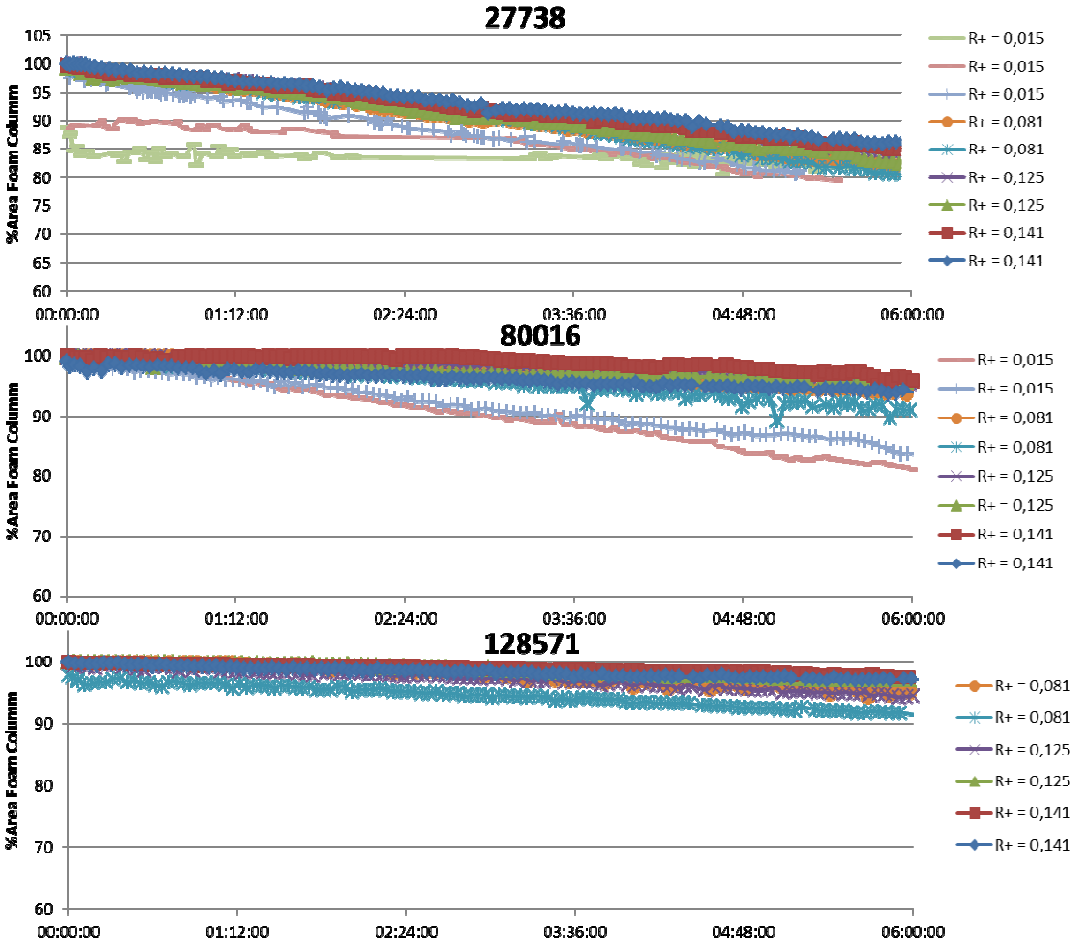

Figure 4-12: Effect of increasing hardness on foam stability of 1AOS:3Betaine formulations at fixed salinities indicated in the top of the plots in mg/L.

When these tests were performed at reservoir temperature (60ºC), the same trends were observed, i.e., the mixtures were more stable than the pure surfactants, both in the absence and presence of crude oil. Since the way the oil is introduced in the system is different in the tests made at reservoir temperature, they presented better reproducibility than the tests at ambient conditions, allowing investigating the effect of salinity and hardness on foam stability in presence of crude oil. The results are shown in Figure 4-14. Both parameters impair foam stability, with hardness seemingly having greater influence.

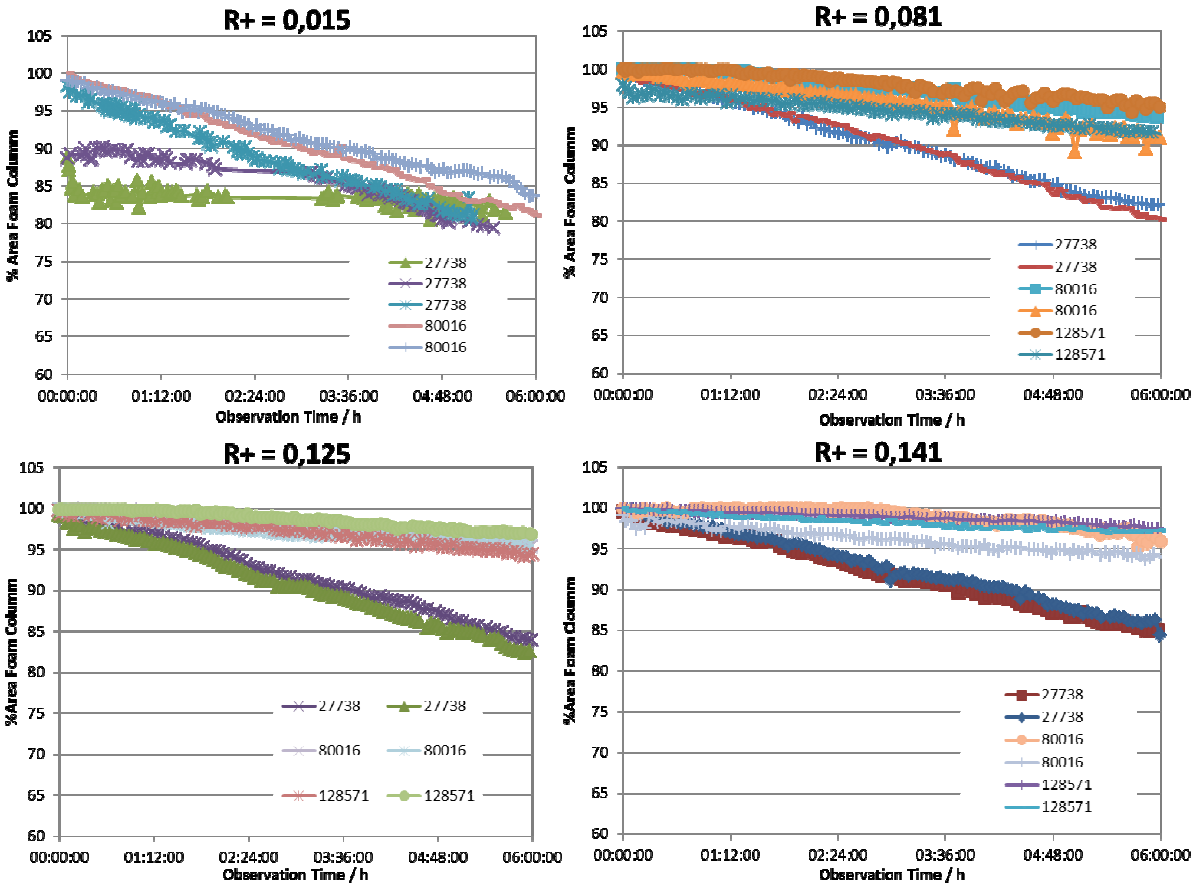

Figure 4-13: Effect of increasing salinity on foam stability of 1AOS:3Betaine formulations at fixed hardnesses.

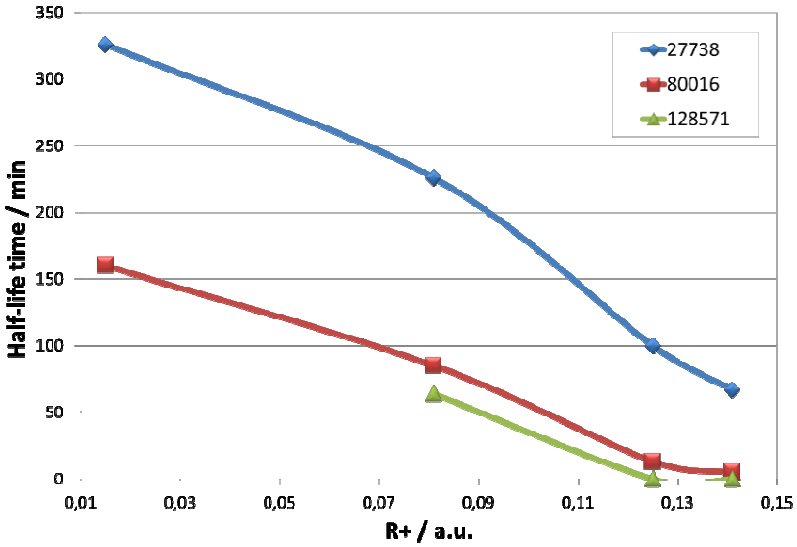

Figure 4-14: Effect of salinity and hardness on half-life time of foams of 1AOS:3Betaine formed at reservoir temperature and in presence of crude oil.

Following the classical characterization of foams (tests at atmospheric pressure), the influence of pressure was evaluated. Being one step closer to actual reservoir conditions, this

kind of tests is very important to achieve a better understanding of foam behavior, ultimately resulting in the more reliable selection of foaming agents.

Pressure, or rather the density of the gas, is thought to be a major parameter in foam properties, especially when CO2 is present. As density increases, the intermolecular interactions become more important. When CO2 is the injected gas (or the major component in a gas mixture) its density can be high enough so that the supercritical phase starts presenting some liquid-like behavior. Consequently, the interactions with the foaming agents might play an important role in the properties and performance of the foam, thus potentially demanding a formulation befitted for such conditions. The previous experience on the collaborations between Solvay and IFPEN of the subject of foams corroborate that idea to such an extent that the whole evaluation of chemical formulation here is divided based on the density of the gas phase.

Table 4-6 shows the conditions and respective density of CO2 for the tests realized with the mixture 1:3 AOS/Betaine in injection water. Since the maximum working pressure was limited at 150 bar on the equipment available, tests were also performed at 40ºC in order to extend the range of densities evaluated. The non-dense formulation presented rather stable foams in all conditions, independently of the pressure/density of CO2.

Table 4-6: Conditions and respective half-life time results (triplicate) obtained in the stability tests at high pressure for the selected non-dense formulation.

Temperature (ºC)	**Pressure (bar)**	**ρ (kg/m^3)**	**Half-life time (1)**	**Half-life time (2)**	**Half-life time (3)**
60	80	192	2,25h – >3h	>3h	
	100	290	>3h	>3h	10 min[†]
	120	416	20 min[†]	>3h	>3h
	150	604	>3h	>3h	>3h
40	120	698	>3h	>3h	>3h
	150	780	>3h	>3h	>3h

Lastly, the adsorption of the selected non-dense formulation was measure on crushed rock samples of Indiana Limestone, Silurian Dolomite, and Clashach sandstone. Adsorption affects the performance of foam by reducing the amount of surfactant available to form and

[†] This replicates presented some instability at the end of gas injection which led to a partial coalescence of the foams within minutes after the injection stopped. Nonetheless, a partial foam column remained stable throughout the 3 hour-tests.

stabilize lamellas, therefore delaying the propagation of foams into the reservoir. Additionally, high adsorption values will demand slugs with bigger volumes and/or higher surfactant concentrations. Both effects will increase the costs of the treatment, impairing the economics of a project, which may ultimately prevent the application [126]. The effect of salinity (Figure 4-15) and hardness (Figure 4-16) were evaluated.

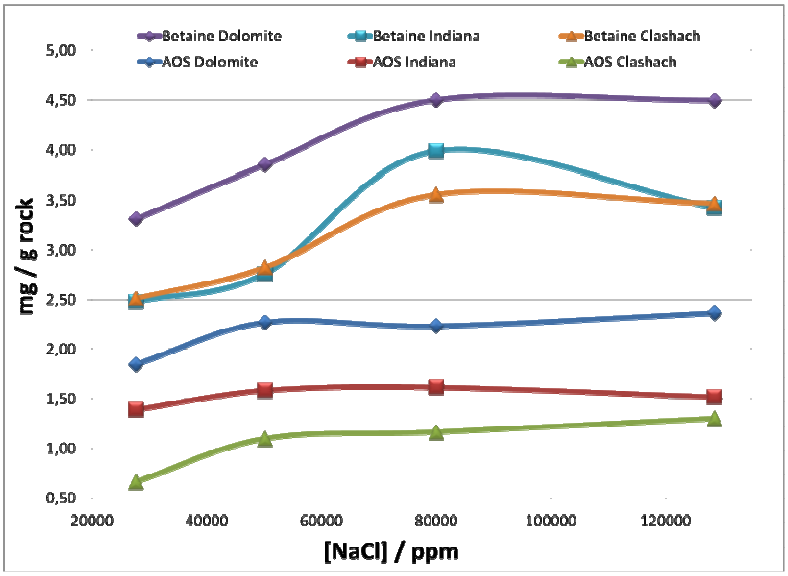

Figure 4-15: Effect of salinity on the adsorption of a 1AOS:3Betaine foaming formulation. Hardness was kept constant at 0,015 in all salinities.

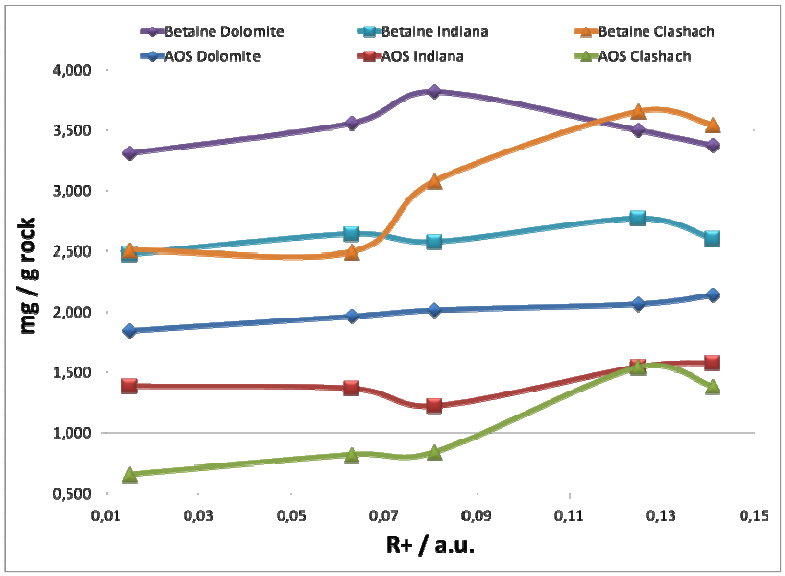

Figure 4-16: Effect of hardness on the adsorption of a 1AOS:3Betaine foaming formulation. Salinity was kept constant at 27738 mg/L in all hardnesses.

The HPLC chromatograms for these analyses presented a poorer resolution of peaks than the usual found in this technique, which increased the error of the measures from 0.1 $mg_{surfactant}/g_{rock}$ to 0.5 $mg_{surfactant}/g_{rock}$. Though this complicates the evaluation of the effect of salinity and hardness, some general trends are nonetheless observable. The results showed that the betaine presented a higher adsorption than AOS in all tested conditions and that, in general, dolomite adsorbed the most of the three rock types. Also, adsorption of both surfactants tends to increase with hardness for the Clashach samples. Likewise, the adsorption of betaine seemed to be more sensitive to the increase of salinity than the adsorption of AOS; regardless, both appeared to increase with salinity. Furthermore, the results suggested that the adsorption of both surfactants on carbonates (either limestone or dolomite) is not affected by hardness within the conditions tested.

4.3.2 Dense formulation

The dense formulation, dC-40R, was tested simultaneously to the non-dense formulation. The conditions were the same as the aforementioned experiments.

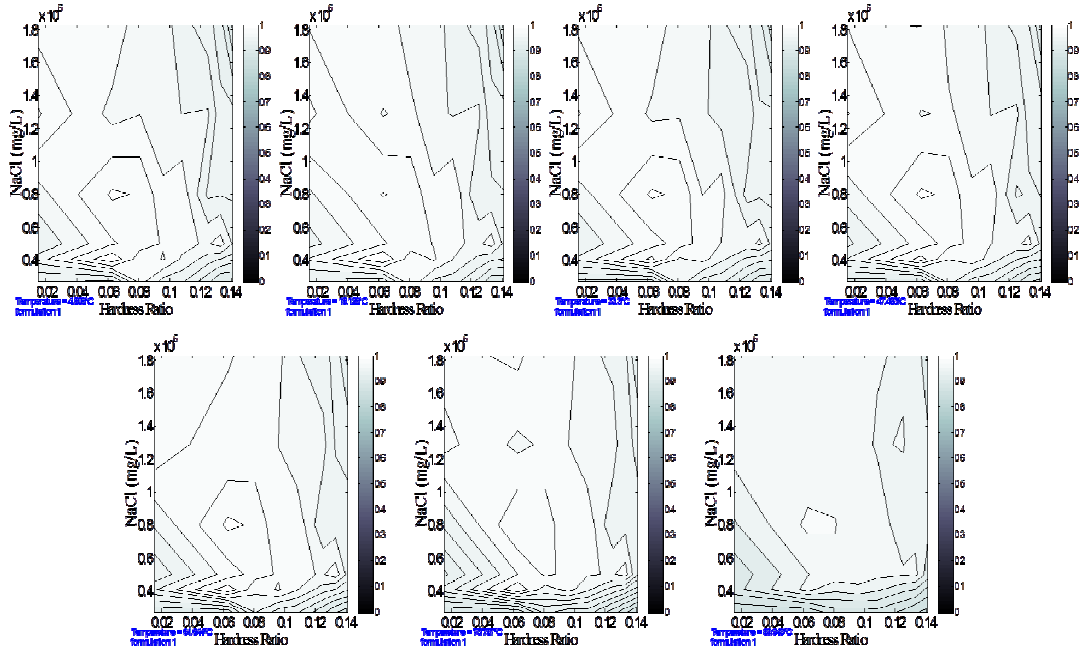

Figure 4-17: Solubility maps of dC-40R at 5ºC, 20ºC, 33ºC, 48ºC, 62ºC, 76ºC, and 90ºC.

Solubility maps show that the formulation is completely soluble in all water compositions and temperatures tested (Figure 4-17). The foams obtained at ambient

conditions are less stable than the ones produced with the non-dense formulation, as demonstrated by the half-life foam curves in Figure 4-18and Figure 4-19, which was expected since this formulation is designed to best performance at high pressures. The curves also indicate that in the absence of an oil phase, the stability increased with both hardness and salinity, though the effect of the latter seems to be more pronounced. The foams of dC-40R were unstable at 60ºC, presenting half-lives shorter than 1.5h. When an oil phase was present, the foams broke within a few minutes in both temperatures.

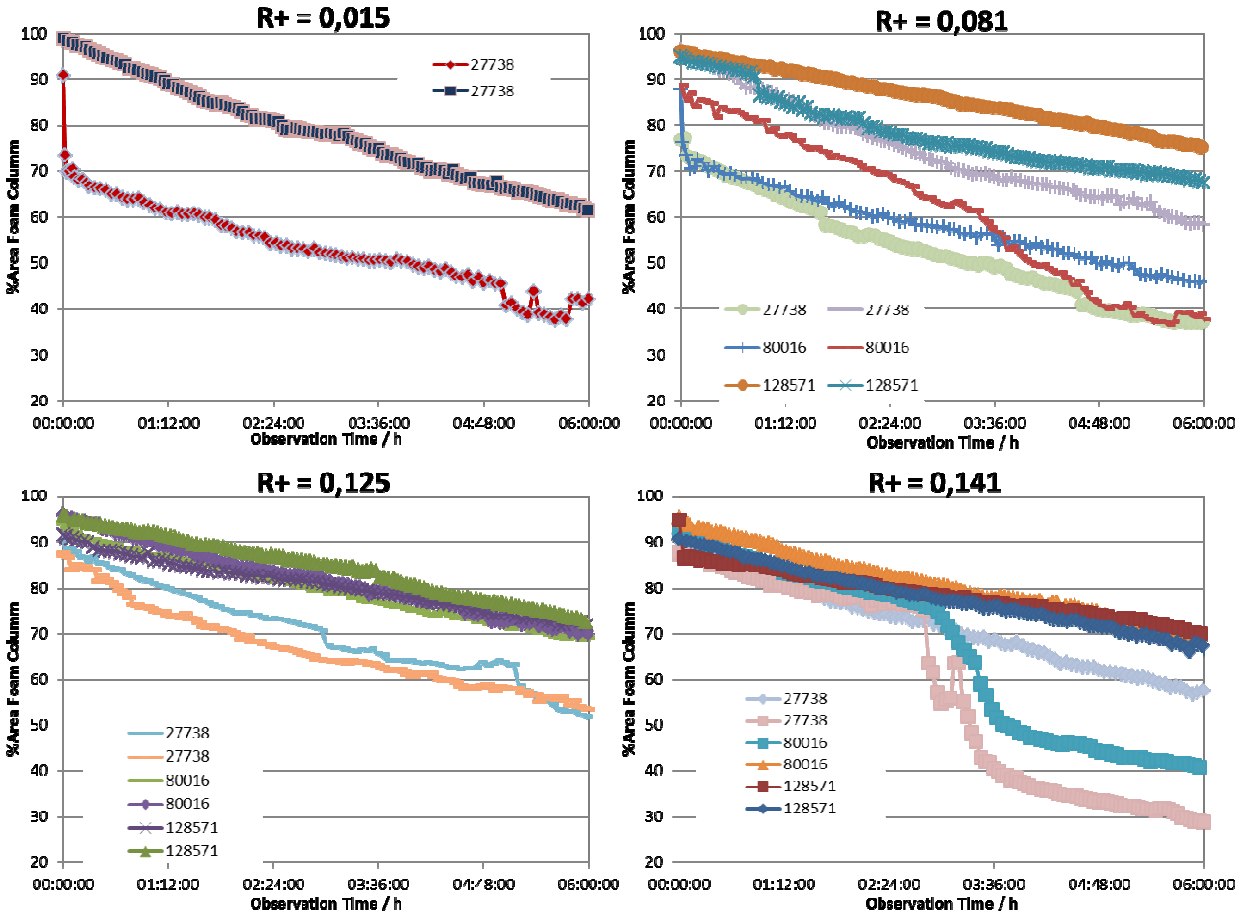

Figure 4-18: Effect of increasing salinity on foam stability of dC-40R solutions at fixed hardnesses.

High-pressure tests were tried at different water compositions, but no foam was ever obtained. According to Solvay, the dC-40R is a formulation still under development, synthesized at lab scale, and the lot that was used during these tests was reported to present some unusual results and labeled inadequate. Therefore, no further tests were done until the synthesis problems have been solved.

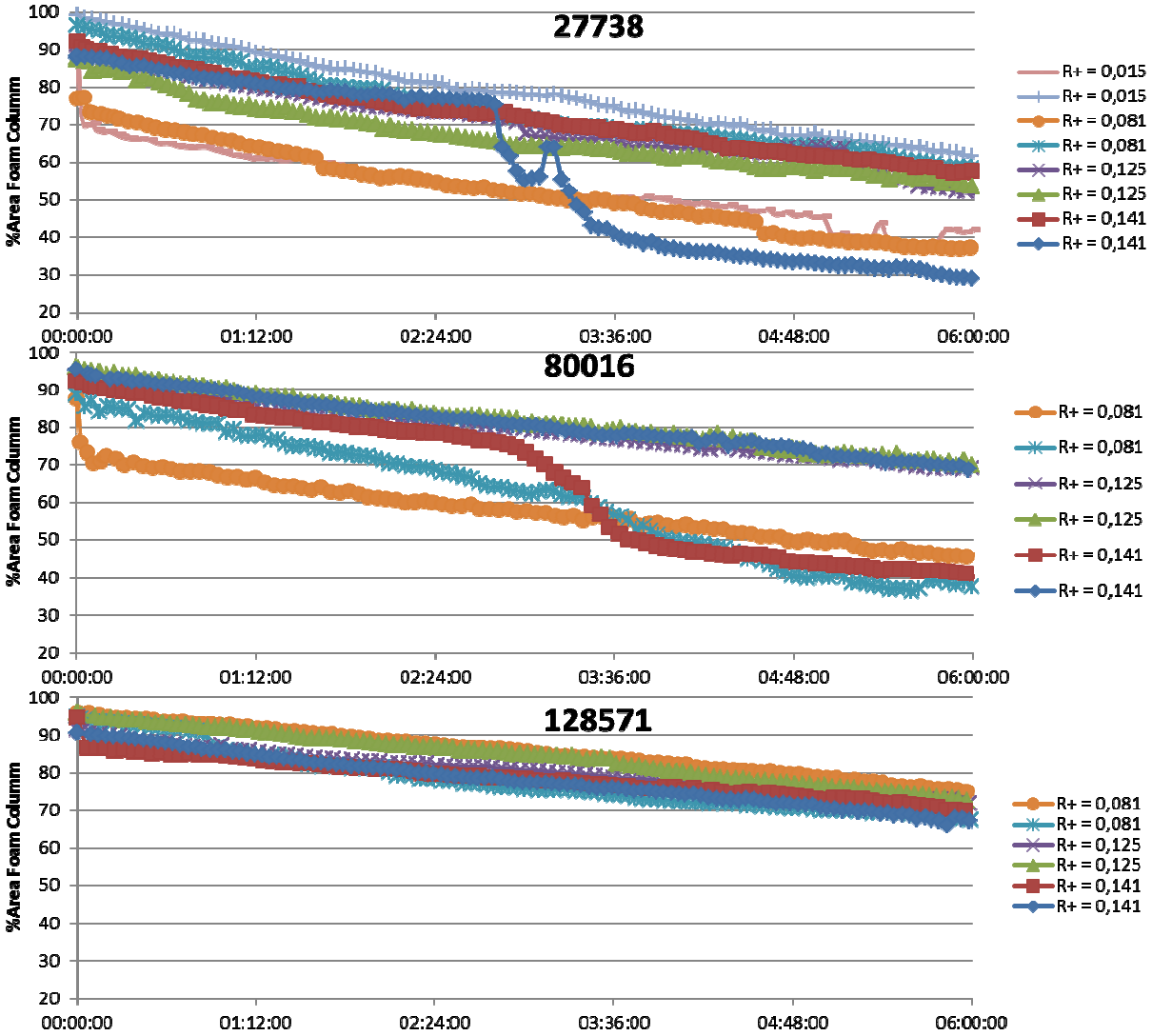

Figure 4-19: Effect of increasing hardness on foam stability of dC-40R solutions at fixed salinities.

4.4 Conclusions

A methodology that combines HTS and automated image processing was successfully applied to evaluate and select foaming agent formulations. It proved to be a powerful and valuable tool for chemical screening for EOR, allowing a great number of formulations and conditions to be rapidly evaluated and compared, demanding small samples. Additionally, it is simple enough to be easily implemented in other EOR laboratories.

The workflow resulted in the selection of a mixture of 1:3 AOS/Betaine as the non-dense formulation to be used in the petrophysical studies for the characterization of foam flow

in porous media. Since it showed good stability even at high pressures, it could be utilized in all the future experiments, should the dense formulation not be available at the time.

Once the two formulations have been selected under static conditions, the next step is to characterize and test their efficiency under dynamic conditions in coreflood tests at IFPEN.

CHAPTER 5.

TESTING FORMULATION IN MICROMODELS

5.1 Introduction

Despite all the tests made during the screening and selection of a foaming agent, they do not ensure that the selected formulation will perform well in a reservoir. The properties of the bulk foam are quite different from the properties presented by foam in porous media. Thus, the first step following the screening is to validate the formulation in a coreflood test. However, at that moment the coreflood system built for this thesis was not yet available, as its delivery was delayed by a series of events. To minimize delays on the project, the confirmation of foaming ability in porous media of the selected formulation was done in an existing micromodel system in IFPEN [127].

Micromodels are important tools in the characterization and understanding of the phenomena occurring at pore scale during EOR flooding, as they allow a direct visualization of how the multiple phases flow within the channels [19,128]. As so, they have been employed to study processes of lamellae creation and destruction, mechanisms of interaction between foam and oil and of oil recovery by foam, as well as foam flow through models with double permeability geometry [19,105,127–129]. In consequence of that, the initial goal of verifying the foaming ability of the selected formulation was expanded to also:

- Evaluate influence of flow rate and fg on the morphology of foam;
- Determine the possibility of obtaining semi-quantitative results from this setup, by comparing the behavior in micromodel experiments with what is usually observed in habitual coreflood tests.

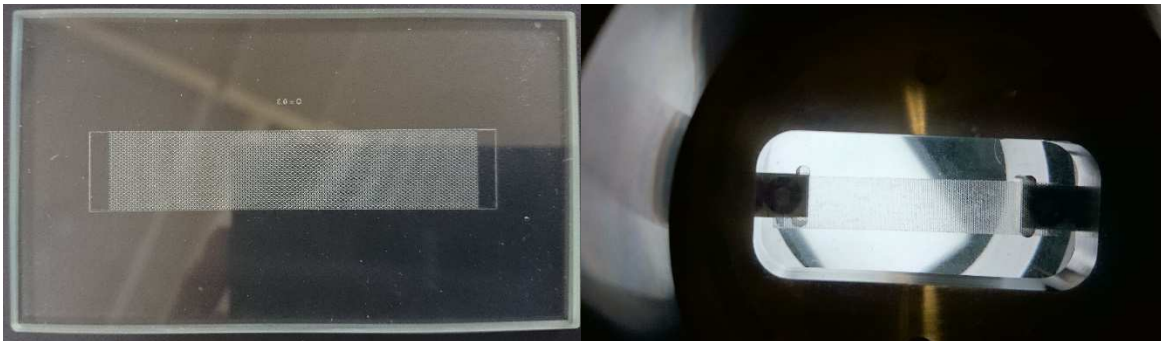

Figure 5-1: Glass Micromodel. Left: etched layer. Right: complete micromodel during flow visualization.

After rendering the setup operational again, as it had been inactive for a few months, tests were performed on a homogeneous glass micromodel (Figure 5-1) consisting of an array of circles with 0.3 mm of diameter and 0.45 mm of distance between centers. Consecutive rows of circles are shifted by 0.225 mm (0.45/2). The porous medium etched has 65.5 mm of length and 12.5mm width. The tests realized and their results are described below.

5.2 Methodology

The experiments were conducted in a high temperature/high pressure (HT/HP) micromodel system, Figure 5-2. A couple of high precision positive displacement pumps together with piston cells were used to inject the fluids in the micromodel. The piston cells were placed inside an oven for temperature control. The glass micromodel was located inside an especially designed confining cell that also regulates the temperature. This cell presents a system that keeps the overpressure (the difference between the pressure applied on the micromodel and the pore pressure inside it) at 2 bar. A stereo microscope combined with a digital camera controlled by a computer allows the visualization and registration of the fluids in the pores. The maxima operational temperature and pressure are 50ºC and 120 bar, respectively.

Figure 5-2: HT/HP Micromodel setup [127].

All tests were performed at 50°C and 80 bar, using CO2 as gas phase, and a solution of 1:3 AOS/Betaine mixture in injection water at 5000 mg/L in active matter. Flow rates of 0.2 mL/h to 40 mL/h were evaluated. Gas fractions (f_g) tested varied from 0.6 to 0.95. Pore pressure was controlled by a backpressure regulator.

5.3 Results and Discussion

The tests started by determining the best conditions for observing the morphology of the foams. Firstly, a screening of total injection flow rate was done at f_g 0.8. The images showed that the formulation presents good foaming ability, as foam quickly formed in all tested conditions. Flow rates lower than 2.5 mL/h were found inadequate for the visualization of foams since the flow proved to be intermittent at such low flow rates due to the opening and closing mechanism of the BPR. Conversely, at flow rates higher than 16 mL/h, the image/video capture became pointless due to the high speed of the bubbles. Flow rates around the middle of this range seemed to give the best conditions for visualizing foam flow.

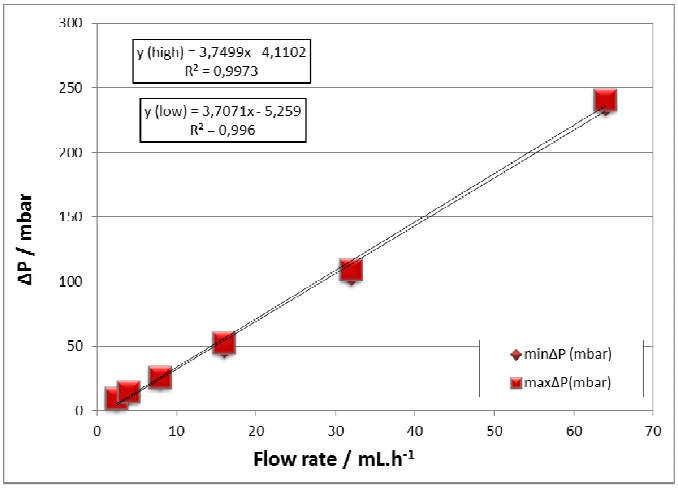

Figure 5-3: Measurements of pressure drop at various brine injection flow rates for assessing the sensitiveness of the pressure gauge connected to the micromodel system.

Consequently, foam flow was observed for f_g's from 0.6 to 0.9 at 8 mL/h total flow rate in order to evaluate the effect of the gas fraction on the morphology of the foam. Unfortunately, flow fluctuations caused a wide range of water/gas ratio inside the micromodel, preventing the visualization of a fixed f_g foam. In fact, such oscillations were so

intense that caused single phase injection (either gas or surfactant solution) for several minutes, independently of the nominal flow rates (value set on the pumps) of each phase. Therefore, no clear difference in the aspect/morphology of foams formed at different f_g's was observed. Nevertheless, it was possible to see that foam could effectively improve sweep efficiency of the gas by limiting the spread of viscous fingering, and "converting" these "fingers" into foam when they were pushed by the fluids behind.

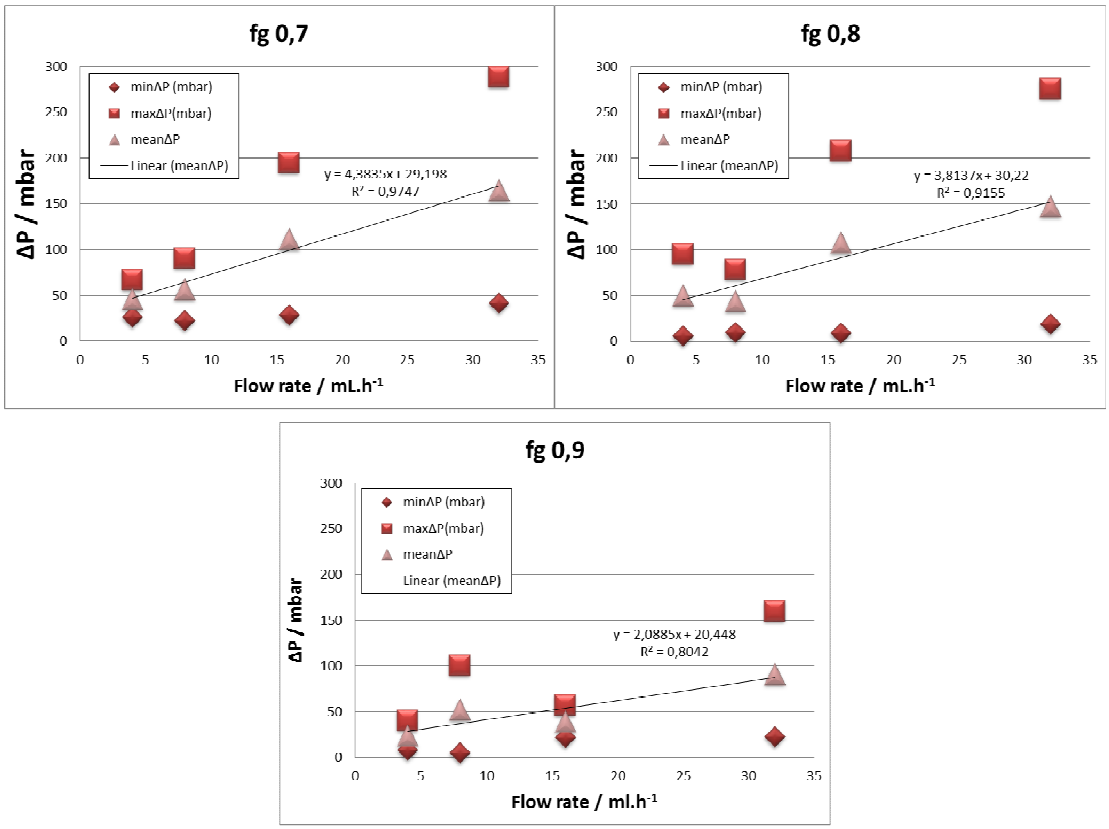

Figure 5-4: Measurements of pressure drop at a range total flow rates for CO2-brine co-injection.

Following these tests, a differential pressure gauge with a range of 0-2 bar was connected to the micromodel in order to determine if a semi-quantitative (comparative) characterization of foam rheology could be done and if the results obtained in this system could be correlated to results from coreflood tests. To accomplish that, the measure of the Mobility Reduction Factor (MRF) was performed as follows:

- Firstly, a permeability-like test (measure of the pressure drop – ΔP – at various flow rates) was conducted with the injection brine to reveal if the pressure gauge was sensitive enough for this system, Figure 5-3;

- Then, CO2 and brine (injection water composition) were co-injected at various total flow rates and at f_g's 0,7, 0,8, and 0,9, to obtain reference values of ΔP, i.e., values of ΔP0, Figure 5-4;
- Next, CO2 was co-injected with the surfactant solution at several flow rates for the three f_g's aforementioned, and their ΔP values were registered as well, Figure 5-5;
- Lastly, the MRF, defined as the ratio between ΔP_{foam} and ΔP_0, was calculated for the range of conditions analyzed, Figure 5-6.

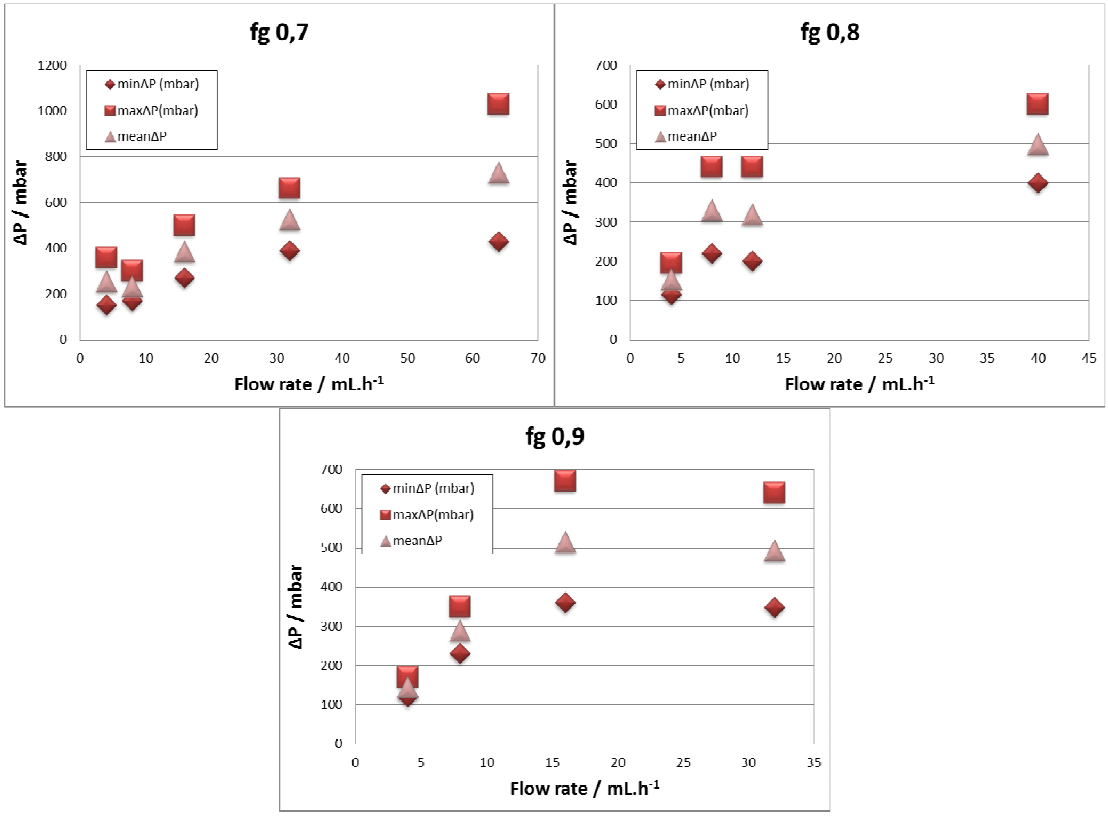

Figure 5-5: Measurements of pressure drop at a range of total flow rates for foams obtained by CO2-surfactant solution co-injection.

ΔP values usually oscillate significantly when there is a multiphase flow, like water and gas co-injection. Normally, the values of pressure drop are recorded by a computer, and then the ΔP for each set of parameters is represented by the mean value over a period of time where the oscillation was roughly uniform. Unfortunately, such acquisition system was not available, and the register was done manually based on the maximum and minimum values observed over a period of about 20 min. Though far from ideal, even such rough data allowed to visualize some patterns.

Comparing the behavior of the maximum and minimum ΔP values presented by the co-injection of CO2-brine (Figure 5-4), the minima ΔP values showed only a slight increase with flow rate, while the respective maxima had a much more significant increase. This behavior suggests that the flow under these conditions is dominated by the opening and closing of the backpressure regulator, resulting in an intermittent flow. However, when the surfactant is added to the system (Figure 5-5), such behavior is no longer observed, revealing that foam not only increased the resistance to flow within the micromodel (higher ΔP values) but also indicates that it can change how the multiphase flow occurs.

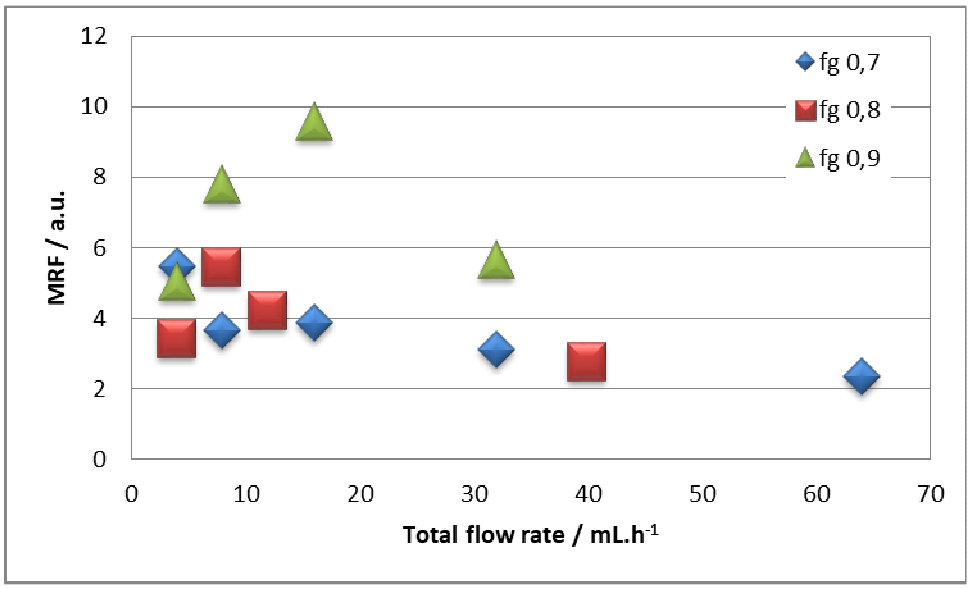

Figure 5-6: Mobility reduction factor measured in the micromodel for different foam qualities.

Figure 5-6 shows the MRF's resultant from the micromodel experiments. They were calculated using the mean ΔP values shown in Figure 5-5. The respective reference pressure drops (ΔP0) were determined using the linear regressions exhibited in Figure 5-4. The typical curve observed for corefloods presents an initial increase in MRF as strong foam forms with increasing velocities up to a maximum, followed by a decreasing profile resulting from a shear-thinning behavior. The same profile is exhibited by the results for fg 0.8 and 0.9, effectively mimicking the typical behavior on corefloods. However, the curve obtained for fg 0.7 presents a different behavior, showing only a decreasing profile. Judging by the shift in flow rate where the maximum MRF is observed for fg's 0.8 and 0.9, it could be that simply the maximum MRF for fg 0.7 occurs at flow rates lower than the range covered in this experiment. Evidently, it could as well indicate that under this condition the system studied presents a different behavior altogether. Despite that, these results support the hypothesis that

micromodels could be used to investigate the rheological behavior of foam flow in other porous media.

5.4 Conclusions and Comments:

The micromodel tests proved to be a useful tool to complement the screening and selection of foaming agents' workflow, as they permit checking their foaming ability during flow through porous media while allowing a direct observation of the foam. Additionally, the data indicates that it is possible to reproduce in the micromodel the same response displayed by foam flow during coreflood tests, suggesting that micromodel systems could improve the selection and evaluation of foaming agents, as well as the understanding of coreflood results by comparing the two systems. Naturally, simulating the rheological behavior of foam flow observed in coreflood tests using a micromodel is undeniably a complex task, and hence it should be expected that not all situations could be represented or display the same response. Though further investigation is needed, these results support the hypothesis that micromodels could be used to study the rheological behavior of foam flow in other porous media nonetheless.

Notwithstanding, the tests revealed some issues with this setup that should be addressed in order to improve the reliability of the data. Firstly, a befitted acquisition system to measure ΔP should be installed. Secondly, the cause of flow instabilities observed throughout the experiments should be inspected. Possibly the co-injection mode (geometry of the point where the phases first meet) and the BPR could be linked to such fluctuations.

CHAPTER 6. CHARACTERIZATION OF FOAM FLOW IN POROUS MEDIA

6.1 Introduction

As discussed in chapters chapter 2 and chapter 3, foam flow in porous media is a dynamic process governed by the density of lamellae n_f (also known as foam texture), which depends on the equilibrium between the creation and destruction of lamellae [15–18]. Many parameters can impact such balance, including reservoir properties (permeability, heterogeneity, wettability, pressure, temperature, mineralogy), reservoir fluids (nature, composition, and saturation), injection conditions, shear rate and surfactant (nature, concentration). As a result, many studies have been done at different scales to investigate different aspects of foam dynamics in porous media in order to understand the impact of each parameter [11,19–21].

Despite the huge volume of studies, foam flooding it is still a developing technology. Major uncertainties remain regarding the rheology and transport of foam in porous media, as much of the available data were obtained in different boundary conditions. Thus, a direct comparison is often not feasible, making it hard to explain contradicting results and hindering the development of a physical model. Consequently, current models are heavily dependent on laboratory results to calibrate their fitting parameters [22]. This dependence makes models less reliable for full-field scale predictions, especially if the results are not representative of the real conditions [21,23,24]. Since the success of foam applications relies on the ability to predict accurately their performance under field conditions, the lack of a physical model is one of the biggest challenges that deter the use of foams in the field.

To overcome this challenge, it is vital to have more experimental studies of foam flow for single formulations over a range of foam qualities and different permeabilities, as pointed out by Farajzadeh et al [130]. The need of more experimental data to advance simulation has also been highlighted by Ma et al. [22] in their recent review on foam simulation.

Thus, the aim of the present work is to advance our understanding of the physics underlying the rheological behavior of foam flow in porous media. To this end, we conducted a systematic experimental study of the impact on foam apparent viscosity of three determining and operational parameters: foam quality (f_g), flow rate (interstitial velocities), and initial permeability. At the best of our knowledge, no such extensive experimental study has been performed before using the same system and under same well-controlled experimental

conditions for consolidated porous media. We show that our data agree with the current understanding of foam flow and then we present an original form to treat coreflood results to obtain experimentally determined expressions for the foam apparent viscosity as a function of the parameters studied. By this methodology, we were able to achieve a foam flow master curve. Finally, we discuss the experimental correlation found and how this methodology may be used to advance foam simulation.

6.2 Materials and Methods

6.2.1 Materials:

Brine solution used was synthetic desulfated sea water (DSW), since its ability to form a stable foam at high pressure both in bulk and in porous media was verified during the experiments discussed in sections 4.2.4 and chapter 5. It has a salinity of 28,112 mg/L (NaCl eq.) and total hardness of 134 mg/L. The brine was prepared by dissolving 27,738 mg/L of NaCl, 607.4 mg/L of $CaCl_2.2H_2O$, and 38.6 mg/L of $MgCl_2.6H_2O$ in deionized water. The brine was filtered with a 0.22µm membrane and de-aerated before injection. The gas phase used in this work was a mixture of 80% of CO_2 and 20% of methane. Table 6.2-1 presents some thermodynamic properties of this gaseous mixture.

Table 6-1: Thermodynamic parameters of the gas 80% CO2 + 20% CH4.

Critical Point	**Properties @ 80 bar, 60°C**		
P_c = 84.28 bar	**Density (kg/m^3)**	**Viscosity (Pa.s)**	**Compressibility factor Z**
T_c = 287.46 K	147.82	1.94×10^{-5}	0.751

The surfactant formulation used was the one selected in chapter 4 and chapter 5. The surfactant solution was prepared by firstly dissolving the surfactant formulation in deionized water at a concentration of 10,000 mg/L. It was then mixed with an equal volume of brine, previously filtered and deaerated, containing the double concentration of the salts used for the DSW preparation, thus resulting in a solution of 5000 mg/L of surfactant in DSW.

Due to the presence of CO_2 in the selected gas mixtures, plugs of Fontainebleau sandstone were chosen as the porous media. Carbonate cores, though more representative, would undergo some dissolution during the tests, altering the permeability and, in extreme

cases, even creating macroscopic channels. These alterations would prevent a proper characterization of the rheology of foams. The samples used had a diameter of 2.5 cm and lengths between 8 and 15 cm. Table 6.2-2 presents the properties of the selected plugs. This diameter was chosen to reduce the porous volumes of the samples, thus increasing the autonomy of the coreflood system. As will be explained in section 6.2.3, foam tests are limited by the volume of the gas piston cell, and because of the hysteresis presented by some foam systems, they cannot be interrupted. The smaller the porous volume, the longer a test can last, thus reducing the chances of losing an experiment thanks to insufficient gas. On the other hand, the smaller diameter limits the injection at interstitial velocities representative of reservoir conditions, as they require very low flow rates. This compromise was considered for the selection of the dimensions of the cores.

Table 6-2: Petrophysical properties of the selected plugs

Core #	Diameter (cm)	Length (cm)	Porosity (%)	K (mD)	Porous Volume (mL)
1	2.461	15.380	10.91	66	7.985
2	2.460	13.130	11.76	120	7.338
3	2.474	8.844	14.29	381	6.074

6.2.2 Experimental Setup:

A coreflood setup was specifically designed for foam studies, based on the experience acquired by IFPEN in previous foam-related projects. Figure 6-1 shows the coreflood setup used. It consists of a Hassler type core holder vertically positioned inside an oven, with injection at the top. The injection head contains two entry points (one for all liquid phases, and the other for gas) and a spiral diffuser at the point of contact with the rock sample. Gas was injected at the center, and the liquid phase at the edge and the gas and brine (or surfactant solution) met at the diffuser. All lines and valves are in Hastelloy to withstand the corrosive conditions derived from CO_2-brine co-injection. The maximum operating conditions are 70°C and 250 bar.

The injection system comprised a pair of dual-piston pumps Quizix-6000 remotely controlled by a computer. One of them was dedicated to brine and surfactant solution injection, while the other was used to inject the gas mixture, which was loaded in a piston cell placed inside the oven.

Differential pressure values were measured by three independent systems to cover all possible ranges of ΔP. Two systems comprised differential pressure transducers connected at each end of the coreholder, one with a pressure range of 0-400 mbar and the other with 0-20 bar. The third system comprised two relative pressure transducers, each placed at one end of the coreholder.

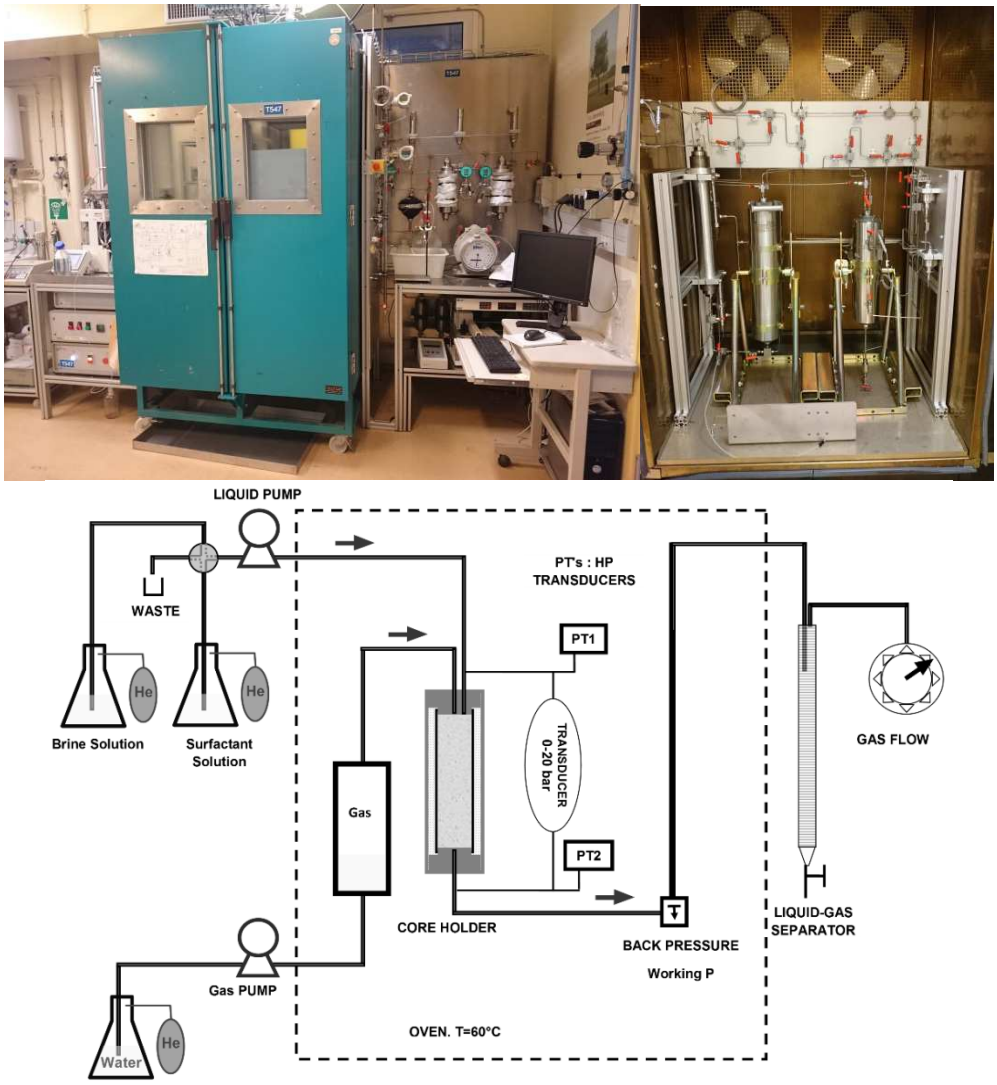

Figure 6-1: Coreflood setup. Upper left- overview; upper right – internal view (coreholder and piston cells); lower image – simplified scheme.

Pore pressure was controlled by two dome-loaded back pressure regulators (BPR) connected in series and placed inside the oven to minimize interference due to lab temperature oscillations. This configuration also helps to attenuate the oscillations in ΔP usually observed three-phase flow. A volumetric burette connected at the exit of the BPR´s worked as -phase

separator. A gas meter attached to the upper exit of the burette measured the produced gas flow.

6.2.2.1 Plug preparation:

When working with gas injection, especially CO_2, the gas may diffuse through the Viton® sleeve and cause a series of issues, like loss of control of confining pressure and/or damaging rubber seals, joints, O-rings, and even the Viton sleeve itself. Based on Petrobras recommendations derived from its experience in WAG essays, and the experience of IFPEN, the following protocol was implemented:

- Firstly, the plug is wrapped with two layers of Teflon® tape, rolled in opposite directions (ascending and descending), and then placed on a support between the injection head and the exit rod;
- Then, it is covered by a layer of aluminum foil made of multiple bands superimposed and fixed in place with adhesive tape;
- Next, an additional layer of Teflon® overlays the aluminum foil, followed by a layer of adhesive tape, which covers all the others and fix them in place;
- Lastly, a small portion of silicone grease is spread over the adhesive tape layer and inside a Viton sleeve, so that the sleeve can slide more easily over the plug.

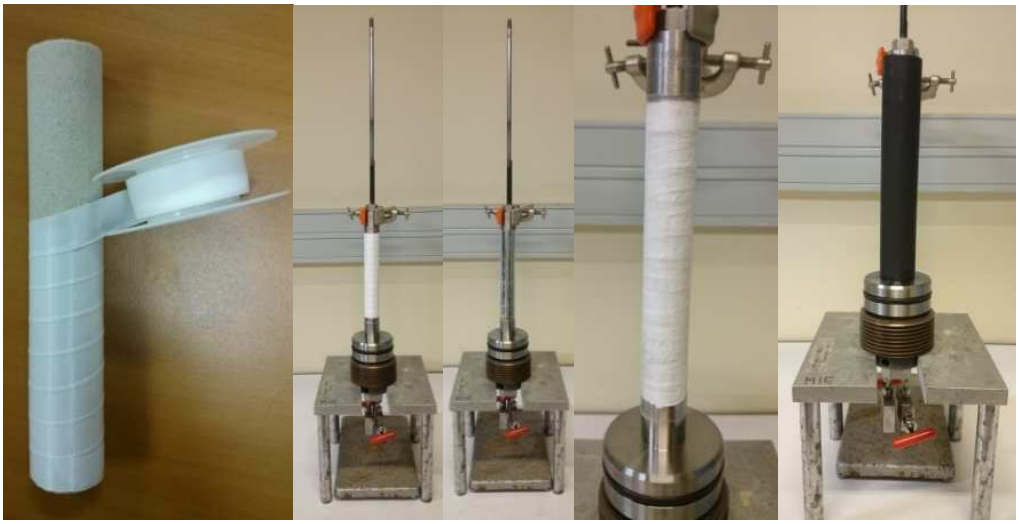

Figure 6-2: Step by step illustration of the procedure for preparing a plug for a coreflood test.

Figure 6-2 illustrates this procedure. After that, the plug is ready to be inserted in the coreholder. Once all connections are properly tightened, the confining pressure may be applied.

6.2.2.2 Plug saturation and determination of porous volume:

Once the confining pressure is applied, an ultra-vacuum pump is connected to both the top and bottom of the coreholder using a plastic line with a T connection and calibrated volume. Vacuum is applied for 3h to 6h. Meanwhile, the rest of the coreflood setup is saturated with a 5 g/L of NaCl brine previously de-aired.

Then, the bottom of the coreholder is connected to the water injection system, while the two entries in the top are connected to the vacuum pump. Vacuum is applied still for a few minutes, and then a valve between the plastic line and the pump is closed. The cumulative injected volume on the water injection pump is set to zero. The injection mode is set to constant pressure delivery, and the pressure is set to 5 bar. The bottom valve is then opened and brine starts to fill the plug. When then injection stops and pressure is stable, the plastic line is checked for air bubbles. If no bubbles are observed, the saturation was successfully executed.

The total injected volume indicated on the pump is noted. The porous volume is determined by subtracting the total dead volume (plastic line, injection head connections, and exit rod) from this value. The empirical value is confronted with the theoretical value determined geometrically in order to check its accuracy. The theoretical volume is calculated by equation 6-1:

6-1.
$$PV = \left(\pi \times \frac{D^2}{4} \times L\right) - \frac{m}{\rho}$$

Where PV is the porous volume, D is the diameter of the plug, L is its length, m is its mass, and ρ is the density of silica (2.64 $g.cm^{-3}$).

6.2.2.3 Permeability measurement:

Initially, both the desired temperature and pore pressure are set. Pressurization of the system is conducted by gradually increasing the pressure in the dome of the BPR's while a 5 g/L of NaCl de-aired brine is injected at a flow rate of 300 mL/h. During this procedure, the injection head is used as a bypass in order to avoid any issues with the core sample.

Once both pressure and temperature are stable, the bypass is closed and brine starts to flow through the core. The brine is then changed for the same water composition that will be employed in experiments that will be performed on the plug, and the system is completely saturated with the new brine. Five flow rates within the range of interest, preferably equidistant, are chosen, and a stair-like injection sequence is initiated, from the lower to the higher flow rate and the respective pressure drops are measured. Each step lasts for at least 20 minutes. Subsequently, the sequence is inverted to confirm the values and to check if there is any kind of hysteresis (which would indicate a problem). During the second part, each step lasts no less than 10 minutes.

The values of flow rate and pressure drop are plotted and the linear correlation is confronted with the Darcy's Law to calculate the value of permeability.

6.2.3 Experimental Procedure:

All experiments presented here were done at 60°C and pore pressure of 80 bar. The experiments were conducted at fixed foam qualities and increasing interstitial velocities. For laboratory work, in-situ foam generation by co-injection mode is preferred to alternate injection, which is the usual operating mode for the application. Co-injection mode allows reaching a steady state flow in the core, while in the alternate mode the results are strongly determined by the core length. Thus, after determining the porous volume and the permeability of the plug, the tests began with the co-injection of brine and gas at the selected f_g and the initial flow rate until the pressure drop is stable. At this point, the 4-way valve was switched from brine to surfactant solution injection.

Figure 6-3 presents a typical result obtained following this procedure. The accumulated produced gas volume is measured at ambient conditions and then converted to

the conditions at the entry of the plug. The high number of injected pore volumes needed to achieve steady state is a consequence of foam generation and gas compression in the system. When the foam starts to form, the entrance pressure increases, and hence the entire gas piston cell needs to be pressurized. Thus, the effective gas flow rate entering the plug (q_g^{eff}) varies during the transient period due to gas compression in the piston cell according to equation 6-2. This behavior is supported by the changing slope of the curve of the accumulated volume of produced gas in Figure 6-3.

6-2. $$q_g^{eff} = n_0 \frac{dv}{dt} + q_{pump}$$

Where n_0 is the initial number of moles, υ is the molar volume of the gas at (P, T), and q_{pump} the displacement pump flow rate. Co-injection of surfactant solution and gas was maintained until pressure drop was stable and the slope of the produced gas curve returned to the original value, i.e., previously to surfactant injection, as shown by the dashed lines in Figure 6-3. This approach ensured that the system was at a steady state at the same fg as injected, and all saturations were constant.

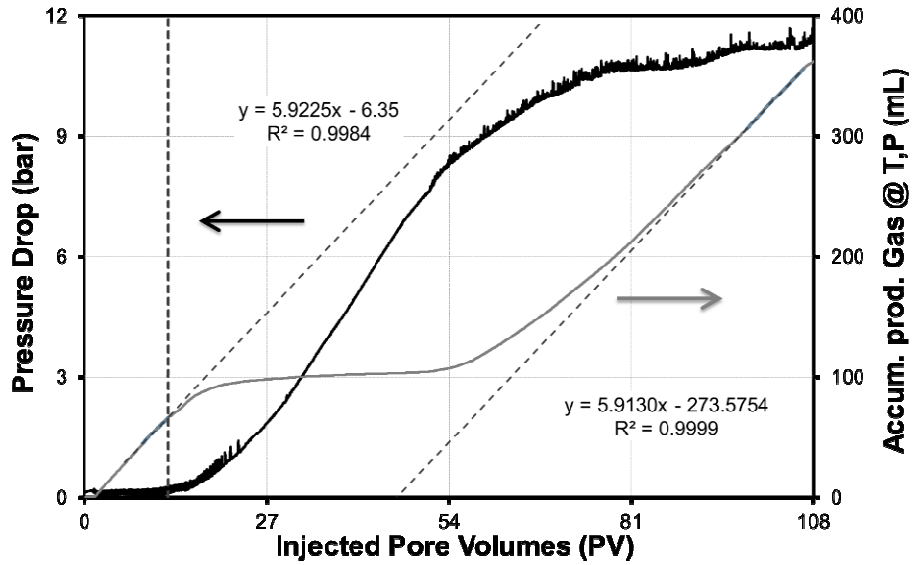

Figure 6-3: Typical result obtained in this study. The pressure drop and accumulated produced gas curves obtained for co-injection at fg 0.7 and total flow rate of 10 mL/h in core #1, showing the formation of foam and the resulting steady state. The vertical dashed line marks the arrival of the surfactant solution to the plug. The diagonal dashed lines show that gas flow rate is the same before and after the transient period.

For each f_g of interest, firstly a sequence of 3-4 increasing total flow rates was established. Each step of interstitial velocity lasted until steady state was achieved. At the end

of the sequence, the injection was reduced to the first (lowest) value of flow rate to verify if the foam flow presented hysteresis feature. The injection was then maintained for at least 20 PV. During each test, pressure drop and fluid (gas and water) production were monitored.

After each f_g was completed, the plug was restored and the permeability was checked before changing to the next f_g.

6.2.4 Summary of experiments

To compare the results from different permeabilities, the total flow rates were adjusted so that the interstitial velocities were kept the same over each plug. Table 6.2-3 presents a summary of the experiments discussed here, with the equivalent flow rates used for each plug for a given interstitial velocity.

Table 6-3: Summary of investigated interstitial velocities and correspondent flow rates of gas and surfactant solution used for each experiment.

Core #	Exp #	f_g	Flow rates of surfactant and gas (mL/h) at total interstitial velocities											
			7.6 ft/d		15.2 ft/d		38.0 ft/d		76.0 ft/d		92.9 ft/d		152.2 ft/d	
			Q_L	Q_g	Q_L	Q_g	Q_L	Q_g	Q_L	Q_g	Q_L	Q_g	Q_L	Q_g
1	1	0.4			6.0	4.0	15.0	10.0	30.0	20.0				
	2	0.6	2.0	3.0	4.0	6.0	10.0	15.0	20.0	30.0				
	3	0.7			3.0	7.0	7.5	17.5	15.0	35.0				
	4	0.8	1.0	4.0	2.0	8.0	5.0	20.0	10.0	40.0				
	5	0.9			1.0	9.0	2.5	22.5	5.0	45.0				
	6	0.9			1.0	9.0	2.5	22.5	5.0	45.0				
2	7	0.4			6.5	4.3	16.2	10.8	32.4	21.6			64.8	43.2
	8	0.6	2.2	3.2	4.3	6.5	10.8	16.2	21.6	32.4			43.2	64.8
	9	0.7	1.6	3.8	3.2	7.6	8.1	18.9	16.2	37.8			32.4	75.6
	10	0.8			2.2	8.6	5.4	21.6	10.8	43.2			21.6	86.4
3	11	0.4			8.0	5.3	19.9	13.3	39.8	26.5			79.6	53.0
	12	0.4			8.0	5.3	19.9	13.3	39.8	26.5			79.6	53.0
	13	0.6			5.3	8.0	13.3	19.9	26.5	39.8			53.0	79.6
	14	0.7			4.0	9.3	9.9	23.2	19.9	46.4			39.8	92.8
	15	0.8			2.7	10.6	6.6	26.5	13.3	53.0			26.5	106.1
	16	0.9			1.3	11.9	3.3	29.8	6.6	59.7	8.1	72.9	13.3	119.3

6.3 Results and Discussion

Table 6.3-1 presents the results of the experiments summarized in Table 6.2-3. To evaluate the impact of foam quality (f_g), interstitial velocity ($v_{interstitial}$), and permeability on

foam flow behavior, the results were expressed as foam apparent viscosity (μ^f_{app}), equation 6-3. Experiments #5 and 6#, and experiments #11 and #12 are duplicates used to check the consistency of the data acquired. Foam experiments are known for giving considerable scatter data, as mentioned by Gauglitz et al. [93]. Although some scatter was noticed in the lowest interstitial velocities when comparing the value from the direct run and the hysteresis, the results were very consistent.

6-3.
$$\mu^f_{app} = \frac{K\Delta P_{foam}}{v_t L}$$

Each line in Table 6.3-1 represents one experiment. Data was obtained following the sequence of interstitial velocities from left to right, and the last two columns present the results of the hysteresis test. In the following sessions, we discuss the impact of each key parameter on μ^f_{app} separately at first. Then, we introduce an approach to combine all these parameters and their impacts in a single variable, shear rate.

Table 6-4: Foam apparent viscosity obtained for the experiments listed in Table 2.

Core #	Exp #	f_g	Foam apparent viscosity μ^f_{app} (mPa.s) @ $v_{interstitial}$							
			7.6 ft/d	15.2 ft/d	38.0 ft/d	76.0 ft/d	92.9 ft/d	152.2 ft/d	Hysteresis data	
									15.2 ft/d	7.6 ft/d
1	1	0.4		48.12	23.45	12.88			51.72	
	2	0.6	94.04	46.41	26.93	16.08				70.34
	3	0.7		60.65	33.22	20.01			59.43	
	4	0.8	98.08	68.03	41.41	25.77				95.80
	5	0.9		69.65	45.30	27.69			66.98	
	6	0.9		68.60	42.67	24.74			66.67	
2	7	0.4		68.66	32.50	18.22		10.13	66.32	
	8	0.6	80.91	72.14	37.98	23.65		14.40		94.29
	9	0.7	73.12	48.85	36.92	21.81		12.38		73.21
	10	0.8		51.53	43.66	26.69		15.86	42.00	
3	11	0.4		96.54	58.82	32.61		18.71	122.24	
	12	0.4		119.83	58.33	32.39		18.41	119.18	
	13	0.6		116.53	62.23	40.43		25.75	131.05	
	14	0.7		103.00	45.51	29.32		20.08	98.75	
	15	0.8		105.75	48.95	26.99		15.12	111.31	
	16	0.9		1.03	1.41	22.77	23.30	15.29	87.37	

6.3.1 Impact of foam quality

Gas fraction or foam quality (f_g) is the main parameter used to characterize the rheological behavior of foams in porous media and establishes two flow regimes: low and high quality. The transition between them occurs at an optimal f_g (f_g*), where maximum

pressure drop is achieved. Figure 6-4 presents the data from Table 6.3-1 as diagrams of Osterloh & Jante for each plug. In these plots, the vertical portion of the isobar curves represents the high-quality regime, while the horizontal region stands for the low-quality regime. The f_g at the transition between low and high-quality regimes is the optimal foam quality (f_g*) and is clearly visible for the plugs of 122 mD and 381 mD. For 66 mD, however, our data covers only the low-quality regime, and all that can be concluded is that $f_g^* \geq 0.9$.

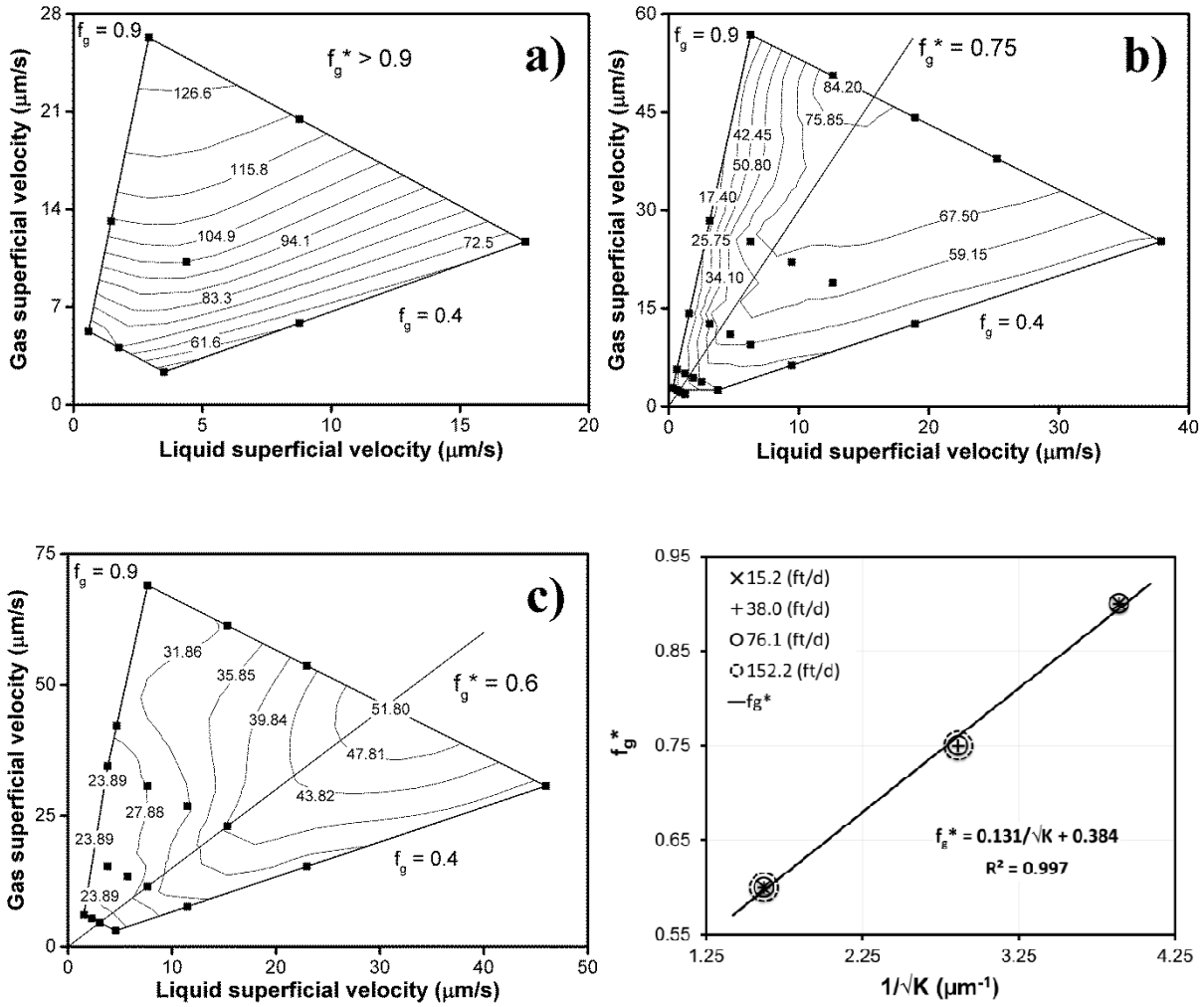

Figure 6-4: Experimental determination of optimal foam quality (f_g*) by diagrams of Osterloh & Jante. a) Core1 = 66 mD; b) Core2 = 122 mD; c) Core3 = 381 mD; d) Experimental correlation between f_g* and permeability [131].

The impact of permeability on optimal foam quality is better visualized in Figure 6-4d, which shows that f_g* is inversely proportional to the square root of the permeability ($f_g^* \propto 1/\sqrt{K}$). Our results agree with Moradi-Araghi et al. [58], who also found that f_g* decreases with increasing permeability (though the relation between f_g* and K is not the same as we

found). Interestingly enough, Farajzadeh et al. [130] and Khatib et al. [70] found a linear correlation between P_c^* and $1/\sqrt{K}$. However, it is not yet clear if there is any connection between our results and the findings of their works.

Table 6.3-2 presents the corresponding values of f_g^* for the plugs at each total interstitial velocity. According to Figure 6-4 and Table 6.3-2, the interstitial velocity had no visible effect on the f_g^*. The impact of interstitial velocity on the rheological behavior of foam flow is further discussed below.

Table 6-5: Effect of interstitial velocity and permeability on the optimal (transition) foam quality (f_g^*).

$K_{initial}$ (mD)	f_g^*			
	15.2 ft/d	**38.0 ft/d**	**76.1 ft/d**	**152.2 ft/d**
66	0.90	0.90	0.90	
120		0.75	0.75	0.75
381	0.60	0.60	0.60	0.60

6.3.2 Impact of interstitial velocity

The impact of interstitial velocity (flow rate) on foam rheology was investigated in numerous studies as well, both experimentally and theoretically [58,92,93]. There is a general agreement that at the low-quality regime, the foam is shear thinning. while the rheology in the high-quality regime is yet to be elucidated, with diverse behaviors reported in the literature, most probably due to the instability of foam in this regime [19]. For example, Rong et al. [132] performed an extensive study in sandpacks of permeabilities between 5 D and 210 D and observed that, in the high-quality regime, foam could either be shear-thinning, Newtonian or even shear-thickening. However, details about the conditions where each behavior was observed are not furnished, nor are all dataset and correlations found.

Figure 6-5 presents the apparent viscosities of foams as a function of interstitial velocity from some experiments performed with core #1 and core #3 to demonstrate the rheological behavior observed in the low and high-quality regime, respectively. Foam apparent viscosity decreased as interstitial velocity increased for the experiments in Figure 6-5a, evincing the characteristic shear thinning behavior expected for the low-quality regime [17,19]. Additionally, μ^f_{app} exhibited a generally increasing trend with f_g, a typical behavior of

this regime as well. Neither foam generation nor hysteresis was observed in any of these curves. All experiments achieved strong foam state even for the lowest interstitial velocity tested.

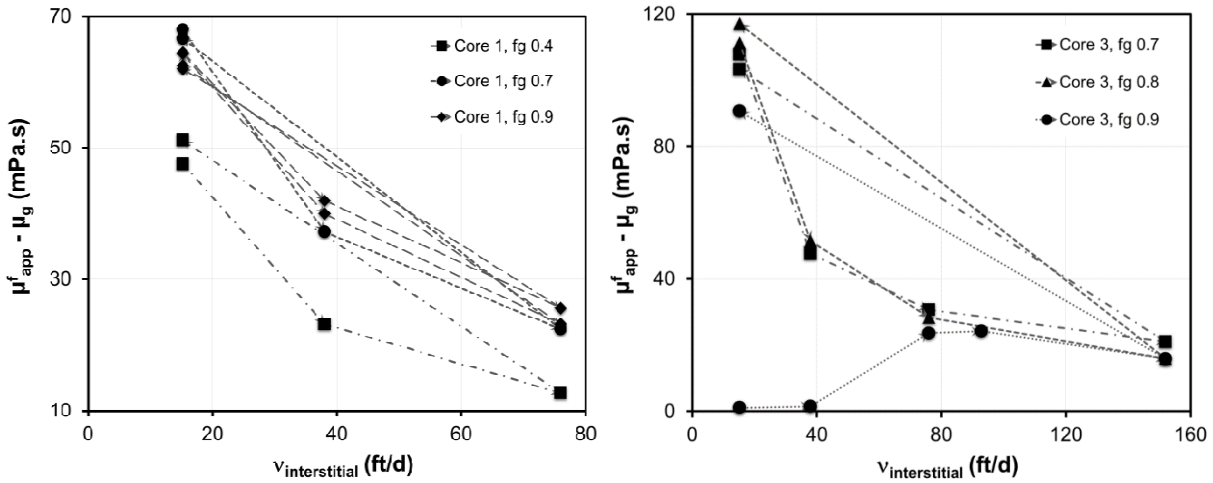

Figure 6-5: Apparent foam viscosity as a function of interstitial velocity for foam co-injection. a) Low quality regime (core #1 experiments 1, 3, 5 and 6); b) High quality regime (core #3 experiments 14–16). The dotted lines and arrows are meant only as visual aids to help to show the sequence at which the data were obtained.

The behaviors observed in the high-quality regime are represented in Figure 6-5b. For experiments 14 and 15 (f_g's 0.7 and 0.8), μ^f_{app} decreased as interstitial velocity increased, denoting shear thinning behavior like it was observed in the low-quality regime. Moreover, these curves presented neither foam generation nor hysteresis as well. Conversely, experiment 16 (f_g 0.9) exhibited a rheological profile corresponding to week foam at low $\nu_{interstitial}$, then a weak-to-strong foam transition (foam generation) followed by a shear thickening region up to a maximum in μ^f_{app} and, finally, shear thinning behavior. This experiment also presented a huge hysteresis (from 1.03 mPa.s when surfactant solution first reached the core, to 87.37 mPa.s after foam flow at high interstitial velocity). An equivalent behavior was observed for f_g 0.9 in core #2 (data not shown).

Multiple behaviors have been reported in the literature for the high-quality regime [11,19,132]. In our study, data obtained for strong foam in this regime presented shear thinning behavior. Gauglitz et al. [93,133] demonstrated that the minimum interstitial velocity for foam generation can be very low when CO_2 is a major component in the gas injected, but the onset of foam generation increases with f_g. This combination of factors may explain why foam generation was observed only at the highest f_g tested. Likewise, the absence of

hysteresis in the curves of Figure 6-5, for both low and high quality, agrees with the findings of Gauglitz et al. [93]. They saw no hysteresis while foam injection was kept within the conditions for strong foam. Hysteresis was only observed when, after reaching the strong foam regime, injection went back to flow conditions before the onset of strong foam formation (region of weak foam), as was the case for experiment 16.

Next, we briefly discuss the observed impact of permeability on strong foam viscosity.

6.3.3 Impact of permeability

The ability of foams to present higher viscosity (reduce gas mobility more) at higher permeabilities is at the core of the importance of foam technology. Yaghoobi and Heller [59] named this property selective mobility reduction (SMR). This effect has been verified in multiple studies both in sand packs, micromodels and corefloods [58,60–63]. Bertin et al. [63] performed a CT-scan study of foam generation and propagation in a heterogeneous system consisted of a Fontainebleau sandstone core encased in Ottawa sand. The permeability contrast between the core and the sand was of 67 to 1. They observed that foam front advanced at the same rate in both zones when they were in capillary contact. When cross flow was not possible, foam front was actually faster in the low permeability zone, evincing the diversion property of foams. The diversion ability has also been showed to work in fracture systems by Hirasaki et al. [62], and more recently, by Gauteplass et al. [60] in both micromodel and 2-D plate systems. However, the effect is not always present. For instance, Tsau and Heller [134] showed that SMR is affected by the surfactant formulation and surfactant concentration.

Figure 6-6 presents the impact of permeability on the foam apparent viscosity for foam flow in the low-quality regime. In these plots μ^{f}_{app} increased linearly with the square root of K, thus demonstrating that foam is more effective in reducing gas mobility in higher permeabilities. This trend was independent of both interstitial velocity and foam quality. The shear thinning behavior discussed in the previous session is also evident here.

The effect of permeability is not presented graphically for the high-quality regime as the data is only available for two permeabilities. Nevertheless, the effect can be deduced from data in Table 6.3-1. Foam apparent viscosity was also observed to increase with permeability,

but at a lesser degree than in the low-quality regime. For instance, at f_g 0.4 and $v_{interstitial}$ 38 ft/d, μ^f_{app} increased 81% from 122 mD to 381 mD, while at f_g 0.8 the increase was 12%. Additionally, the correlation between μ^f_{app} and K varied with both foam quality and interstitial velocity. Therefore, foam viscosity is more sensitive to permeability in the low quality than in the high-quality regime. These findings agree with conjectures and results of Alvarez et al. [17] and of Rong et al [132].

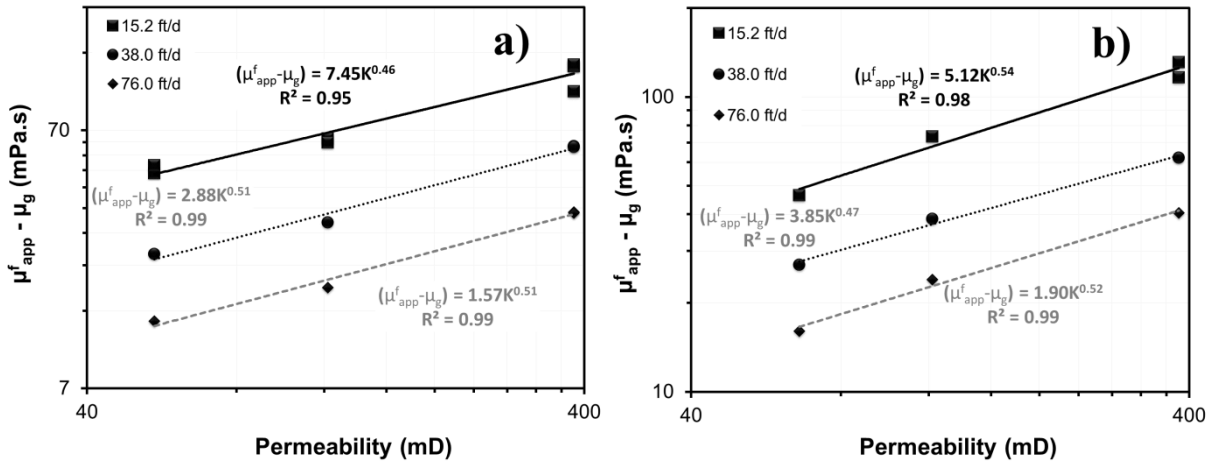

Figure 6-6: Experimental correlation between foam apparent viscosity and permeability at fixed foam quality. a) f_g= 0.4; b) f_g=0.6.

The previous sessions showed that the impact on foam apparent viscosity of each of the key parameters depends on the flow conditions imposed by the other parameters. In order to tackle the complex behavior of foams, we present in the following session an approach that allows us to combine the effect of all the above parameters and hence handle their interdependence.

6.3.4 Combined impact of key parameters

The impact of each parameter that affects foam flow is usually determined by fixing all other parameters, thus assuming that they are independent of each other. However, the multiple trends observed in the literature, with results sometimes in direct opposition, shows that this is not the case. As a non-Newtonian fluid, a better way to evaluate the rheological behavior of foam flow is to analyze the results as a function of shear rate. The shear rate computes the combined impact of permeability, interstitial velocity, and pore structure. To the

best of our knowledge, this is the first time that this approach is used to analyze coreflood results for foam flow.

We analyze our data as a function of shear rate based on an experimental correlation obtained from the work of Chauveteau & Zaitoun [135], which is valid for flow in homogenous sandstones and sandpacks. According to the authors, the shear rate in sandstones is given by equation 6-4:

6-4. $$\dot{\gamma} = \alpha \times 4\, v_{interstitial} \times \sqrt{\phi/8K}$$

Where α is a scaling factor. The value of α is given by the experimental correlation obtained from their data, Figure 6-7, and accounts for the pore structure.

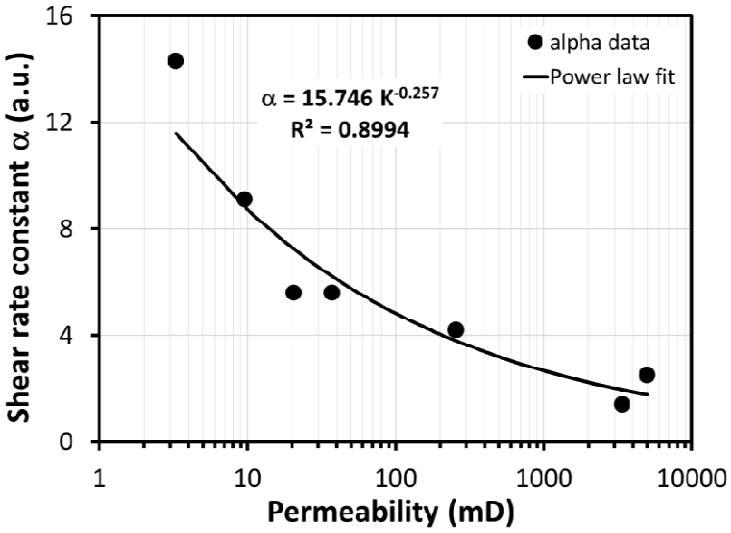

Figure 6-7: Empirical correlation for the scaling factor α obtained from the data presented by Chauveteau & Zaitoun [135].

The simplest rheological model to describe the shear thinning behavior showed by foams in our experiments (evidenced in Figure 6-5) is the Ostwald-de Waele power law, equation 6-5:

6-5. $$\mu = C\dot{\gamma}^{n-1}$$

Where μ is the viscosity, C is the flow consistency index, $\dot{\gamma}$ is the shear rate, and n is the flow behavior index. For shear thinning behavior, n<1. Figure 6-8 shows the strong foam apparent viscosity as a function of the shear rates calculated as indicated in the Appendix.

Interestingly, when μ^f_{app} was plotted as a function of shear rate, all data in the shear thinning behavior of strong foam, regardless of foam quality, permeability, and even foam regime, collapsed in a single curve. Though data is a little scattered (as we are limited by the precision of the correlation for shear rate in Figure 6-7), the trend is clear. The master curve of foam viscosity as a function of shear rate obeys a power law with a universal exponent of -2/3 (thus, n = 1/3), as showed in equation 6-6:

6-6. $$\left(\mu^f_{app} - \mu_g\right) = 2535.27\dot{\gamma}^{-0.63}$$

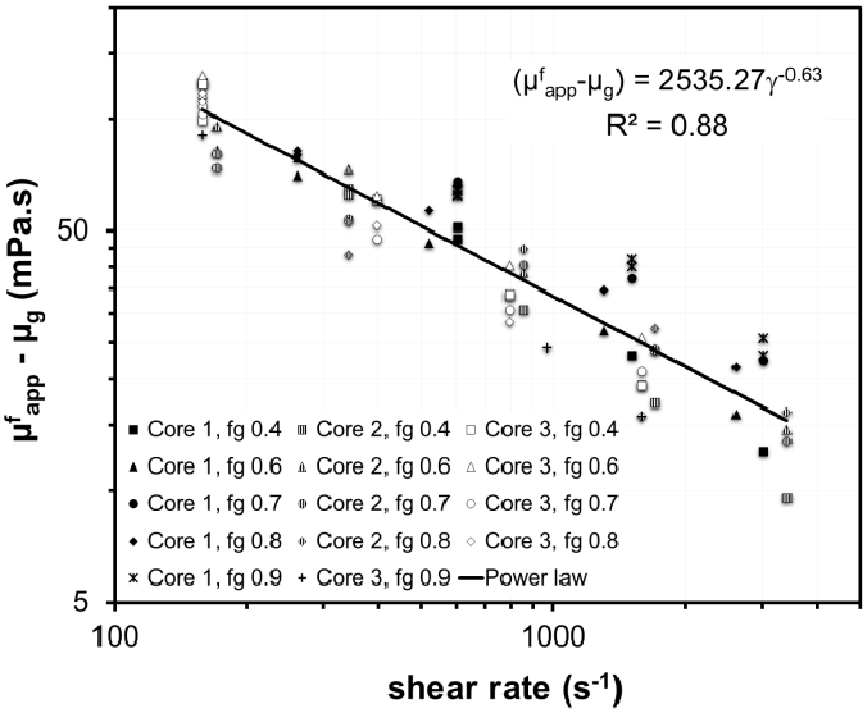

Figure 6-8: Master curve, in linear and log-log scale, of foam apparent viscosity as a function of shear rate obtained for all data in Table 6.3-1 presenting shear thinning behavior, independently of the quality regime, fg, or permeability.

Comparing equations 6-5 and 6-6, and substituting the definition for the shear rate term from equation 6-4, we obtained the following empirical correlation between μ^f_{app}, K and $v_{interstitial}$:

6-7. $$\mu^f_{app} = \mu_g + 2^{-1/3}\beta^{-2/3}C\sqrt{K}\phi^{-1/3}v_{interstitial}^{-2/3}$$

Where β is the coefficient of the correlation between the shear rate obtained in Figure 6-7, i.e., β = 15.746.

Equation 6-7 has the same formulation as the mathematical expressions in most of the current population balance models for foam flow [22]. Thus, the approach proposed here to treat foam flow data from coreflood tests can be used to obtain expressions for the parameters of many foam models in terms of properties of the porous media, as permeability and porosity. This has the potential to reduce the effective number of parameters, and possibly facilitate the upscaling of foam simulation from the laboratory to the reservoir scale. Furthermore, equation 5 itself can be used as a mathematical expression for μ^f_{app} in population balance models.

Comparing equation 6-7 with the models with expressions for μ^f_{app} reviewed by Ma et al. [22], we see that about half of the models assume that μ^f_{app} to vary as the -1/3 power of $v_{interstitial}$, in contrast to the value of -2/3 in equation 6-7. The exponent of -1/3 is the theoretical value from the work of Bretherton [136] and is found in the original work of Hirasaki and Lawson (1985) [68] for smooth capillaries. However, Falls et al. [69] extended this model to account for the constrictions present in porous media and showed that it underestimates μ^f_{app} and that the exponent of -2/3 characterizes a foam with very fine texture. Additionally, they found that at low shear rates, μ^f_{app} varies with the -1 power of $v_{interstitial}$. These findings were supported experimentally by bead pack micromodel tests.

Further evidence of the value of -2/3 for the exponent can be found in the rheological study of foam flow in a small pipe viscometer by Enzendorfer et al. [137], and in a more recent model for foam flow in diverging-converging channels (simplified for clarity in equation 6-8), developed by Nguyen [138].

6-8. $$\mu^f_{app} = \mu_g + n_f K^{3/2}\left\{A v^{-2/3}_{interstitial} + B v^{-1}_{interstitial}\right\}$$

Despite the different physical model, the conclusions that emerge from the expression showed in eq. 6 are similar to the ones from the work of Falls et al. [69]: foam apparent viscosity is proportional to either -2/3 or -1 power of interstitial velocity depending on the balance between the parameters A and B, and on the value of $v_{interstitial}$, with the second term on the brackets being more important at lower velocities, and the first term being dominant of the behavior at higher velocities.

To confirm the -1 exponent present in both works of Falls et al. [69] and Nguyen [138], we performed an additional coreflood test at lower shear rates by using a plug with a

permeability 4340 mD. The test followed the same procedure described for the other experiments and was done at f_g 0.6. Figure 6-9 shows the comparison between the results obtained in this test and the previous experiments. As predicted by the models, at lower shear rates the power law exponent decreased to -1, evincing a qualitative agreement between our data set and the experimental correlation with these theoretical models.

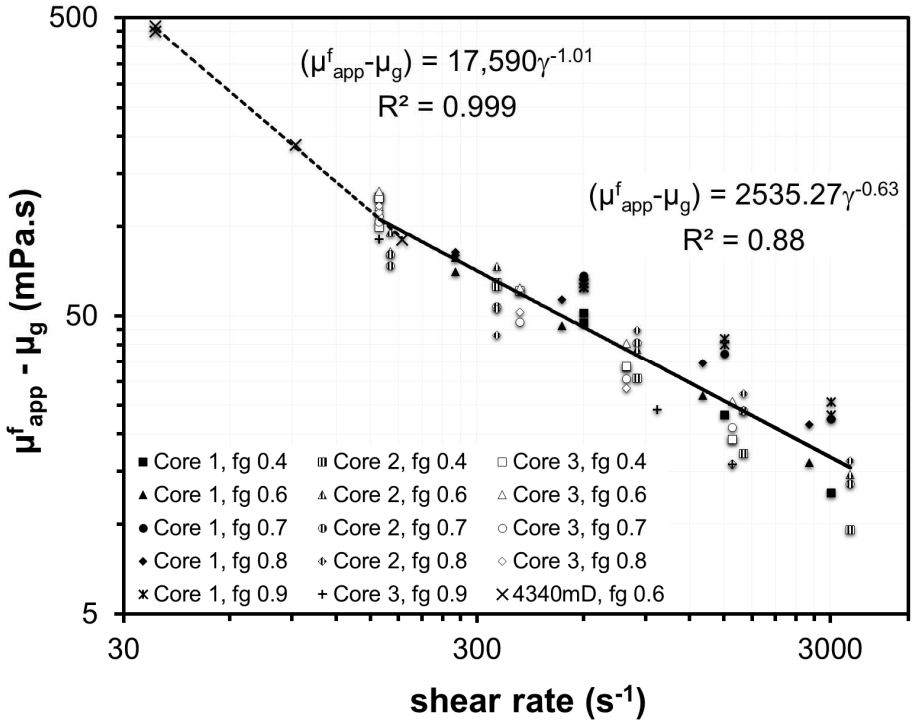

Figure 6-9: Verification of the power law exponent for foam apparent viscosity at low shear rates and comparison with the master curve showed in Figure 6-8.

In addition to the dependence of foam apparent viscosity with interstitial velocity, the experimental correlation obtained for our data (equation 6-7) also establishes that at fixed interstitial velocities, μ^f_{app} varies with the square root of K. This correlation was observed experimentally (Figure 6-6). This result differs from the explicit dependence between μ^f_{app} and K in the Nguyen's model, where μ^f_{app} varies with the 3/2 power of K. This difference could imply that n_f has an implicit dependence with 1/K, which would render both our results and the Nguyen's model consistent.

Considering all of the exposed above, we believe that the empirical correlations presented here can help to justify and refine the mathematical expressions used in current foam models, particularly the population balance ones, thus advancing the capabilities of flow simulation.

6.4 Conclusions

We performed an extensive experimental study on foam flow in porous media. Our results showed good agreement with the current understanding of foam flow and the expected rheological behavior of strong foams in the low-quality regime. For our conditions, we observed that the f_g^* decreased linearly with the square root of permeability. This result agrees with the work of Moradi et al. [58].

We presented an original approach to analyzing experimental data from foam flow that is valid for homogenous sandstones and sand packs. This approach consists in plotting the apparent foam viscosity as a function of shear rate. In doing so, we obtained a master curve for the behavior of foams in porous media independent of foam quality, permeability, and the flow regime. The master curve obeys a power law with a universal exponent of -2/3. We found experimental and theoretical evidence in the literature for the value of the exponent [68,69,137,138].

The experimental correlations presented here can be used to determine the parameters appearing in the equations of foam models in terms of the foam flow parameters, as permeability and porosity. Thus, such correlations hold great potential to advance the physical modeling of foam flow in porous media and to improve the Foam-EOR process modeling in the reservoir simulators, which are mostly based on the “steady state” phenomenological model, with limited predictive abilities. Additionally, the data supplied here can be used in simulation studies.

CHAPTER 7. INFLUENCE OF PRESSURE AND GAS COMPOSITION ON FOAM FLOW

7.1 Introduction

The previous chapters showed the complexity of foam flow in porous media. Both foam stability and performance are highly influenced by the balance of intermolecular forces at the interface of the fluids, as well as flow conditions and rock properties. While some of these factors have been extensively investigated, others are yet poorly explored, such as gas pressure and composition and their influence on foam behavior.

At low pressures, most gases behave ideally, and the intermolecular forces between the gas itself and the gas with the surfactants and water molecules at the liquid interface can be neglected. However, at the high pressures found in oil reservoirs, the gas can be as dense as the oil, and even be in a liquid or supercritical state. Under such conditions, the interactions between gas and oil, brine, and hydrophobic tails of the foaming agents become relevant to the behavior and performance of foams. These interactions can affect many foam properties, as rheology [139–141], stability [12,128,141,142], resistance to oil [12,128,141], and oil displacement [12,128].

Farajzadeh et al [139] compared the flow in porous media of N_2 and CO_2-foams, in the absence of oil, at both low (1 bar) and high (90 bar) pressures. They found that N_2-foams were stronger (higher pressure drop) than CO_2-foams at all conditions examined. N_2-foams presented a greater entrance effect, needing more space to properly form a foam. Their results also showed that foams were stronger at high pressure than at low pressure for both gases.

Solbakken et al [140] investigated the effect of CO_2 density on foam flow in porous media and found that the MRF of CO_2-foams decreases as CO_2 density increases, i.e., as pressure increases. Contrarily to the findings of Farajzadeh et al [139], the authors observed a decrease in pressure drop for CO_2-foams flow as pressure was increased. Nevertheless, both works agree that N_2 was capable of generating stronger foams than CO_2.

Emadi et al [128] compared the recovery efficiency of CO_2-foams and N_2-foams in pressurized micromodels. Their results showed that N_2-foams were not only stronger than CO_2-foams but also more stable in presence of oil because of the non-spreading of oil over the lamellae when N_2 was the gas phase. Still, CO_2-foams were more effective in recovering oil.

The authors credited the better performance of CO_2-foams to the reduction of oil viscosity due to the interactions between the oil and CO_2.

Farajzadeh et al [12] also evaluated the impact of pressure on foam stability and recovery efficiency in presence of oil, by comparing immiscible and miscible conditions. They found that low pressure, immiscible CO_2 was not able to foam in presence of oil at 1 and 90 bar, but strong CO_2-foams were formed when CO_2 achieved miscibility (137 bar). The formed foam at a high pressure increased oil recovery in comparison to co-injection of only brine and gas. The authors also tested N_2-foams, but only at 1 bar. Like the results of Emadi et al [128], these foams were more resistant to oil impact, presenting a very homogeneous advancing front and higher oil recovery when compared either gas co-injection or CO_2-foams under these conditions.

Pressure can also impact the selection of a foaming formulation. Holt et al [141] compared the impact of pressure on foams made with either an AOS surfactant or a fluorinated sulfobetaine. Their results showed an increase of pressure drop with increasing pressures for the AOS-based foams, while the opposite behavior was observed for fluorosurfactant-based foams. The same behavior was observed when the experiments were performed in presence of oil. The authors concluded that a proper screening and selection of foaming formulations can only be achieved through flooding experiments realized at the actual pressure of the target reservoir.

The works discussed above highlight the importance of pressure and gas composition on the performance of foam-EOR. Nevertheless, these effects have not received much attention so far, as evinced by the limited literature available on the subject. For instance, the impact of pressure was done mostly with pure CO_2, with some results reporting stronger foams at higher pressures [139], while others observed the opposite behavior [140]. N_2 is often used to compare the impact of gas type at low pressures but rarely used at high pressures. Regarding the impact of composition, as only the work of Harris [143] was performed with varying mixtures of CO_2 and N_2.

The impacts of pressure and gas composition are critical operationally since both reservoir and injection conditions can vary considerably from well to well, field to field, and even during the operation of a single well. For pre-salt scenarios, for example, the composition of the re-injected gas will vary depending on the produced gas characteristics,

and on operational conditions of the gas processing and injection units. Moreover, the extremely high pressures of pre-salt reservoirs deter experimentation at actual reservoir conditions, hence one would need to extrapolate the behavior of foams as a function of pressure to evaluate it. Thus, it is vital to understand the impact of such variables on foam properties.

Hence, we investigated the impact of pressure and gas composition on foam flow through porous media with the objective of finding correlations that allow extrapolating these effects. To this end, we performed corefloods with three gas compositions at multiple foam qualities and fixed total flow rate. To our knowledge, this is the first time that the impact of gas composition (mixtures of natural gas and CO_2) has been evaluated over multiple f_g's and pressures. The impact of pressure and gas composition was evaluated through the calculated foam apparent viscosity and foam relative permeability for each condition. K^f_{rg} increased with increasing pressure for all gas compositions following a similar profile. We found a master curve that allows estimating the efficiency of foam in reducing gas mobility at real pre-salt conditions.

7.2 Materials and Methods

7.2.1 Materials

Both brine and surfactant solution used for the experiments on the impact of pressure and gas composition were the same already described in section 6.2.1. Core #3 in Table 6.2-2 was used for all the coreflood experiments discussed in this chapter.

We selected the compositions of the gases based on the information provided by Petrobras on the projects for WAG injection in Pre-Salt reservoir, more specifically, the pilot in Lula field. The three compositions selected needed a few adjustments to meet the gas synthesis capabilities at IFPEN. The final compositions were as follows:

- Rich gas: 80% molar CO_2 + 20% molar CH_4;
- Intermediate gas: 50% molar CO_2 + 50% molar CH_4;

- Poor gas / produced gas: 11.7% molar CO_2 + 66.7% molar CH_4 + 13.8% molar C_2H_6 + 7.6% molar C_3H_8.

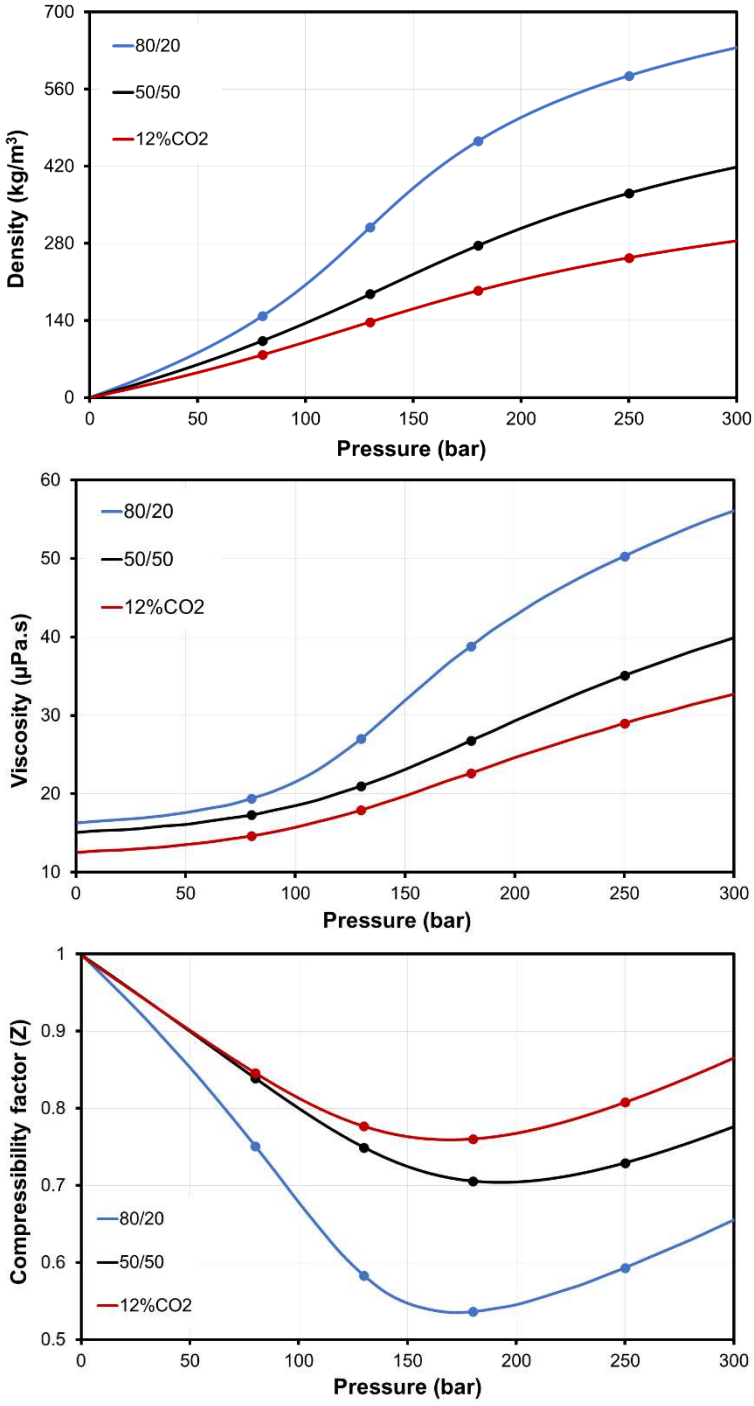

Figure 7-1: Density (ρ), viscosity (μ) and compressibility factor (Z) of the three gas mixtures as a function of pressure.

Final gas compositions were verified by gas chromatography and their thermodynamic properties were calculated by the PVT team using an equation of states. Figure 7-1 shows

how the compressibility factor (Z), density (ρ), and viscosity (μ) of the three gas mixtures vary as a function of pressure. Based on these curves, we selected four pressures to perform the coreflood tests: 80, 130, 180, and 250 bar. These points are highlighted in Figure 7-1.

7.2.2 Experimental Procedure:

Plug preparation, saturation, determination of porous volume and permeability measurements were done as described in chapter 6. Likewise, the same experimental setup detailed there was used to investigate the impact of pressure and gas composition.

Differently from the experiments in chapter 6, the coreflood tests were conducted at a fixed total flow rate of 66.3 mL/h (interstitial velocity of 72 ft/d) and increasing foam qualities. Thus, after characterizing the plug, the tests began with the co-injection of brine and gas at the selected total flow rate and initial f_g of 0.5 until the pressure drop was stable. At this point, the 4-way valve was switched from brine to surfactant solution injection.

Once stable pressure drop was achieved again, the next step of foam quality was initiated. For each pressure of interest, firstly a sequence of 4 increasing foam qualities was established, at steps of 0.1. During each test, pressure drop and fluid (gas and water) production were monitored. All experiments were done at 60°C, and after each sequence of foam qualities was completed, the plug was restored and the permeability was checked before changing to the next pressure.

7.3 Results and Discussion

Figure 7-2 presents the values of foam apparent viscosity as a function of foam quality for the three distinct gas compositions at the four pressures studied. For all conditions tested, μ^f_{app} increases with f_g, indicating that all data was obtained in the low-quality regime. Hence, the impact of pressure and gas composition on the optimal foam quality could not be determined.

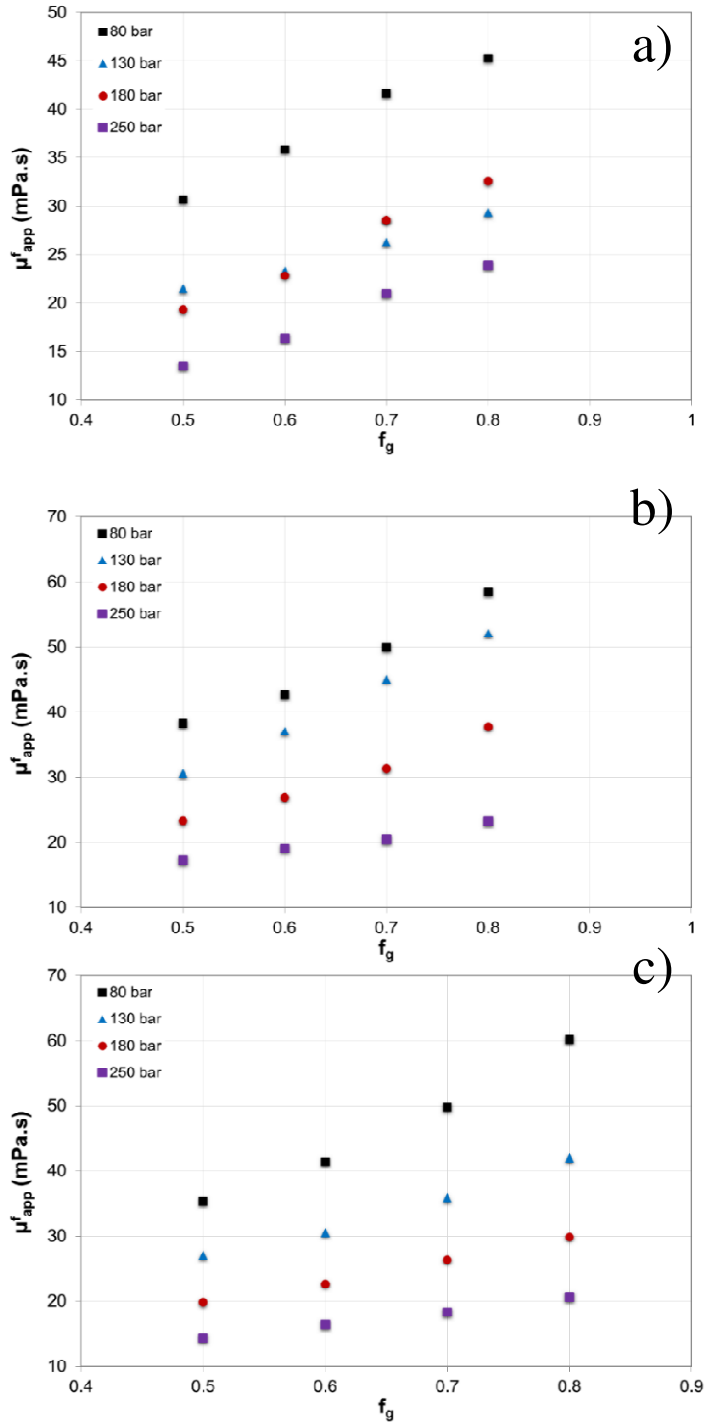

Figure 7-2: Foam apparent viscosity as a function of foam quality at 80, 130, 180 and 250 bar. a) rich gas; b) intermediate gas; c) poor gas.

Figure 7-2 shows that the slope of the curves, of μ^f_{app} vs. f_g, depends both on gas composition and pressure. For the poor gas, the slope decreases as pressures increases. This effect is less visible for the intermediate gas and practically vanishes for the rich gas. In terms of Osterloh-Jante diagrams, this behavior corresponds to squeeze the isobar curves closer together. The data in Figure 7-2 also shows an overall reduction on μ^f_{app} as pressure increases.

Hence, an increase in pressure not only compresses the isobar curves, it also displaces them closer to the origin.

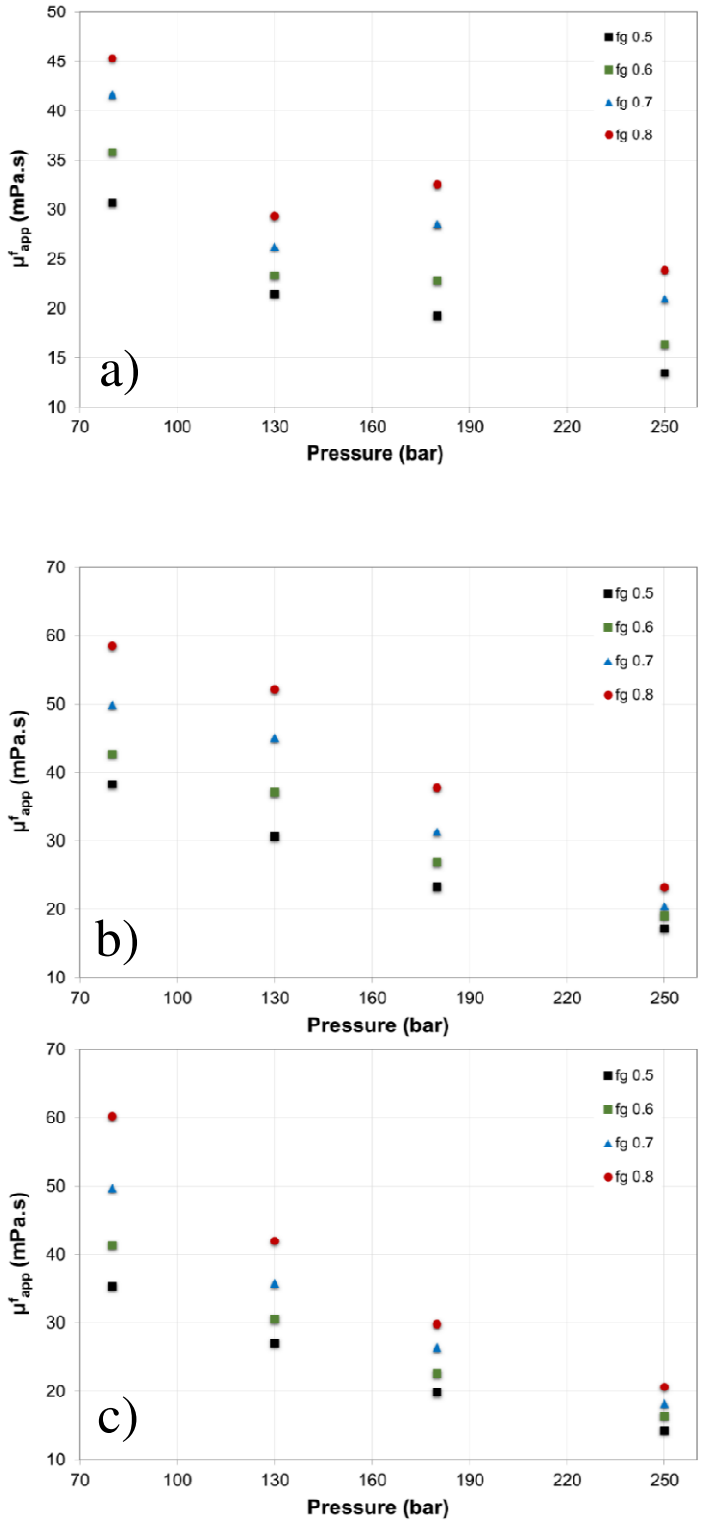

Figure 7-3: Foam apparent viscosity as a function of pressure. a) rich gas; b) intermediate gas; c) poor gas.

The impact of pressure on foam apparent viscosity is better visualized in Figure 7-3. Despite the overall trend of reducing μ^{f}_{app} as pressure increases, Figure 7-3 evinces the existence of a discontinuity on this behavior around the pressures near the minimum compressibility factor for the rich gas mixture. Between 130 and 180 bar, foam apparent viscosity actually increases with pressure for f_g's 0.7 and 0.8, remains almost constant for f_g 0.6, and decreases for f_g 0.5. For the intermediate and poor gases, only a decrease of μ^{f}_{app} is observed. This behavior could help to explain why some authors, such as Farajzadeh et al [139], observed an increase in foam strength with pressure, while others, as Solbakken et al [140], observed the opposite trend.

To evaluate the impact of gas composition on foam flow, first we needed to find a way to convert the data for each composition in Figure 7-3 in a single curve, and then compare them. We tried all the characterization parameters described by the equations in subsection 3.2.4.1 and found that gas relative permeability was fairly constant for a single composition at a given pressure, regardless the foam quality. Figure 7-4 presents the data points and corresponding fitted curves for the three gases.

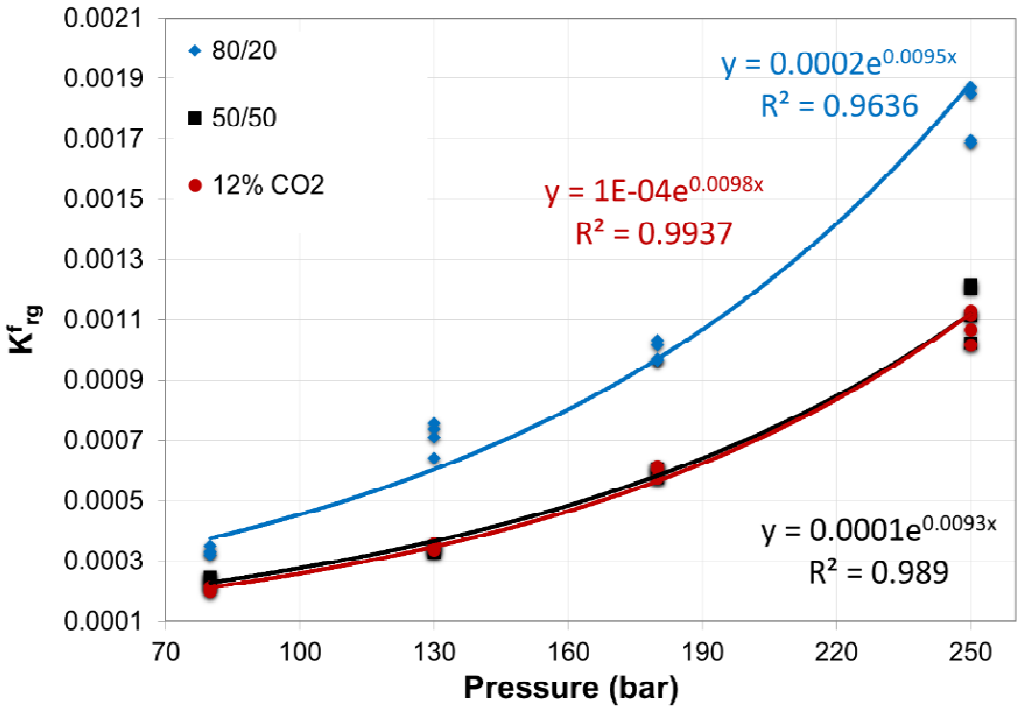

Figure 7-4: Gas relative permeability in presence of foam as a function of pressure.

This representation of coreflood data corroborates that, for the selected foaming formulation, the foam is less effective in reducing gas mobility as pressures increases for all

conditions tested. Even the discontinuity observed for the rich gas in Figure 7-3 is no longer present. Additionally, both intermediate and poor gas presented very similar values, despite the different compositions. Moreover, the rich gas also presented a curve parallel to the other two compositions, even though the rich gas was more mobile than the other gaseous mixtures. Hence, it seems that gas composition has no influence on foam flow up to an undetermined CO_2 content. This finding is similar to the results obtained by Harris [143], who performed tests in a loop viscometer, using mixtures of CO_2 and N_2. He found that foams produced with gaseous mixtures with only 20% of N_2 had the same half-life as a pure N_2-foam.

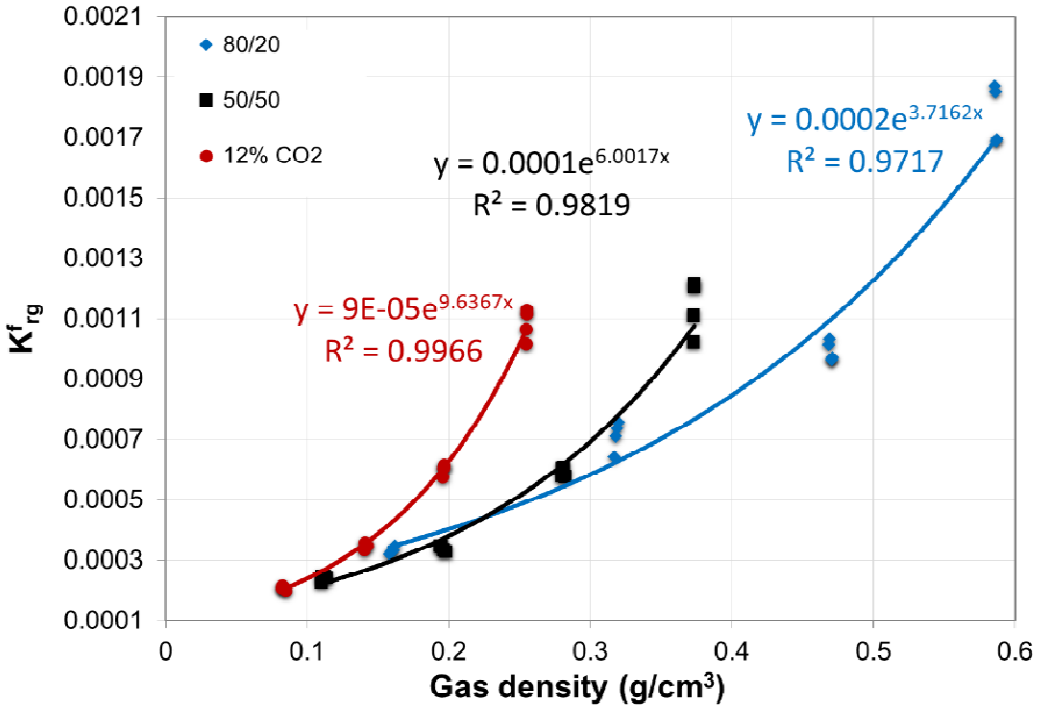

Figure 7-5: Gas relative permeability in presence of foam as a function of gas density.

However, when the K^f_{rg} is expressed as a function of gas density, Figure 7-5, the complexity of the effect of gas composition on foam flow is more visible. Figure 7-5 shows that if the density is low enough, the gas composition has no effect on foam efficiency. But at higher densities, the higher the CO_2 content, the more effective foam is in reducing gas mobility, for a given gas density. Nonetheless, as shown in Figure 7-4, at a given pressure, a foam made of a CO_2-rich gas mixture is less efficient than a foam made with CO_2-poor gas because the negative impact of a high density overbalances the favorable impact of a high CO_2 content.

The fact that the three gas compositions follows very similar mathematical expressions in both Figure 7-4 and Figure 7-5 tell us that, with the proper parametrization and normalization, a master curve that describes the behavior of K^f_{rg} as a function of both pressure and composition can be obtained. As a first approach to try to achieve such master curve, we normalized the data in Figure 7-4 by the CO_2 content of each gas. Figure 7-6 presents the resulting curves.

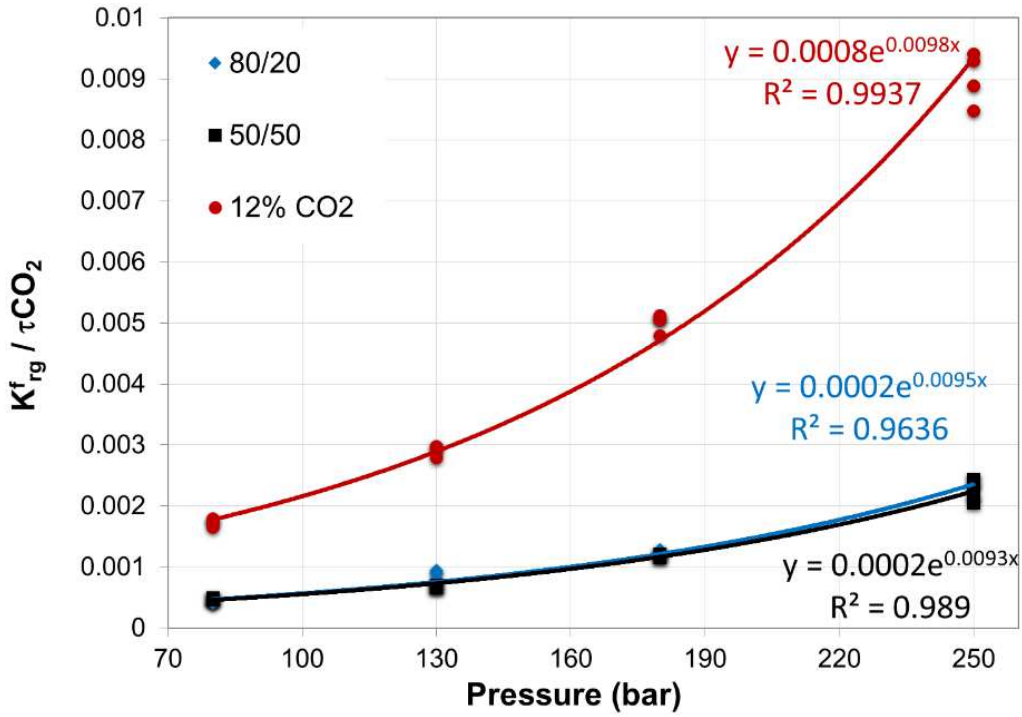

Figure 7-6: Gas relative permeability in presence of foam as a function of pressure, normalized by the CO2 content in each gaseous mixture.

Figure 7-6 shows that the two binary gas compositions could be normalized by just considering the CO_2 context. The poor gas composition follows an exponential expression that is very similar to the binary mixtures, but it did not fall on the otherwise-would-be master curve. This indicates that all components in the gas mixture matter in describing the foam flow behavior.

Hence, another parameter must be used to achieve a master curve, one that considers the presence of ethane and propane as well. Thus, the parameter should consider the intermolecular forces at play in the gas mixture, such as the molar density, ρ_m. Figure 7-7 shows the K^f_{rg} as a function of ρ_m. This last representation finally unifies the behavior of

foams across different foam qualities (as long as in the low-quality regime), pressures, and gas compositions investigated here in a master curve.

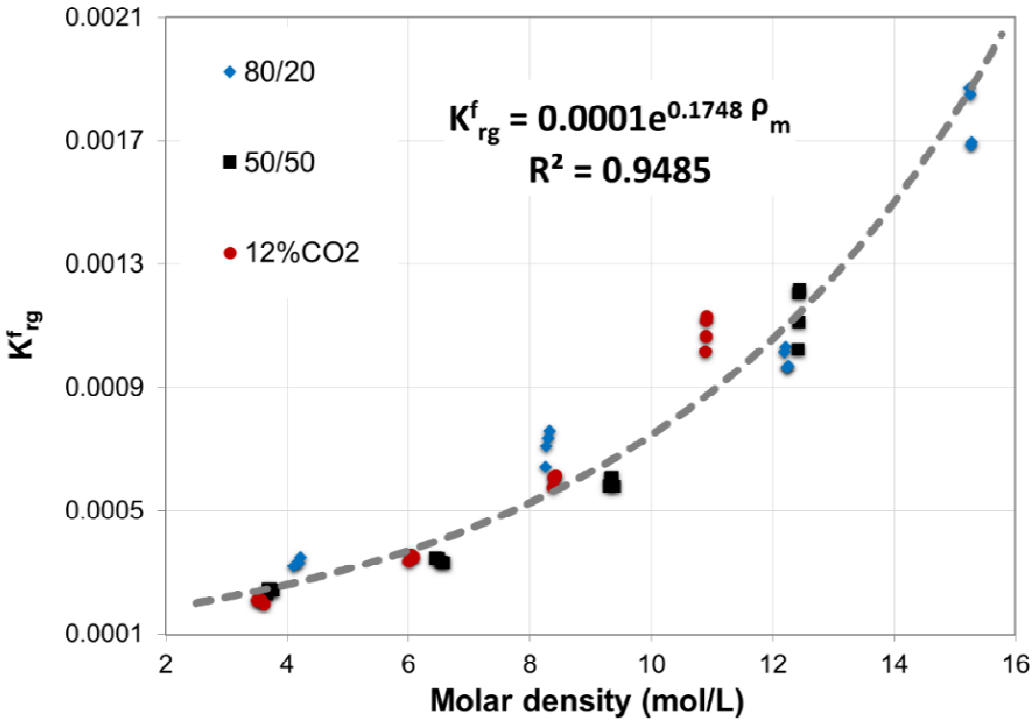

Figure 7-7: Gas relative permeability in presence of foam as a function of molar density. The dotted grey line is the unified master curve for all foam qualities, pressures, and gas compositions evaluated.

7.4 Conclusions

We studied the impact of pressure and gas composition on foam flow through porous media. For all experiments performed, foam was less effective in reducing gas mobility as pressure increased. We found a unified behavior when presenting the results as gas relative permeability in presence of foams as a function of gas molar density. The master curve obtained follows an exponential equation and allows us to extrapolate foam efficiency for different compositions at different pressures. This allows to estimate foam behavior at actual pre-salt reservoir conditions and to consider composition variations during field operation. However, the accuracy of such estimates, as well as the validity of this master curve for other foaming agents needs to be confirmed by more experiments that extend the range of formulations, compositions, and pressures covered in this work.

CHAPTER 8.
CONCLUSIONS, PERSPECTIVES AND FUTURE WORK

8.1 Conclusions and Perspectives

In this dissertation, we investigated the impact of foam quality, flow rate (interstitial velocity), permeability, pressure and gas composition on foam flow in porous media. Our main objective was to advance our knowledge of the physics underlying the rheological behavior of foams. For that, our studies comprised a careful evaluation and selection of a foaming formulation, which was then validated by micromodel tests at high pressure, before performing a comprehensive and systematic petrophysical study of foam flow in porous media. A critical review of the literature was essential to guide the experiments and to analyze and understand our results.

Our findings showed that it is possible to obtain in micromodels the same characteristic rheological behavior observed for foam flow during coreflood experiments. Though further investigation is needed, these results support the hypothesis that micromodels could be used to greatly improve our understanding of foam flooding, as they allow a direct observation and characterization of the foaming ability during flow through porous media, fraction of trapped gas, saturation of fluids and the texture of foam in-situ. Furthermore, micromodel floods can be more easily incorporated in high throughput systems, allowing a finer characterization of complex systems such as foams, since many formulations and conditions can be rapidly evaluated and compared at much lower costs than conventional coreflood tests. Indeed, a Ph.D. project with this objective has been initiated at IFPEN in 2015.

Our findings also showed that the innovative approach proposed here to treat the results of coreflood tests of foam flooding allowed us to represent the rheological behavior of strong foam with a master curve. This curve follows a power law with a universal exponent of -2/3, regardless flow regime, foam quality, interstitial velocity, or permeability. The ability to gather so many parameters (foam quality, interstitial velocity, permeability, and porosity) in a single empirical expression shows the potential of this approach to help elucidate the physics of foam flow in porous media. In fact, the empirical expression found closely resembles a population balance expression that considers the forces acting in the moving lamellae in the pores of the rock. Thus, we believe that this approach can greatly improve the modeling of foam flooding processes by helping to justify and refine the mathematical expressions used in current foam models.

Besides the innovative method of analysis of foam flow in porous media, our work provides an extensive and set of coreflood data that can be used in simulation studies to advance modeling techniques. The need of systematic and extensive foam flow data obtained using the same system and under very well controlled experimental conditions has been highlighted by diverse groups in the literature. Such data is vital to understand foam behavior and hence, improve the predictive capabilities of foam simulation tools. In fact, they are already being used in a Ph.D. project on foam simulation initiated at IFPEN in 2014.

The results of the influence of pressure on foam flow in porous media exhibited an overall trend of increasing gas mobility as pressure increases, i.e., foam efficiency reduced with pressure. Only the rich gas mixture presented a more complex behavior around its minimum compressibility factor. Regarding the impact of gas composition, our results revealed no influence of gas composition on foam efficiency at low pressures. However, as pressure increases, the gas composition becomes an important parameter to foam behavior. Our results showed that every component must be considered to correctly address the impact of gas composition on foam performance.

We obtained a master curve that describes the impact of both pressure and gas composition by expressing the coreflood results as K^{f}_{rg} as a function of gas molar density, thus accounting for both flow conditions and intermolecular forces. The obtained master curve is an important tool to estimate foam efficiency for different compositions at different pressures. This is crucial for evaluating the potential of this technology for scenarios with ever-changing conditions, such as the pre-salt fields. The results of the influence of both pressure and gas composition on foam performance highlighted the importance of evaluating foam flow behavior under conditions as close as possible to the desired application.

Considering all the remarks above, we believe that both the innovative approaches to evaluate foam flooding data presented here, and their resulting empirical correlations, hold an immense potential to advance our understanding of foam flow in porous media. Our results indicate that these approaches and empirical correlations can be used to can help to justify and refine the mathematical expressions used in current foam models, thus improving the simulation of Foam-EOR process and its reliability.

8.2 Future work

As often happens during a research project, many ramifications from the initial planning appeared. We started to study a few of them during the making of this dissertation. We believe that these topics should be developed in further projects due to their relevance not only for the application of foams in pre-salt reservoirs but for the advancement of foam EOR technology. The initial results and observations, and their implications for both future research and on foam technology are briefly presented below:

8.2.1 Impact of core heterogeneity on foam performance

In subsection 6.3.4, we discussed additional coreflood tests made with a high permeability core to verify the existence of the -1 exponent for the power law curve that represents the rheological profile of foam flow in porous media at low shear rate. During these tests, a few experiments were performed in a plug presenting a very distinct longitudinal heterogeneity (layered permeability).

Figure 0-1 shows the pressure drop curves obtained during foam injection at constant flow rate and changing f_g in this layered plug. Our findings revealed that when the flow experiments were conducted from low to high foam qualities, foam was rapidly formed and remained effective throughout the role range of f_g's tested. However, when the experiments were conducted in the opposite direction, i.e., starting from high f_g and gradually reducing it, foam was not observed even at foam qualities as low as 0.3.

Our hypothesis is that when we started at a low gas fraction, there was enough surfactant solution to form stable and strong foam in the low-quality regime, which filled all the pore space. In that case, foam injection reduced gas mobility as expected for the entire range of foam qualities tested. However, by starting at a high gas fraction, foam was unable to form immediately in our system, and fluid segregation occurred. Hence, gas flowed through the high permeability layer, while surfactant solution flowed through the low permeability one. It seems that the initial segregation continued throughout the range of foam qualities tested, thus preventing the proper mixture of gas and surfactant, which inhibited foam generation.

This behavior has serious implications for field operation of foams in heterogeneous reservoirs. Foam flooding is usually conducted as FAWAG, i.e., by continuously alternating between the two directions regarding foam quality mentioned above. If the proper mixture of surfactant solution and gas is not achieved in the reservoir, the channeling issues will not be addressed, and the project may fail. The fact that segregation issues could be visualized in a vertical core of only 2.5 cm of diameter raises concern on how to avoid this issue on the field. More research is needed to determine the real severity of this issue.

8.2.2 Impact of the injection history on foam performance

An impact of the history of foam injection was also observed in homogenous cores during the tests for the influence of pressure and gas composition. We observed that the f_g^* was displaced to higher values when we compared the results obtained in chapter 6 (fixed foam quality and increasing flow rate) with the analogous results in chapter 7 (fixed flow rate and increasing foam quality). Figure 0-2 shows the compared curves of foam apparent viscosity as a function of foam quality. All the results were obtained during foam injection using core 3 at 80 bar.

Therefore, our results revealed a hysteresis to foam flow in porous media regarding gas fraction. The hysteresis with interstitial velocity is well known, but a similar effect with varying foam quality has never been reported, to the best of our knowledge. These findings evinced that hysteresis behavior of foam flow is more complex than previously thought, and reinforces the dependence of the results with the injection history in the plug. This has a significant impact in evaluating and comparing the results in the literature.

The fact that such a key parameter as f_g^* depends on how the experiments are done, and not just on the system studied (brine, gas, foaming agent, rock sample, pressure, and temperature), is yet another reason to concern about the reliability of the models. If the results change with the injection protocol used, the simulation parameters calculated during the model calibration process are not representative of the foam and the system alone, but of how the experiments are done as well. This conclusion has strong implications for studies that compared Osterloh & Jante diagrams obtained in different conditions, as well as studies that

made assumptions and forecasts on foam flow behavior by extrapolating the curves in these diagrams.

The evaluation of foam flow data by Osterloh & Jante diagrams assumes that the pressure drop data for the isobar curves is the same regardless the "path" that the experiments made in the diagram. The studies in the literature that compared these diagrams never question the injection protocol used. In fact, some works propose alternative "paths" for acquiring coreflood data for determining model parameters, with the objective of simplifying and reducing the number of experiments required.

Usually, authors build these diagrams by injecting foam at either: constant flow rate and changing foam quality, constant foam quality and varying flow rate, or even by keeping either liquid or gas flow rate constant while changing the other. Our findings indicate that the relative slope of the isobar curves will change as a function of how the data were obtained, thus possibly changing some of the trends and conclusions reported in the literature. For instance, the conclusions made by Alvarez et al on foam behavior by extrapolating these diagrams might not be accurate, as these curves should change depending on how data were obtained.

It is important to clarify and to stress that the Osterloh & Jante diagrams are not in question here since the typical L-shaped curves were observed in several studies, including for foam flow in pipes. Indeed, the verification of the same type of L-shaped curves in such a variety of conditions may indicate that these diagrams capture the intrinsic physics of foam flow. It is the interpretation and extrapolation of data according to these diagrams that we discuss here.

Therefore, performing more thorough and systematic experiments, as recommended by multiple research teams in the literature, is vital to advance our understanding of foam flow in porous media, thus determining which parameters are relevant and the experimental procedures more adequate for each study. As we said before, the fact that the available data in the literature were obtained in many distinct conditions and different procedures, hampers the development of a physical model of foam flow in porous media, hence impairing the advancement of foam technology.

8.2.3 Impact of oil on foam performance

To test the impact of oil on foam flow in porous media, three experiments were performed and are summarized in the Table A-1. The initial oil saturation was very reproducible. The results of oil recovery were coherent in general, except for the step of water flooding in the first experiment. Apparently, some of the oil in the dead volume could not be produced during brine injection. One hypothesis is that at the injection conditions, brine could not displace all the oil inside the BPR's (each one has a dead volume of 0.871 mL, which corresponds to almost 15% of the PV). Whatever the cause of this imprecision, it seems to not affect the oil production during co-injection of either brine and gas or surfactant solution and gas (i.e., foams).

Unfortunately, as is often the case for a new experimental setup, we had some technical issues during these tests. The total dead volume was three times the pore volume of the rock sample used, thus greatly impacting the accuracy and precision of the measurements of the volume of produced oil. Likewise, the emulsification of oil when surfactant was present significantly impaired the measurements of oil produced. And though the experimental procedure used was the same already validated in another setup, our conditions proved to need some adaptations. Hence, despite our best efforts, the tests were inconclusive.

Nevertheless, as a fundamental topic for foam EOR, the impact of oil on the performance of foam in the studies discussed in this dissertation should be investigated in future projects.

8.3 Final Considerations

The different injection modes and the range of issues that foams can solve make this technology flexible and versatile. Likewise, the possibility to combine foam with nearly any other EOR method to improve their sweep efficiency grants foams great versatility and potential to positively impact oil recovery. However, the absence of a physical model to accurately describe and predict foam flow in porous media is one of the greatest challenges for the development foam flooding.

Current models, though useful, are not yet predictive, and the quality of their forecasts relies on the capability of correctly reproduce real field conditions with laboratory scale experiments, which is another challenge. Moreover, the lack of understanding of the underlying physics of foam flow in porous media makes it difficult to justify the choice of one or another model.

Indeed, Weaire [83] highlights that a great flaw in advancing our knowledge on foam rheology is the overemphasis given to fitting limited experimental data to theoretical models rather than attempting to acquire more significant and complete data sets. Thus, he advocates devoting efforts in performing more detailed and systematic experiments is needed, as the end of what he called “undisciplined empiricism” would naturally lead us to experimental and theoretical progress in characterizing foam rheology. Similar pleas for performing more comprehensive and systematic experiments were made by Ma et al [22] and Farajzadeh et al [92].

Our results stressed some of the gaps in the literature and understanding of foam flow in porous media, and corroborate the claims above. Therefore, we join our voices in the plea for experimental progress that leads to the end of the “undisciplined empiricism”, and for more systematic and comprehensive data that will unlock the theoretical development needed for improving the predictive capabilities of foam models

NOMENCLATURE:

A, B: combination of parameters

B: bridging coefficient

C: flow consistency index

E: entry coefficient

E_{con}: connected volume factor (proportion of the total reservoir volume connected to wells)

E_D: microscopic displacement efficiency

E_{ec}: economic efficiency factor

E_{VA}: areal sweep efficiency

E_{VV}: vertical sweep efficiency

E_V: total sweep efficiency

E_R: total recovery efficiency

f_g: foam quality (gas fraction)

FM: gas mobility reduction factor

fmmob: maximum gas mobility reduction factor

F_1, F_2, F_3…F_N: functions that capture the contributions of the main parameters impacting the gas mobility

K: permeability, mD

K_{rg}: relative permeability of gas

K^f_{rg}: relative permeability of gas in presence of foam

L: lamella number

M: mobility ratio

MRF: mobility reduction factor

n: flow behavior index

n_0: initial number of moles of gas in the piston cell, mol

N_C: capillary number

n_f: lamella density (foam texture) – number of flowing lamella per unit volume, lamella/m^3

P_l: pressure in the liquid phase

P_g: pressure in the gas phase

PV: porous volume

q_g^{eff}: Effective injected gas flow rate, mL/h

q_{pump}: water flow rate injected in the gas piston cell, mL/h

R_1 and R_2: curvature radii in the center of a lamella and at a node, respectively

S: spreading coefficient

V_g: volumetric fraction of gas in foam

V_l: volumetric fraction of liquid in foam

Greek letters:

α: scaling factor for the shear rate in porous media

β: coefficient relating α and permeability

$\dot{\gamma}$: shear rate, s^{-1}

ΔP: pressure drop, bar

$\Delta P_{no\text{-}foam}$: pressure drop of gas and brine co-injection, bar

ΔP_{foam}: foam pressure drop, bar

ϕ: Porosity

σ: surface or interfacial tension

σ_{og}: interfacial tension between oil and gas

σo_s: interfacial tension between surfactant solution and oil

σ_{sg}: interfacial tension between surfactant solution and gas

θ: contact angle (brine-oil-rock)

μ: viscosity, mPa.s

μ^f_{app}: foam apparent viscosity, mPa.s

Π_d: disjoining pressure

τ: shear stress

λ_{foam}: gas mobility in presence of foam

λ^f_r: gas relative mobility in presence of foam

v: surface velocity, ft/d

$v_{interstitial}$: Interstitial velocity, ft/d

υ: molar volume of the gas, mL/mol

REFERENCES

[1] C.M. Jones, H. Chaves, Assessment of Yet-To-Find Oil in the Brazilian Pre-Salt Region, SPE, Society of Petroleum Engineers, 2011/1/1.

[2] A.H.A. Pepin, N. Bize-Forest, S.J. Montoya Padilla, C. Abad, P. Schlicht, A. de Castro Machado, I. Lima, A. de Paiva Teles, R. Tadeu Lopes, Pre-Salt Carbonate Reservoir Analog Selection for Stimulation Optimization, IPTC, International Petroleum Technology Conference, 2014/12/10.

[3] J.O.D.S. Pizarro, C.C.M. Branco, Challenges in Implementing an EOR Project in the Pre-Salt Province in Deep Offshore Brasil, SPE, Society of Petroleum Engineers, 2012/1/1.

[4] A.S. Almeida, S.T.C. Lima, P.S. Rocha, A.M.T. Andrade, C.C.M. Branco, A.C. Capeleiro Pinto, CCGS Opportunities in the Santos Basin Pre-Salt Development, SPE, Society of Petroleum Engineers, 2010/1/1.

[5] P.R.S. Johann, R.C. Monteiro, Geophysical Reservoir Characterization and Monitoring at Brazilian Pre-Salt Oil Fields, OTC, Offshore Technology Conference, 2016/5/2.

[6] Recent production growth from presalt resources increases Brazil's total crude output - Today in Energy - U.S. Energy Information Administration (EIA), available at https://www.eia.gov/todayinenergy/detail.php?id=13771 (accessed on April 6, 2017).

[7] Nossa produção de petróleo no pré-sal ultrapassa 1 milhão de barris por dia, available at http://www.petrobras.com.br/fatos-e-dados/nossa-producao-de-petroleo-no-pre-sal-ultrapassa-1-milhao-de-barris-por-dia.htm (accessed on April 6, 2017).

[8] Petrobras Slashes $32 Billion from Five-Year Expenditure Plan - Oil & Gas 360, available at http://www.oilandgas360.com/petrobras-slashes-32-billion-from-five-year-expenditure-plan/ (accessed on April 7, 2017).

[9] R.E. Sweatman, S. Crookshank, S. Edman, Outlook and Technologies for Offshore CO2 EOR/CCS Projects, OTC, Offshore Technology Conference, 2011/1/1.

[10] P.L. Bondor, J.R. Hite, S.M. Avasthi, Planning EOR Projects in Offshore Oil Fields, SPE, Society of Petroleum Engineers, 2005/1/1.

[11] R.M. Enick, D.K. Olsen, J.R. Ammer, W. Schuller, Mobility and Conformance Control for CO2 EOR via Thickeners, Foams, and Gels -- A Literature Review of 40 Years of Research and Pilot Tests.

[12] R. Farajzadeh, A. Andrianov, P.L.J. Zitha, Investigation of Immiscible and Miscible Foam for Enhancing Oil Recovery, INDUSTRIAL & ENGINEERING CHEMISTRY RESEARCH 49 (4) (2010) 1910–1919.

[13] J.-S. Tsau, H. Yaghoobi, R.B. Grigg, Smart Foam to Improve Oil Recovery in Heterogeneous Porous Media, in: SPE/DOE Improved Oil Recovery Symposium, Tulsa, Oklahoma, 1998-04-19.

[14] A.T. Turta, A.K. Singhal, Field Foam Applications in Enhanced Oil Recovery Projects: Screening and Design Aspects, PETSOC-02-10-14 (2002).

[15] A.R. Kovscek, G.-Q. Tang, C.J. Radke, Verification of Roof snap off as a foam-generation mechanism in porous media at steady state, Colloids and Surfaces A: Physicochemical and Engineering Aspects 302 (1-3) (2007) 251–260.

[16] K. Ma, J.L. Lopez-Salinas, M.C. Puerto, C.A. Miller, S.L. Biswal, G.J.H. Hirasaki, Estimation of Parameters for the Simulation of Foam Flow through Porous Media. Part 1: The Dry-Out Effect, ENERGY & FUELS 27 (5) (2013) 2363–2375.

[17] J.M. Alvarez, H.J. Rivas, W.R. Rossen, Unified Model for Steady-State Foam Behavior at High and Low Foam Qualities, SPE-74141-PA (2001).

[18] T.C. Ransohoff, C.J. Radke, Mechanisms of Foam Generation in Glass-Bead Packs, SPE-15441-PA (1988).

[19] Q.P. Nguyen, A.V. Alexandrov, P.L.J. Zitha, P.K. Currie, Experimental and Modeling Studies on Foam in Porous Media: A Review, in: SPE-58799-MS 2000.

[20] P. Spirov, S. Rudyk, A. Khan, Foam Assisted WAG, Snorre Revisit with New Foam Screening Model, in: SPE-150829-MS, Society of Petroleum Engineers, SPE, 2012.

[21] S.H. Talebian, R. Masoudi, I.M. Tan, P.L.J. Zitha, Foam assisted CO2-EOR: A review of concept, challenges, and future prospects, Journal of Petroleum Science and Engineering 120 (2014) 202–215.

[22] K. Ma, G. Ren, K. Mateen, D. Morel, P.R. Cordelier, Modeling Techniques for Foam Flow in Porous Media, SPE-169104-PA (2015).

[23] M. Chabert, L. Nabzar, A. Cuenca, V. Beunat, E. Chevallier, Improved Mobility Reduction of Non Dense Gas Foam in Presence of High Residual Oil Saturation, in: IOR 2015 - 18th European Symposium on Improved Oil Recovery, Dresden, Germany, EAGE Publications BVNetherlands, 2015.

[24] F. Roggero, B. Bourbiaux, B. Braconnier, P. Delaplace, F. Douarche, A. Fourno, L. Nabzar, Q.-L. Nguyen, Essential contributions of simulation models to the assessment and design of Chemical EOR projects, in: 21st Word Petroleum Congress, Moscow 2014.

[25] International Energy Agency, World Energy Outlook 2015: Executive Summary - English Version, available at https://www.iea.org/Textbase/npsum/WEO2015SUM.pdf (accessed on April 8, 2017).

[26] P. Zitha, R. Felder, D. Zornes, K. Brown, and K. Mohanty, Increasing Hydrocarbon Recovery Factors | Society of Petroleum Engineers, available at http://www.spe.org/industry/increasing-hydrocarbon-recovery-factors.php (accessed on April 8, 2017).

[27] A. Muggeridge, A. Cockin, K. Webb, H. Frampton, I. Collins, T. Moulds, P. Salino, Recovery rates, enhanced oil recovery and technological limits, Philosophical Transactions of the Royal Society of London A: Mathematical, Physical and Engineering Sciences 372 (2006) (2013).

[28] S. Thomas, Enhanced Oil Recovery - An Overview, Oil & Gas Science and Technology - Rev. IFP 63 (1) (2008) 9–19.

[29] J.J. Sheng, Introduction, in: J.J. Sheng (Ed.), Modern Chemical Enhanced Oil Recovery, Gulf Professional Publishing, Boston, 2011, pp. 1–11.

[30] V. Alvarado, E. Manrique, Chapter 2 - Enhanced Oil Recovery Concepts, in: V. Alvarado, E. Manrique (Eds.), Enhanced Oil Recovery, Gulf Professional Publishing, Boston, 2010, pp. 7–16.

[31] A. Mandal, Chemical flood enhanced oil recovery: A review, IJOGCT 9 (3) (2015) 241.

[32] G.J. Stosur, J.R. Hite, N.F. Carnahan, K. Miller, The Alphabet Soup of IOR, EOR and AOR: Effective Communication Requires a Definition of Terms, SPE, Society of Petroleum Engineers, 2003/1/1.

[33] J. Sheng, Modern chemical enhanced oil recovery: Theory and practice, 1st ed., Gulf Professional Pub, Amsterdam, Boston, 2011.

[34] S. Kokal, A. Al-Kaabi, Enhanced Oil Recovery: challenges and opportunities, World Petroleum Council: Official Publication 12 (1) (2010) 64–68.

[35] Enhanced Oil Recovery: Prospects for CO2-based EOR, available at http://www.rigzone.com/news/oil_gas/a/135662/Enhanced_Oil_Recovery_Prospects_for_CO2based_EOR (accessed on April 7, 2017).

[36] J. Mathonnier, The Global Prospects For Enhanced Oil Recovery, available at http://oilprice.com/Energy/Energy-General/The-Global-Prospects-For-Enhanced-Oil-Recovery.html (accessed on April 7, 2017).

[37] Al-Mjeni, Arora, Cherukupalli, Wunnik, Edwards, Felber, Gurpinar, Hirasaki, Miller, Jackson, Kristensen, Lim, Ramamoorthy, E. Andersen, Has the Time Come for EOR?, Oilfield Review 22 (4) (2010/2011) 16–35.

[38] Short-Term Energy Outlook - U.S. Energy Information Administration (EIA), available at https://www.eia.gov/outlooks/steo/report/global_oil.cfm (accessed on April 9, 2017).

[39] C. Lefebvre, P. Lemouzy, D. Sorin, G. Roy, S. Serbutoviez, Building a Roadmap for Enhanced Oil Recovery Prefeasibility Study, in: Society of Petroleum Engineers.

[40] Vladimir Alvarado, Eduardo Manrique, Chapter 8 - EOR's Current Status, in: V. Alvarado, E. Manrique (Eds.), Enhanced Oil Recovery, Gulf Professional Publishing, Boston, 2010, pp. 133–156.

[41] R. Martel, A. Hébert, R. Lefebvre, P. Gélinas, U. Gabriel, Displacement and sweep efficiencies in a 5DNAPL6 recovery test using micellar and polymer solutions injected in a five-spot pattern, Journal of Contaminant Hydrology 75 (1–2) (2004) 1–29.

[42] Displacement efficiency of immiscible gas injection -, available at http://petrowiki.org/Displacement_efficiency_of_immiscible_gas_injection (accessed on April 9, 2017).

[43] Gravity Effect on Macroscopic Displacement Efficiency | Fundamentals of Fluid Flow in Porous Media, available at http://perminc.com/resources/fundamentals-of-fluid-flow-in-porous-media/chapter-5-miscible-displacement/fluid-properties-miscible-displacement/macroscopic-displacement-efficiency/gravity-effect/ (accessed on April 11, 2017).

[44] R.E. Terry, Enhanced Oil Recovery, in: R.A. Meyers (Ed.), Encyclopedia of Physical Science and Technology (Third Edition), Academic Press, New York, 2003, pp. 503–518.

[45] Abdallah, W., Buckley, J. S., Carnegie, A., Edwards, J., Herold, B., Forham, E., Graue, A., Habashy, T., Seleznev, N., Signer, C., Hussain, H., Montaron, B., Ziauddin, M., Fundamentals of Wettability, Oilfield Review 19 (2) (2007) 44–61.

[46] James J. Sheng, Chapter 7 - Surfactant Flooding, in: J.J. Sheng (Ed.), Modern Chemical Enhanced Oil Recovery, Gulf Professional Publishing, Boston, 2011, pp. 239–335.

[47] A. Turta, Chapter 18 - In Situ Combustion, in: J.J. Sheng (Ed.), Enhanced Oil Recovery Field Case Studies, Gulf Professional Publishing, Boston, 2013, pp. 447–541.

[48] S. Lee, S.I. Kam, Chapter 2 - Enhanced Oil Recovery by Using 5CO26 Foams: Fundamentals and Field Applications, in: J.J. Sheng (Ed.), Enhanced Oil Recovery Field Case Studies, Gulf Professional Publishing, Boston, 2013, pp. 23–61.

[49] R.T. Johns, B. Dindoruk, Chapter 1 - Gas Flooding, in: J.J. Sheng (Ed.), Enhanced Oil Recovery Field Case Studies, Gulf Professional Publishing, Boston, 2013, pp. 1–22.

[50] M.H. Holtz, Immiscible Water Alternating Gas (IWAG) EOR: Current State of the Art, SPE, Society of Petroleum Engineers, 2016/4/11.

[51] E.I. Dale, Modelling of immiscible WAG with emphasis on the effect of capillary pressure, The University of Bergen, 2008.

[52] W. Ren, R.G. Bentsen, L.B. Cunha, A Study of the Gravity Assisted Tertiary Gas Injection Processes, PETSOC-05-02-02.

[53] V. Kuuskraa, M. Wallace, CO2-EOR set for growth as new CO2 supplies emerge, Oil and Gas Journal 112 (4) (2014) 92–105.

[54] Shell explores using CO2 for enhanced oil recovery, available at http://www.energydigital.com/utilities/2710/Shell-explores-using-CO2-for-enhanced-oil-recovery (accessed on April 10, 2017).

[55] H.L. Chang, Chapter 10 - ASP Process and Field Results, in: J.J. Sheng (Ed.), Enhanced Oil Recovery Field Case Studies, Gulf Professional Publishing, Boston, 2013, pp. 203–249.

[56] E. Delamaide, P. Moreau, R. Tabary, A New Approach for Offshore Chemical Enhanced Oil Recovery, in: Offshore Technology Conference, Houston, Texas, USA, 2015-05-04.

[57] James J. Sheng, Chapter 11 - Foams and Their Applications in Enhancing Oil Recovery, in: J.J. Sheng (Ed.), Enhanced Oil Recovery Field Case Studies, Gulf Professional Publishing, Boston, 2013, pp. 251–280.

[58] A. Moradi-Araghi, E.L. Johnston, D.R. Zornes, K.J. Harpole, Laboratory Evaluation of Surfactants for CO2-Foam Applications at the South Cowden Unit, in: SPE-37221-MS, Society of Petroleum Engineers, SPE, 1997.

[59] H. Yaghoobi, J.P. Heller, Laboratory Investigation of Parameters Affecting CO2-Foam Mobility in Sandstone at Reservoir Conditions, in: SPE-29168-MS, Society of Petroleum Engineers, SPE, 1994.

[60] J. Gauteplass, K. Chaudhary, A.R. Kovscek, M.A. Fernø, Pore-level foam generation and flow for mobility control in fractured systems, Colloids and Surfaces A: Physicochemical and Engineering Aspects 468 (2015) 184–192.

[61] E. Chevallier, O. Tchamba, M. Chabert, S. Bekri, F. Martin, S. Gautier, Foams with Ultra-Low Interfacial Tensions for an Efficient EOR Process in Fractured Reservoirs, in: SPE-174567-MS, Society of Petroleum Engineers, SPE, 2015.

[62] W. Yan, C.A. Miller, G.J. Hirasaki, Foam sweep in fractures for enhanced oil recovery, Colloids and Surfaces A: Physicochemical and Engineering Aspects 282–283 (2006) 348–359.

[63] H.J. Bertin, O.G. Apaydin, L.M. Castanier, A.R. Kovscek, Foam Flow in Heterogeneous Porous Media: Effect of Cross Flow, SPE JOURNAL 4 (2) (1999) 75–82.

[64] D.C. Bond, O.C. Holbrook, Gas drive oil recovery process, Google Patents, 1958, available at http://www.google.com.na/patents/US2866507.

[65] L.W. Holm, Foam Injection Test in the Siggins Field, Illinois, SPE-2750-PA (1970).

[66] J.M. Alvarez, H.J. Rivas, W.R. Rossen, Unified model for steady-state foam behavior at high and low foam qualities, SPE JOURNAL 6 (3) (2001) 325–333.

[67] W.T. Osterloh, Jante, M.J., Jr., Effects of Gas and Liquid Velocity on Steady-State Foam Flow at High Temperature, in: SPE-24179-MS, Society of Petroleum Engineers, SPE, 1992.

[68] G.J.H. Hirasaki, J.B. Lawson, Mechanisms of Foam Flow in Porous Media: Apparent Viscosity in Smooth Capillaries, SPE-12129-PA (1985).

[69] A.H. Falls, J.J. Musters, J. Ratulowski, The Apparent Viscosity of Foams in Homogeneous Bead Packs, SPE-16048-PA (1989).

[70] Z.I. Khatib, G.J.H. Hirasaki, A.H. Falls, Effects of Capillary Pressure on Coalescence and Phase Mobilities in Foams Flowing Through Porous Media, SPE-15442-PA (1988).

[71] M.G. Aarra, A. Skauge, H.A. Martinsen, FAWAG: A Breakthrough for EOR in the North Sea, in: SPE-77698-MS, Society of Petroleum Engineers, SPE, 2002.

[72] S.H. Talebian, R. Masoudi, I.M. Tan, P.L.J. Zitha, Foam assisted CO2-EOR; Concepts, Challenges and Applications, in: SPE-165303-MS, Society of Petroleum Engineers, SPE, 2013.

[73] B. Dollet, C. Raufaste, Rheology of aqueous foams, COMPTES RENDUS PHYSIQUE 15 (8-9) (2014) 731–747.

[74] A. Bureiko, A. Trybala, N. Kovalchuk, V. Starov, Current applications of foams formed from mixed surfactant–polymer solutions, ADVANCES IN COLLOID AND INTERFACE SCIENCE 222 (2015) 670–677.

[75] D. Weaire, S. Hutzler, W. Drenckhan, A. Saugey, S.J. Cox, The Rheology of Foams, in: W. Richtering (Ed.), Smart Colloidal Materials, Springer Berlin Heidelberg, Berlin, Heidelberg, 2006, pp. 100–105.

[76] L.L. Schramm, F. Wassmuth, Foams: Basic Principles, in: L.L. Schramm (Ed.), Foams: Fundamentals and Applications in the Petroleum Industry, American Chemical Society, Washington, DC, 1994, pp. 3–45.

[77] Z.F. Zhang, V.L. Freedman, L. Zhong, Foam Transport in Porous Media - A Review, 2009.

[78] V. Bergeron, P. Walstra, Foams, Fundamentals of Interface and Colloid Science 5 (2005) 7.1 - 7.38.

[79] A. Andrianov, R. Farajzadeh, M.M. Nick, M. Talanana, P.L.J. Zitha, Immiscible Foam for Enhancing Oil Recovery: Bulk and Porous Media Experiments, INDUSTRIAL & ENGINEERING CHEMISTRY RESEARCH 51 (5) (2012) 2214–2226.

[80] TensideHyrophilHydrophob.png (500×315), available at https://upload.wikimedia.org/wikipedia/commons/d/d1/TensideHyrophilHydrophob.png (accessed on July 3, 2017).

[81] A.B.J. Kroezen, J.G. Wassink, C.A.C. Schipper, The flow properties of foam, Journal of the Society of Dyers and Colourists 104 (10) (1988) 393–400.

[82] D.D. Joseph, Questions in Fluid Mechanics: Understanding Foams and Foaming, Journal of Fluids Engineering 119 (3) (1997) 497–498.

[83] D. Weaire, The rheology of foam, CURRENT OPINION IN COLLOID & INTERFACE SCIENCE 13 (3) (2008) 171–176.

[84] S. Cohen-Addad, R. Hoehler, Rheology of foams and highly concentrated emulsions, CURRENT OPINION IN COLLOID & INTERFACE SCIENCE 19 (6) (2014) 536–548.

[85] A. Haugen, M.A. Fernø, A. Graue, H.J. Bertin, Experimental Study of Foam Flow in Fractured Oil-Wet Limestone for Enhanced Oil Recovery, SPE-129763-PA (2012).

[86] R.A. Ettinger, C.J. Radke, Influence of Texture on Steady Foam Flow in Berea Sandstone, SPE-19688-PA (1992).

[87] A. Huerre, V. Miralles, M.-C. Jullien, Bubbles and foams in microfluidics, Soft Matter 10 (36) (2014) 6888–6902.

[88] M.M. Almajid, A.R. Kovscek, Pore-level mechanics of foam generation and coalescence in the presence of oil, ADVANCES IN COLLOID AND INTERFACE SCIENCE (2015) In Press, Corrected Proof.

[89] D. Tiab, E.C. Donaldson, Chapter 5 - Capillary Pressure, in: D. Tiab, E.C. Donaldson (Eds.), Petrophysics (Fourth Edition), Gulf Professional Publishing, Boston, 2016, pp. 279–317.

[90] A.R. Kovscek, C.J. Radke, FUNDAMENTALS OF FOAM TRANSPORT IN POROUS-MEDIA, in: FOAMS: FUNDAMENTALS AND APPLICATIONS IN THE PETROLEUM INDUSTRY, AMER CHEMICAL SOC, 1155 SIXTEENTH ST NW, WASHINGTON, DC 20036, 1994, pp. 115–163.

[91] R. Farajzadeh, A. Andrianov, R. Krastev, G.J.H. Hirasaki, W.R. Rossen, Foam-oil interaction in porous media: Implications for foam assisted enhanced oil recovery, ADVANCES IN COLLOID AND INTERFACE SCIENCE 183 (2012) 1–13.

[92] R. Farajzadeh, M. Lotfollahi, A.A. Eftekhari, W.R. Rossen, G.J.H. Hirasaki, Effect of Permeability on Implicit-Texture Foam Model Parameters and the Limiting Capillary Pressure, Energy Fuels 29 (5) (2015) 3011–3018.

[93] P.A. Gauglitz, F. Friedmann, S.I. Kam, W.R. Rossen, Foam generation in homogeneous porous media, CHEMICAL ENGINEERING SCIENCE 57 (19) (2002) 4037–4052.

[94] T. Dicksen, G.J.H. Hirasaki, C.A. Miller, Conditions for Foam Generation in Homogeneous Porous Media, in: SPE-75176-MS, Society of Petroleum Engineers, SPE, 2002.

[95] Z.F. Dholkawala, H.K. Sarma, S.I. Kam, Application of fractional flow theory to foams in porous media, Journal of Petroleum Science and Engineering 57 (1-2) (2007) 152–165.

[96] K.G. Kornev, A.V. Neimark, A.N. Rozhkov, Foam in porous media: thermodynamic and hydrodynamic peculiarities, ADVANCES IN COLLOID AND INTERFACE SCIENCE 82 (1-3) (1999) 127–187.

[97] V.Q. Le, Q.P. Nguyen, A. Sanders, A Novel Foam Concept With CO2 Dissolved Surfactants, in: SPE-113370-MS, Society of Petroleum Engineers, SPE, 2008.

[98] M. Chabert, L. Nabzar, M. Morvan, S. Rohaida Mohd Shafian, P. Abdul Hamid, M. Faizal Sedaralit, N. Darman, An Integrated Laboratory Workflow for the Design of a Foam Pilot in Malaysia, Saint Petersburg, Russia, EAGE Publications BVNetherlands, 2013.

[99] A.A. Eftekhari, R. Farajzadeh, Effect of Foam on Liquid Phase Mobility in Porous Media, Scientific Reports 7 (2017) 43870 EP -.

[100] Q. Li, Foam generation and propagation in homogeneous and heterogeneous porous media. PhD dissertation, 2006, available at https://repositories.lib.utexas.edu/bitstream/2152/2567/2/liq50449.pdf.

[101] A.H. Falls, G.J. Hirasaki, T.W. Patzek, D.A. Gauglitz, D.D. Miller, T. Ratulowski, Development of a Mechanistic Foam Simulator: The Population Balance and Generation by Snap-Off, SPE-14961-PA.

[102] S.A. Jones, V. van der Bent, R. Farajzadeh, W.R. Rossen, S. Vincent-Bonnieu, Surfactant screening for foam EOR: Correlation between bulk and core-flood

experiments, Colloids and Surfaces A: Physicochemical and Engineering Aspects 500 (2016) 166–176.

[103] K. Osei-Bonsu, N. Shokri, P. Grassia, Foam stability in the presence and absence of hydrocarbons: From bubble- to bulk-scale, Colloids and Surfaces A: Physicochemical and Engineering Aspects 481 (2015) 514–526.

[104] L.L. Schramm (Ed.), Foams: Fundamentals and Applications in the Petroleum Industry, American Chemical Society, Washington, DC, 1994.

[105] L.L. Schramm, A.T. Turta, J.J. Novosad, Microvisual and Coreflood Studies of Foam Interactions With a Light Crude Oil, SPE-20197-PA (1993).

[106] J.J. Novosad, K. Mannhardt, The Interaction Between Foam And Crude Oils, in: PETSOC-89-40-29, Petroleum Society of Canada, PETSOC, 1989.

[107] K. Mannhardt, J.J. Novosad, L.L. Schramm, Foam/Oil Interations at Reservoir Conditions, in: SPE-39679-MS, Society of Petroleum Engineers, SPE, 1998.

[108] K. Mannhardt, J.J. Novosad, L.L. Schramm, Comparative Evaluation of Foam Stability to Oil, SPE-60686-PA (2000).

[109] A.K. Vikingstad, A. Skauge, H. Høiland, M. Aarra, Foam–oil interactions analyzed by static foam tests, Colloids and Surfaces A: Physicochemical and Engineering Aspects 260 (1) (2005) 189–198.

[110] R. Aveyard, B.P. Binks, P.D.I. Fletcher, T.G. Peck, C.E. Rutherford, Aspects of aqueous foam stability in the presence of hydrocarbon oils and solid particles, ADVANCES IN COLLOID AND INTERFACE SCIENCE 48 (1994) 93–120.

[111] K Koczo, L.A Lobo, D.T Wasan, Effect of oil on foam stability: Aqueous foams stabilized by emulsions, Journal of Colloid and Interface Science 150 (2) (1992) 492–506.

[112] Laurier L. Schramm, Jerry J. Novosad, Enhanced Oil Recovery The destabilization of foams for improved oil recovery by crude oils: Effect of the nature of the oil, Journal of Petroleum Science and Engineering 7 (1) (1992) 77–90.

[113] V. BERGERON, M.E. FAGAN, C.J. Radke, GENERALIZED ENTERING COEFFICIENTS - A CRITERION FOR FOAM STABILITY AGAINST OIL IN POROUS-MEDIA, LANGMUIR 9 (7) (1993) 1704–1713.

[114] H. A. Martinsen, F. Vassenden, Foam Assisted Water Alternating Gas (FAWAG) Process on Snorre, Brighton, UK, EAGE Publications BVNetherlands, 1999.

[115] D. Levitt, A. Jackson, C. Heinson, L.N. Britton, T. Malik, V. Dwarakanath, G.A. Pope, Identification and Evaluation of High-Performance EOR Surfactants, SPE-100089-PA.

[116] P. Gao, B.F. Towler, Y. Li, X. Zhang, Integrated Evaluation of Surfactant-Polymer Floods, SPE, Society of Petroleum Engineers, 2010/1/1.

[117] C. Watkins, Chemically enhanced oil recovery stages a comeback, available at https://www.aocs.org/stay-informed/read-inform/featured-articles/chemically-enhanced-oil-recovery-stages-a-comeback-november-2009 (accessed on March 13, 2017).

[118] J.F. Casteel, N.F. Djabbarah, Sweep Improvement in CO2 Flooding by Use of Foaming Agents, SPE-14392-PA (1988).

[119] F.M. Llave, F.-H. Chung, R.W. Louvier, D.A. Hudgins, Foams as Mobility Control Agents for Oil Recovery by Gas Displacement, SPE, Society of Petroleum Engineers, 1990/1/1.

[120] J.-S. Tsau, J.P. Heller, How Can Selective Mobility Reduction of CO2-Foam Assist in Reservoir Floods?, SPE, Society of Petroleum Engineers, 1996/1/1.

[121] B. Bazin, M. Morvan, F. Douarche, R. Tabary, An Integrated Workflow for Chemical EOR Pilot Design, SPE, Society of Petroleum Engineers, 2010/1/1.

[122] M. Morvan, R. Koetitz, P. Moreau, B. Pavageau, P. Rivoal, B. Roux, A Combinatorial Approach for Identification of Performance EOR Surfactants, SPE, Society of Petroleum Engineers, 2008/1/1.

[123] M. Chabert, M. Morvan, L. Nabzar, Advanced Screening Technologies for the Selection of Dense CO2 Foaming, in: SPE-154147-MS, Society of Petroleum Engineers, SPE, 2012.

[124] Y. Liu, R.B. Grigg, B. Bai, Salinity, pH and Surfactant Concentration Effects on CO2-Foam, in: SPE-93095-MS 2005.

[125] Y. Liu, R.B. Grigg, R.K. Svec, CO2 Foam Behavior: Influence of Temperature, Pressure, and Concentration of Surfactant, in: SPE-94307-MS, Society of Petroleum Engineers, SPE, 2005.

[126] J.-S. Tsau, A.E. Syahputra, R.B. Grigg, Economic Evaluation of Surfactant Adsorption in CO2 Foam Application, in: SPE-59365-MS 2000.

[127] M. Robin, J. Behot, V. Sygouni, CO2 Injection in Porous Media: Observations un Glass Micromodels Under Reservoir Conditions, in: SPE-154147-MS, Society of Petroleum Engineers, SPE, 2012.

[128] A. Emadi, M. Jamiolahmady, M. Sohrabi, S. Irland, Visualization of Oil Recovery by CO2-Foam Injection; Effect of Oil Viscosity and Gas Type, in: SPE-152996-MS 2012.

[129] A. Emadi, M. Sohrabi, M. Jamiolahmady, S. Irland, G. Robertson, Mechanistic Study of Improved Heavy Oil Recovery by CO2-Foam Injection, in: SPE-144968-MS, Society of Petroleum Engineers, SPE, 2011.

[130] R. Farajzadeh, M. Lotfollahi, A.A. Eftekhari, W.R. Rossen, G.J.H. Hirasaki, Effect of Permeability on Implicit-Texture Foam Model Parameters and the Limiting Capillary Pressure, ENERGY & FUELS 29 (5) (2015) 3011–3018.

[131] L.G. Pedroni, L. Nabzar, New Insights On Foam Rheology In Porous Media, in: Rio Oil & Gas Expo and Conference, 24-27 October, Rio de Janeiro/Brazil, 2016.

[132] C.K. Mamun, J.G. Rong, S.I. Kam, H.M. Liljestrand, W.R. Rossen, Extending Foam Technology from Improved Oil Recovery to Environmental Remediation, in: SPE-77698-MS, Society of Petroleum Engineers, SPE, 2002.

[133] W.R. Rossen, P.A. Gauglitz, Percolation theory of creation and mobilization of foams in porous media, AIChE Journal 36 (8) (1990) 1176–1188.

[134] J.-S. Tsau, J.P. Heller, Evaluation of Surfactants for CO2-Foam Mobility Control, SPE, Society of Petroleum Engineers, 1992/1/1.

[135] G. Chauveteau, A. Zaitoun, Basic rheological behavior of xanthan polysaccharide solutions in porous media: effects of pore size and polymer concentration, in: F.J. Fayers (Ed.), Enhanced oil recovery: Proceedings of the third European Symposium on Enhanced Oil Recovery, held in Bournemouth, U.K., September 21-23, 1981, Elsevier Scientific Pub. Co; Distributors for the U.S. and Canada, Elsevier/North-Holland, Amsterdam, New York, New York, 1981, pp. 197–212.

[136] F.P. Bretherton, The motion of long bubbles in tubes, J. Fluid Mech. 10 (02) (1961) 166.

[137] C. Enzendorfer, R.A. Harris, P. Valkó, M.J. Economides, P.A. Fokker, D.D. Davies, Pipe viscometry of foams, JOURNAL OF RHEOLOGY 39 (2) (1995) 345–358.

[138] Q.P. Nguyen, Dynamics of foam in porous media, [s.n.], [S.l.], 2004.

[139] R. Farajzadeh, A. Andrianov, H. Bruining, P.L.J. Zitha, Comparative Study of CO2 and N-2 Foams in Porous Media at Low and High Pressure-Temperatures, INDUSTRIAL & ENGINEERING CHEMISTRY RESEARCH 48 (9) (2009) 4542–4552.

[140] M.G. Aarra, A. Skauge, J.S. Solbakken, Supercritical CO Foam - The Importance of CO Density on Foams Performance, in: SPE-165296-MS 2013.

[141] T. Holt, F. Vassenden, I. Svorstol, Effects of Pressure on Foam Stability; Implications for Foam Screening, in: SPE-35398-MS 1996.

[142] R. Farajzadeh, R.M. Muruganathan, R. Krastev, W.R. Rossen, Effect Of Gas Type On Foam Film Permeability And Its Implications For Foam Flow In Porous Media, in: SPE-131297-MS, Society of Petroleum Engineers, SPE, 2010.

[143] P.C. Harris, A Comparison of Mixed Gas Foams With N2 and C02 Foam Fracturing Fluids on a Flow Loop Viscometer, SPE-20642-PA (1995).

[144] M. Bogdanovic, R.N. Gajbhiye, S.I. Kam, Experimental study of foam flow in horizontal pipes: Two flow regimes and its implications, Colloids and Surfaces A: Physicochemical and Engineering Aspects 344 (1-3) (2009) 56–71.

APPENDIX

Appendix A

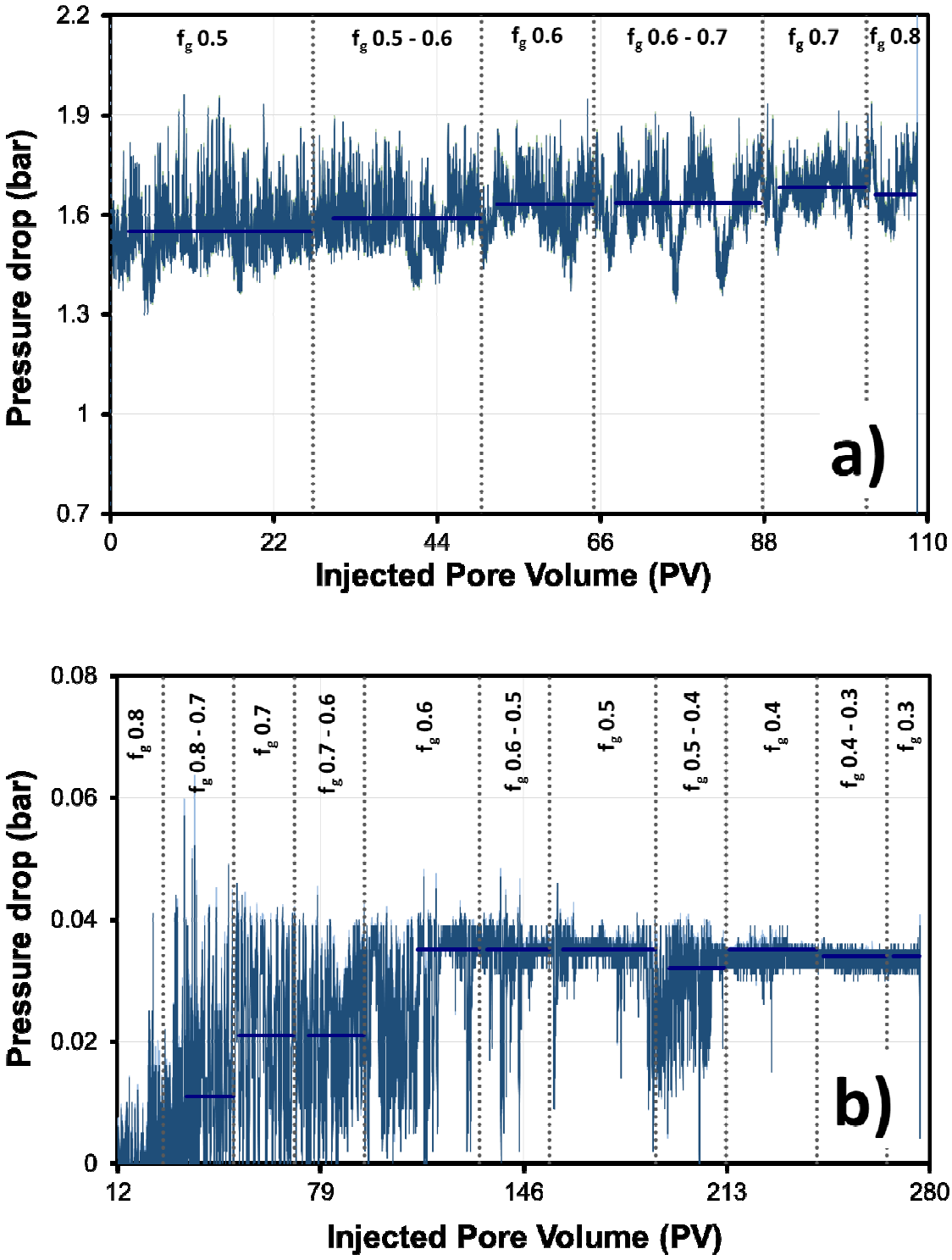

Figure A-1: Pressure drop curves of foam injection at a fixed total flow rate and varying foam quality in a heterogeneous core of 4800 mD. a) from f_g 0.5 to f_g 0.8; b) from f_g 0.8 to f_g 0.3.

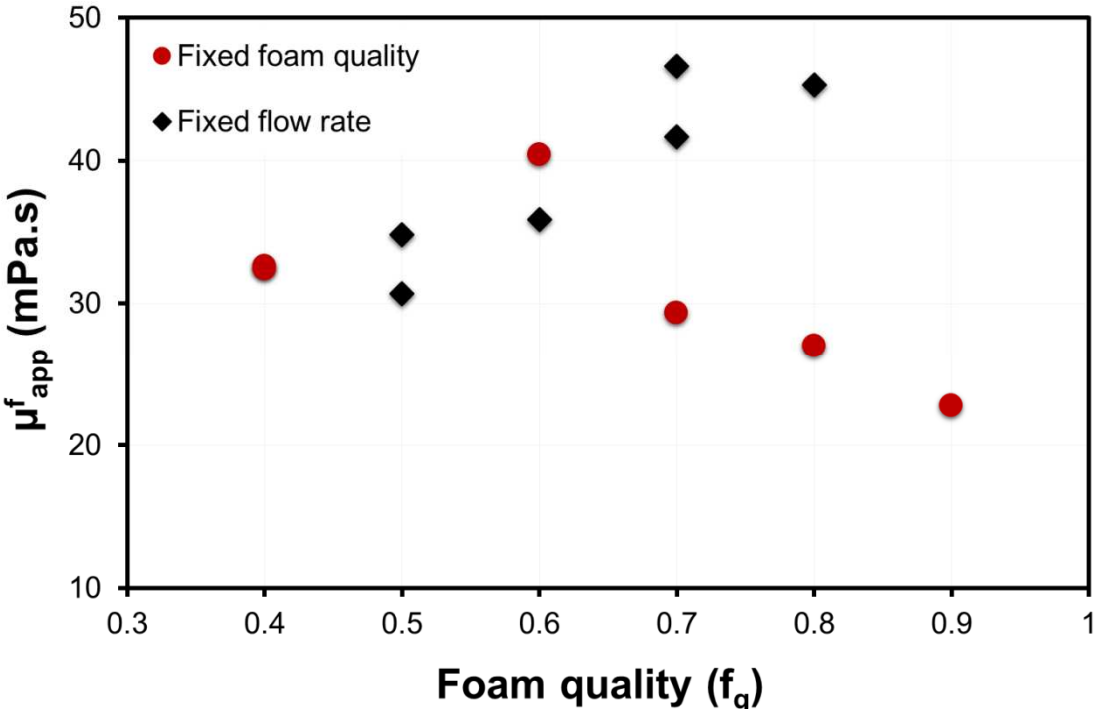

Figure A-2: Comparison of foam response as a function of the injection protocol.

Table A-1: Summary of results from foam flooding experiments in presence of crude oil.

Exp.	Oil Injection up to Swi			Oil Production					
				Brine injection		Co-injection		Foam flooding	
	V_{brine}	S_{wi}	S_o	V_{oil}	S_{orw}	V_{oil}	S_{org}	V_{oil}	S_{or}^{mousse}
#1	16.8 mL	41.3%	58.7%	12.2 mL	74.6%	2.4 mL	34.6%	Emulsion	Unknown
#2	16.8 mL	41.2%	58.8%			15.3 mL	10.4%	Emulsion	Unknown
#3	16.5 mL	46.2%	53.8%					14.3 mL*	22.1%*

*great volume of emulsion visible. Exact final values cannot be determined